University of Alberta

Sandwich Plate System Panels under In-plane Load and Uniform Lateral Pressure

by

Joshua Little

A thesis submitted to the Faculty of Graduate Studies and Research in partial fulfillment of the requirements for the degree of Master of Science

in

Structural Engineering

Department of Civil and Environmental Engineering

Edmonton, Alberta

Spring 2007

Library and Archives Canada

Published Heritage Branch

395 Wellington Street
Ottawa ON K1A 0N4
Canada

Bibliothèque et Archives Canada

Direction du Patrimoine de l'édition

395, rue Wellington
Ottawa ON K1A 0N4
Canada

Your file Votre référence
ISBN: 978-0-494-29988-3
Our file Notre référence
ISBN: 978-0-494-29988-3

NOTICE:
The author has granted a non-exclusive license allowing Library and Archives Canada to reproduce, publish, archive, preserve, conserve, communicate to the public by telecommunication or on the Internet, loan, distribute and sell theses worldwide, for commercial or non-commercial purposes, in microform, paper, electronic and/or any other formats.

The author retains copyright ownership and moral rights in this thesis. Neither the thesis nor substantial extracts from it may be printed or otherwise reproduced without the author's permission.

AVIS:
L'auteur a accordé une licence non exclusive permettant à la Bibliothèque et Archives Canada de reproduire, publier, archiver, sauvegarder, conserver, transmettre au public par télécommunication ou par l'Internet, prêter, distribuer et vendre des thèses partout dans le monde, à des fins commerciales ou autres, sur support microforme, papier, électronique et/ou autres formats.

L'auteur conserve la propriété du droit d'auteur et des droits moraux qui protège cette thèse. Ni la thèse ni des extraits substantiels de celle-ci ne doivent être imprimés ou autrement reproduits sans son autorisation.

In compliance with the Canadian Privacy Act some supporting forms may have been removed from this thesis.

While these forms may be included in the document page count, their removal does not represent any loss of content from the thesis.

Conformément à la loi canadienne sur la protection de la vie privée, quelques formulaires secondaires ont été enlevés de cette thèse.

Bien que ces formulaires aient inclus dans la pagination, il n'y aura aucun contenu manquant.

Canada

Abstract

Three Sandwich Plate System (SPS) specimen sets were tested under uniaxial in-plane compression and uniform lateral pressure. Each specimen set consisted of two SPS panels glued and clamped together in a test frame designed to enforce fixed boundaries on the panel perimeter and apply the loads uniformly, with the lateral load applied using a pressurized water-filled cavity between the two panels. Elastic load combinations were applied, then each specimen set was taken well into the plastic range at a different load combination to generate three points on the in-plane load versus lateral pressure interaction diagram for this SPS panel geometry. The test frame maintained adequate boundary conditions and provided accurate load application throughout all tests. SPS specimens exceeded full in-plane yield capacity without local faceplate buckling or bond delamination between sandwich layers. Comparison with finite element analyses showed good correlation for in-plane load versus deflection behaviour and for all interaction diagram points.

Acknowledgements

The contributions of Intelligent Engineering to this project were what made it possible. They provided the funding and the Sandwich Plate System test specimens, as well as the finite element analysis work and the rendered drawings of the test frame. Their advice and technical support throughout the project was much appreciated. Additional funding was provided by NSERC and by the University of Alberta, for which the author is grateful.

The author thanks Dr. G. Grondin and Dr. S.D.B. Alexander, who provided guidance and invaluable assistance throughout the project. The contribution of Dr. D.J.L. Kennedy in helping to shape the scope and direction of the project is also appreciated.

The contribution of C-FER laboratory in the use of their facilities was indispensable in achieving the goals of the testing portion of this project.

Table of Contents

1.0 Introduction 1

1.1 Background 1

1.2 Scope and Objectives 1

2.0 Background Information 3

2.1 Introduction and SPS Overview 3

2.2 Problem Description and Report Purpose 5

2.3 Related Work Done by Others 7

2.4 Basic Plate Theory and Behavior 9

2.5 Summary 10

3.0 Experimental Program 12

3.1 Overview 12

3.2 Test Specimens 13

3.3 Design of Test Frame 15

3.3.1 Design Overview 15

3.3.2 Panel Spacer and Gasket Setup 16

3.3.3 Perimeter Clamping and Loading System 16

3.3.4 Roller Bearing Setup 18

3.3.5 Test Frame Assembly Procedure 19

3.4 Test Setup and Instrumentation 22

3.4.1 Test Equipment Setup 22

3.4.2 Data Collection and Instrumentation 23

3.5 Test Protocol – Loading Procedures 25

3.5.1 Test Phase 1: Elastic Loading Range 25

3.5.2 Test Phase 2: Loading to Ultimate 26

3.6 Ancillary Tests 27

4.0 Experimental Results and Analysis 55

4.1 Elastic Loading Phase 55

4.1.1 In-plane Load of 7200 kN and No Lateral Pressure 55

4.1.2 Internal Pressure of 276 kPa and No In-plane Load 58

4.1.3 Intermediate Load Combinations 60

4.2 Loading to Ultimate Panel Failure 64

4.2.1 SPS-2: 415 kPa Internal Pressure 64

4.2.2 SPS-1: 207 kPa Internal Pressure 65

4.2.3 SPS-3: 690 kPa Internal Pressure 67

4.2.4 Test Results 69

4.2.5 Points on the Interaction Diagram 71

4.3 Test Frame Performance 72

4.3.1 Frame Behaviour - Elastic Range of Test Specimens 73

4.3.2 Frame Behaviour – Loading to Ultimate 74

5.0 Finite Element Analysis 98

5.1 Finite Element Model Overview 98

5.1.1 Model Geometry and Material Properties 98

5.1.2 Kinematic Boundary Conditions 99

5.1.3 Loading Conditions 100

5.2 Results of Elastic Analysis – Comparison of Finite Element Analysis Results with Test Results 100

5.2.1 Load Case 1 – 7200 kN Axial Load and No Lateral Pressure 101

5.2.2 Load Case 2 – 280 kPa Lateral Pressure and No Axial Load 101

5.2.3 Intermediate Load Cases 102

5.3 Loading to Ultimate – Comparison of Finite Element Analysis Results with Test Results 103

5.3.1 In-plane Deflections 103

5.3.2 Out-of-plane Deflections 104

5.3.3 Von Mises Equivalent Strains 105

5.4 Interaction Diagram – Comparison of Finite Element Analysis Results with Test Results 107

5.4.1 Methods to Determine Interaction Points 107

5.4.2 Interaction Results for Finite Element Model Version 1 108

5.4.3 Interaction Results for Finite Element Model Version 2 109

5.4.4 Comparison of Interaction Results between Version 1 and Version 2 111

6.0 Summary and Conclusions 126

6.1 Summary 126

6.2 Conclusions 127

6.3 Recommendations 128

References 130

Appendix A 132

List of Tables

Table 3.1:	Elastomer Material Properties (Brooking and Kennedy, 2003)	28
Table 3.2:	Adhesive Properties	28
Table 3.3:	Steel Spacer Bar Material Properties	28
Table 3.4:	Details of the Roller Bearing Assembly Components	29
Table 3.5:	SPS Plate Steel Tension Coupon Test Results	29
Table 4.1:	Data for Elastic Load Case of 7200 kN In-plane Load and No Lateral Pressure	77
Table 4.2:	Data for Elastic Load Case of 276 kPa Lateral Pressure and No In-plane Load	77
Table 4.3:	Data for Three Intermediate Elastic Load Cases	78
Table 5.1:	Summary of Finite Element Analyses	113
Table 5.2:	Comparison of Finite Element Analyses with Test Results for Elastic Load Combination of 7200 kN In-plane Load and No Lateral Pressure	114
Table 5.3:	Comparison of Finite Element Analyses with Test Results for Elastic Load Combination of 276 kPa Lateral Pressure and No In-plane Load	114
Table 5.4:	Comparison of Finite Element Analyses with Test Results for Three Intermediate Elastic Load Combinations	115
Table 5.5:	Comparison of Finite Element Analyses with Test Results for the Three Ultimate Load Cases after the Application of Initial Transverse Pressure but Prior to Application of In-plane Load	116

List of Figures

Figure 3.1:	Plan View of SPS Specimen	30
Figure 3.2:	SPS Specimen Section	30
Figure 3.3:	SPS Panel Specimen	31
Figure 3.4:	SPS Specimen Section	31
Figure 3.5:	SPS Test Specimen Fabrication - Photo Sequence	32
Figure 3.6:	Panel Spacer Bar Layout	33
Figure 3.7:	Spacer Bar Layout	33
Figure 3.8:	Water Inlet Spacer Insert	34
Figure 3.9:	Plan View of Test Frame	34
Figure 3.10:	Rendered Test Frame	35
Figure 3.11:	Assembled Test Frame	35
Figure 3.12:	Top Clamp Section	36
Figure 3.13:	Rendered Top Clamp Section	36
Figure 3.14:	Edge Clamp Section	37
Figure 3.15:	Rendered Edge Clamp Section	37
Figure 3.16:	Top and Edge Clamp Sections	38
Figure 3.17:	Plan View of Portion of Roller Bearing Assembly	38
Figure 3.18:	Section of Portion of Roller Bearing Assembly	39
Figure 3.19:	Rendered Cutaway View of Portion of Roller Bearing Assembly	39
Figure 3.20:	Roller Strip – Outer Bearing Plates Removed	40
Figure 3.21:	Close-up of Roller Bearing Strip	40
Figure 3.22:	Specimen Set Assembly	41
Figure 3.22:	Specimen Set Assembly (Cont'd)	42

Figure 3.23:	Test Frame Assembly Sequence	43
Figure 3.23:	Test Frame Assembly Sequence (Cont'd)	44
Figure 3.24:	Specimen Vertical Lifting Assembly – Top Brackets and Links	45
Figure 3.25:	Specimen Vertical Lifting Assembly – Bottom Brackets and Rods	45
Figure 3.26:	Specimen Mounted in the Testing Machine – Front View	46
Figure 3.27:	Specimen Mounted in the Testing Machine – Side View	47
Figure 3.28:	Specimen Mounted in the Testing Machine – Front View	48
Figure 3.29:	Specimen Mounted in the Testing Machine – View from Above	49
Figure 3.30:	Specimen Mounted in the Testing Machine – Bottom Loading Beams	49
Figure 3.31:	Strain Rosette Layout	50
Figure 3.32:	Channel Numbers Corresponding to Strain Rosette Components	50
Figure 3.33:	Strain Rosette Locations on One SPS Panel Face	51
Figure 3.34:	LVDT Layout on Specimen Set	51
Figure 3.35:	Channel Numbers Corresponding to LVDT Positions	52
Figure 3.36:	Typical Out-of-plane LVDT Setup	52
Figure 3.37:	Typical In-plane LVDT Setup	53
Figure 3.38:	Typical Outer Edge Clamp LVDT Setup (Channel 34 and 35)	53
Figure 3.39:	Load Combinations Applied to Each Specimen Set in the Elastic Range	54
Figure 3.40:	Dimensions of Tension Coupon	54
Figure 3.41:	Failed Section of Typical Tension Coupon	54

Figure 4.1:	In-plane Load versus In-plane Deflection for 7200 kN Axial Load and No Lateral Pressure	79
Figure 4.2:	In-plane Load versus Average Vertical Panel Strain for Axial Load of 7200 kN and No Lateral Pressure	79
Figure 4.3:	In-plane Load versus Average Top and Bottom von Mises Stress	80
Figure 4.4:	In-plane Load versus Average Panel Edge von Mises Stress	80
Figure 4.5:	In-plane Load versus Average Panel Midpoint von Mises Stress	81
Figure 4.6:	Transverse Pressure versus Mid Panel Out-of-plane Deflection for 280 kPa Lateral Pressure and No In-plane Load	81
Figure 4.7:	Transverse Pressure versus Panel Quarter Point Out-of-plane Deflection for 280 kPa Lateral Pressure and No In-plane Load	82
Figure 4.8:	Transverse Pressure versus Average Panel Top and Bottom von Mises Stresses	82
Figure 4.9:	Transverse Pressure versus Average Panel Edge von Mises Stresses	83
Figure 4.10:	Transverse Pressure versus Average Panel Midpoint von Mises Stresses	83
Figure 4.11:	In-plane Load versus In-plane Deflection for Three Intermediate Load Cases	84
Figure 4.12:	In-plane Load versus Panel Midpoint Out-of-plane Deflection	84
Figure 4.13:	In-plane Load versus Panel Quarter Point Out-of-plane Deflection	85
Figure 4.14:	In-plane Load versus Average Panel Top and Bottom von Mises Stress	85
Figure 4.15:	In-plane Load versus Average Panel Edge von Mises Stress	86

Figure 4.16:	In-plane Load versus Average Panel Midpoint von Mises Stress	86
Figure 4.17:	Welded and Ground Bottom Corner of SPS-3 Specimen Set	87
Figure 4.18:	Welded Top Corner and Water Inlet Port of SPS-3 Specimen Set	87
Figure 4.19:	Nylon Reinforced Neoprene Rubber Top Gasket Material Added to SPS-3 Specimen Set – Top Corner Close-up with Outer Clamp Bars Removed	88
Figure 4.20:	Extra Neoprene Edge Gasket and Steel Retaining Strip added to SPS-3 Specimen Set	88
Figure 4.21:	Steel Block for Axial Support of Gasket Retaining Strip on SPS-3 Specimen Set	89
Figure 4.22:	In-plane Load versus In-plane Deflection for All Three Tests	89
Figure 4.23:	Progression of Out-of-plane Deflected Shape During Loading of SPS-1	90
Figure 4.24:	Progression of Out-of-plane Deflected Shape During Loading of SPS-2	91
Figure 4.25:	Progression of Out-of-plane Deflected Shape During Loading of SPS-3	92
Figure 4.26:	Interaction Point From In-plane Load versus In-plane Deflection Curve for SPS-1 Test	93
Figure 4.27:	Interaction Points Calculated From All Three Test Results	93
Figure 4.28:	Yield Line Pattern Assumed in Calculating Upper Bound Plastic Collapse Pressure	94
Figure 4.29:	Comparison of Applied In-plane Load to Calculated In-plane Load	94
Figure 4.30:	Half-height In-plane Deflection of SPS-1	95
Figure 4.31:	Transverse Pressure versus Top and Bottom Clamp Motion for SPS-3	95

Figure 4.32:	In-plane Load versus Top and Bottom Clamp Motion for SPS-3	96
Figure 4.33:	Transverse Pressure versus Edge Clamp Motion for SPS-3	96
Figure 4.34:	In-plane Load versus Edge Clamp Motion for SPS-3	97
Figure 5.1:	Description of Finite Element Model	117
Figure 5.2:	Steel and Elastomer Stress-Strain Curves Used in FE Models	118
Figure 5.3:	In-plane Load versus In-plane Deflection – FEA versus Test Results	119
Figure 5.4:	In-plane Load versus Out-of-plane Deflection of Panel Midpoint – FEA versus Test	119
Figure 5.5:	In-plane Load versus Out-of-plane Deflection at Panel Quarter Point – FEA versus Test	120
Figure 5.6:	In-plane Load versus von Mises Strain for SPS-1 (207 kPa) – FEA versus Test	120
Figure 5.7:	In-plane Load versus von Mises Strain for SPS-2 (415 kPa) – FEA versus Test	121
Figure 5.8:	In-plane Load versus von Mises Strain for SPS-3 (690 kPa) – FEA versus Test	121
Figure 5.9:	Determination of Interaction Point using 0.2% Strain Offset Method – SPS-1	122
Figure 5.10:	Determination of Interaction Point using 0.5% Allowable Deflection Method – SPS-1	122
Figure 5.11:	In-plane Load versus In-plane Deflection – Eight Load Cases for FEA Version 1 Model	123
Figure 5.12:	Interaction Diagram - FEA Version 1 and Test Results	123
Figure 5.13:	In-plane Load versus In-plane Deflection – Eight Load Cases for FEA Version 2 Model	124
Figure 5.14:	Interaction Diagram - FEA Version 2 and Test Results	124
Figure 5.15:	Interaction Diagram Obtained Using the 0.2% Offset Method – FEA Version 1 and 2	125

Figure 5.16: Interaction Diagram Obtained Using the 0.5% Allowable Deflection Method – FEA Version 1 and 2 125

Figure A1: Top Outer Clamp Bar (4 Pieces Required) – Fabrication Drawing with Imperial Units 133

Figure A2: Top In-plane Loading Bar (4 Pieces Required) – Fabrication Drawing with Imperial Units 134

Figure A3: Edge Clamp Outer Bar (4 Pieces Required) – Fabrication Drawing with Imperial Units 135

Figure A4: Edge Clamp Spacer Bar (2 Pieces Required) – Fabrication Drawing with Imperial Units 136

Figure A5: Top Panel Spacer Bar (2 Pieces Required per Specimen Set) – Fabrication Drawing with Imperial Units 137

Figure A6: Edge Panel Spacer Bar (2 Pieces Required per Specimen Set) – Fabrication Drawing with Imperial Units 138

Figure A7: Water Inlet Spacer Insert (2 Pieces Required per Specimen Set) – Fabrication Drawing with Imperial Units 139

Figure A8: Nylon Retaining Strip for Roller Bearing Assemblies (40 Pieces Required) – Fabrication Drawing with Imperial Units 140

Figure A9: Inner Bearing Plate for Roller Bearing Assemblies (40 Pieces Required) – Fabrication Drawing with Imperial Units 141

Figure A10: Outer Bearing Plate for Roller Bearing Assemblies (20 Pieces Required) – Fabrication Drawing with Imperial Units 141

1.0 Introduction

1.1 Background

The patented Sandwich Plate System (SPS) is a three layer composite panel made up of two parallel steel outer faceplates separated and bonded with a solid homogeneous core composed of a polyurethane elastomer. This relatively new heavy engineering material is a replacement for traditional orthotropic stiffened steel plate, a construction method used extensively in ship structures and bridge decking. Uses for SPS thus far have been primarily in the rehabilitation of ship and ferry decking, however these panels show substantial promise for use in a ship hull plating application. In this particular case, the panels below the waterline of the ship would undergo both uniform transverse pressure from the surrounding water and in-plane load induced from global bending of the overall hull girder.

1.2 Scope and Objectives

Three sets of SPS panels were tested for this report, with each set having two identical specimens loaded simultaneously. In all tests, panels were subjected to various combinations of uniaxial in-plane compression and uniform transverse pressure. A set of tests was carried out in the elastic range of loading on each test specimen, after which each of the specimen sets were taken to their ultimate capacity under a different combination of in-plane compression and transverse pressure. In order to effectively apply these load combinations while enforcing a clamped boundary edge all around the panel perimeter, it was necessary to design a restraining frame that would contain the SPS specimens during testing. In addition, ancillary tests were performed on tension coupons to determine material properties for the SPS steel faceplates.

There were two main objectives for this test program. The primary objective was to document the behaviour of SPS panels under the combined loading scenario of in-plane compression and transverse pressure. Included in this was the development of an interaction diagram for in-plane load versus lateral pressure showing the failure envelope

for SPS plates of the geometry tested. The second objective was to design and fabricate a test frame to contain the specimens by enforcing rigid boundaries on all sides and enable the accurate application of the load combinations. Ideally, this test frame would be re-usable for future more comprehensive testing programs on SPS panels undergoing combined loading.

2.0 Background Information

2.1 Introduction and SPS Overview

The focus of composite construction, or more specifically sandwich panel construction, is to capitalize on the strengths and compensate for the weaknesses of the components and materials involved. A typical sandwich panel consists of two separated but parallel faceplates of relatively strong and stiff material bonded together using a lightweight core compound. The faceplates are generally quite thin with respect to the core depth, and the core itself must have enough shear strength to keep the faces aligned during plate bending. In addition, the core functions to keep the faces flat and at the proper separation under loading, and thus must have a certain minimum modulus of elasticity. The bond between the core and the faces is another critical element of a stiff sandwich. Enough shear strength must exist at this interface to prevent slip between the faceplates and the core while the panel undergoes loading.

The patented Sandwich Plate System (SPS) is a three layer structural panel made up of two relatively thin outer face plates of metal separated by a thicker core composed of a polyurethane elastomer. This multi-layer method of plate construction is used to increase flexural stiffness and improve buckling capacity over a simple steel plate without greatly increasing the mass of material involved, and without need for the added complexity of discrete transverse stiffeners welded to the plate at regular intervals (Brooking and Kennedy, 2003). In an SPS panel undergoing flexure, the metal outer faces function like the flanges of an I-beam, with the core transferring the shear between the steel plates and thus playing the role of the web. The faceplates also receive continuous out-of-plane support from the core material. In comparison to a typical steel plate of a given thickness, an SPS panel with the same mass per unit area is both a stiffer and a stronger system. An SPS panel is a simplified substitute for a traditional stiffened steel plate, which typically consists of a single steel panel that is braced laterally with many discrete closely-spaced secondary steel members welded to it (Brooking and Kennedy, 2003).

The capacity and performance of SPS plating is a function of the thickness of the various layers, as well as the material properties of the metal used in the faceplates. The faceplates of SPS panels can in theory be made up of many different metals, but in practice it is various grades and types of steel that are most commonly used. The SPS core is an engineered plastic developed and produced by Elastogran GmbH. It is a polyurethane elastomer, initially a two-part liquid that is injected into a sealed cavity formed between the metal faceplates. As the elastomer cures, it hardens and bonds with the faceplates such that once fully cured, the composite plate can reach full plastic moment or axial compressive capacity without any local buckling of the faceplates or delamination occurring between the sandwich elements (Brooking and Kennedy, 2003). When referring to the various arrangements of SPS panel layer thicknesses, a notation of xx-yy-zz is used, with all dimensions in millimetres. Thus a panel with 5 mm thick top and bottom faceplates and a 30 mm thick core would be SPS 5-30-5.

Construction of a typical SPS panel begins with the surface preparation of the steel faceplates. The side of the plates that faces the core must be grit-blasted to a minimum surface roughness of 60 microns, a value that has been established from extensive testing of the bond behaviour between the metal and elastomer (Brooking and Kennedy, 2003). Once appropriately roughened, the surface must be thoroughly cleaned of any dust, moisture or contaminants. The metal plates are positioned face to face and separated by spacer bars around the perimeter which are welded or glued in place to form an airtight cavity between the plates. Holes are drilled in the plates to form injection and venting ports, and the elastomer is then pumped into the core cavity. During both the injection and curing process, the faceplates are restrained against out-of-plane motion in order to attain a flat and deformity-free surface. Typical injection time is between 8 and 12 minutes, and the elastomer fully cures in 3 to 4 hours. The curing process is exothermic, which results in a residual stress distribution consisting of compression in the steel and tension in the elastomer (Brooking and Kennedy, 2003).

The sandwich plate system was invented by Dr Stephen Kennedy in the early 1990's, and over the past decade has undergone an extensive array of testing in an effort to

understand its behaviour under various conditions of loading and usage. These testing programs focused on a number of aspects of the product, including material characterization, structural behaviour under different load scenarios, fatigue testing and fire resistance (Brooking and Kennedy, 2003). Up until this point in time, the primary use of SPS has been in the rehabilitation and upgrading of the wearing surface of existing ship and ferry decking. It is conceivable, however, that with its simplicity of design, high rigidity, impact and fire resistance and vibration damping ability, the maritime uses for SPS could go beyond that of simply the decking surfaces of the ship. The Sandwich Plate System would potentially be a candidate for use as a ship hull plating material as well. The testing documented in this report is carried out as a means of characterizing the performance of SPS panels for use in this particular scenario.

2.2 Problem Description and Report Purpose

The primary objective of this report is to test and characterize the behaviour of Sandwich Plate System material in a ship hull plating application. In order to properly test the plate specimens however, it is necessary to determine just what the load case and boundary conditions are for a typical ship hull panel.

There are two fundamental elements of a ship hull structure, the skeleton support framework and the hull plating (Hughes, 1983). The primary components of the skeleton are the transverse frames and transverse bulkheads, which run perpendicular to the length of the ship and are essentially giant hoop-shaped girders. These transverse frames are spaced at regular intervals down the length of the ship and form the main girders of the hull support system. Longitudinal supports connect perpendicularly to the transverse frames and run parallel to the length of the ship. These longitudinal members act like beams and are spaced around the circumference of the ship hull at intervals typically smaller than the spacing of the transverse frames. With traditional steel plating, there would also be many secondary stiffeners running perpendicular to the longitudinal beams, spaced closely together and functioning much like floor joists to support and stiffen the hull plating in the out-of-plane direction (Hughes, 1983). Due to its built-in stability and stiffness, SPS hull plating material eliminates the need for these secondary

stiffeners (Brooking and Kennedy, 2003). As a result, a typical rectangular plate in an SPS ship hull would span entirely between two longitudinal members with no added stiffeners, and is thus supported on two parallel sides by the longitudinal beams and on its other two sides by the transverse frames.

The loading present on a ship hull comes from a combination of gravity, water pressure and from the motion of the ship though its surrounding environment (Hughes, 1983). The hull itself is really a giant beam or box girder that carries the loading imposed by its cargo and that is supported by its buoyancy. Wave action causes an unequal and ever-changing distribution of buoyancy, essentially creating continuously moving support conditions. A combination of this wave action and unevenly distributed gravity loads along the length of the ship introduce global bending moments in the hull structure. Vertical bending, which is bending about a horizontal axis perpendicular to the length of the ship, is by far the most significant load effect the hull girder will see, and the maximum value of this moment is the most critical load parameter for ship hull design (Hughes, 1983). The hull resists this bending in the same manner as a beam would, with the upper deck and bottom hull structure acting as flanges and the vertical hull side walls functioning as the web. Bending produces in-plane tension or compression in the flanges, implying that the hull skeleton and plating will see significant in-plane loads as a result of this hull bending moment. In addition to the in-plane load, the pressure of the surrounding water is ever present on hull plates below the waterline of the ship. This transverse pressure becomes more and more significant as the depth of the plate below the water surface increases, with hull plates on the very bottom of the ship undergoing the worst possible case of maximum in-plane load and maximum transverse pressure from the surrounding water.

The SPS hull plates would typically span with their long axis running parallel to the length of the ship. Moment due to global hull bending produces in-plane loads that are also primarily in the longitudinal direction, with transverse in-plane loads being negligible in comparison (Hughes, 1983). A theoretical worst case scenario thus occurs when the global bending moment puts the bottom hull plating into in-plane compression

parallel to the long axis of the panel, in combination with the uniform transverse pressure from the surrounding water. Boundary conditions for this load case can be most closely approximated as clamped on all four edges. This is due to the fact that the SPS plates are assumed to run continuously over all supports, with the transverse pressure acting uniformly on all spans from one side only.

2.3 Related Work Done by Others

There has been no testing done by others in terms of previous work on Sandwich Plate System panels under the combined load case of uniaxial in-plane compression and uniform transverse pressure. There are, however several related tests and analyses that have been done in which the results are applicable or helpful in gaining an understanding of the behaviour of at least one aspect of the tests done here.

Intelligent Engineering Ltd has carried out a wide range of tests on various aspects of SPS behaviour, including material properties and strength characteristics for the elastomer core, bond properties of the core-faceplate interface, fire and heat resistance of the panels, and overall panel structural performance under various load cases (Brooking and Kennedy, 2003). Fatigue tests on SPS beam specimens were also carried out by G. Lui and S.D.B. Alexander. In terms of structural behaviour test results that are of interest in this report, Intelligent Engineering has done testing of SPS beam specimens under compressive in-plane load only, and under lateral load only. Note that these tests were done on beams that were supported only on their two ends and not on plate specimens with continuous support around all boundaries. It was determined from these tests that SPS specimens can reach their full plastic moment in flexural capacity or their full compressive strength without local buckling or steel-elastomer delamination. In addition, the strength predictions from finite element analyses were very close to the actual test results, with an average test-to-predicted ratio of 0.98 for flexure and 1.05 for compression (coefficient of variation less than 5%) (Brooking and Kennedy, 2003).

Tests on reinforced concrete plates under combined in-plane load and flexure were carried out by M.G. Ghoneim and J.G. Macgregor in 1992. They investigated among

other things the influence of loading sequence on the maximum strength of square plate specimens. They varied the loading sequence and rate, and their conclusion was that the maximum strength of the plate specimen was independent of the path taken to reach that failure point. This testing was only done for slender square plates and not for plates of varying aspect ratios.

Roberts, Boyle, Wienhold, Ward and White (2002) tested rectangular sandwich panels made of glass fibre reinforced plastic under the load case of uniform lateral pressure only. The sandwich core material was either balsa or polyvinylchloride foam. Boundary conditions consisted of clamped edges on the two short sides of the panel and simply supported edges on the two long sides. Lateral pressure was applied using water-inflated bladders, and strains and deflections were measured and compared to results from finite element analyses. Results indicated that in general, the test and finite element model strains compared much better on the tensile side of the panels than on the compressive side.

Foo, Chai and Seah (2006) investigated low velocity impact in aluminium honeycomb sandwich panels, comparing test results to finite element analyses using the commercially available ABAQUS software. It was determined that the software was able to model the characteristics of the impact loading, and that the energy absorbed during impact was not a function of the density of the sandwich core material.

Cao, Grenestedt and Maroun (2006) tested a small scale ship hull built from sandwich panels with glass fibre reinforced vinyl ester faceplates and foam cores. These panels were glued to a three-dimensional steel truss. The hull was tested under both hogging and sagging loads. At the design load there was no apparent failure in the sandwich panels or the bonds between the panels and the steel truss, although substantial plastic deformation of the truss had occurred. Good correlation existed between test results and finite element analyses.

2.4 Basic Plate Theory and Behaviour

To design the test setup and loading procedure for the SPS plate specimens, it is essential to have a basic knowledge of plate behaviour. Plate behaviour can be quite complex, in particular under loading that produces both elastic and inelastic deformations.

It is possible to roughly compare a two-dimensional plate under in-plane compression and transverse pressure to a one-dimensional beam-column. It should be noted however, that the behaviour of the plate is very different than that of the beam column as loading progresses from the elastic to the plastic range. A simple column under a compressive point load will buckle and fail once the critical load is reached, whereas a rectangular plate under uniaxial compressive in-plane load has a far greater reserve of strength. This is due to the fact that when the applied load on the plate reaches the point required to cause buckling, a reconfiguration of the load carrying mechanism occurs (Bleich, 1952). The center portion of the plate buckles, but since the edges of the plate that are parallel to the line of application of the load are laterally supported, they are restrained from out-of-plane motion and thus redistribute the stresses and stabilize the plate in the deformed configuration. In a similar manner, a plate subjected to transverse loading has a much larger reserve of strength than a beam. Under large plastic deflections, the two-dimensional plate has many more potential means of stress redistribution than does a one-dimensional beam (Bleich, 1952).

In addition to the bending and torsional stresses that occur in plates under loading, another load carrying mechanism can develop in the form of membrane stresses. These membrane stresses form due to the change in length of the middle surface of the plate as it deforms under load (Salvadori and Levy, 1981). If the plate boundaries are prevented from moving in the in-plane direction, then the curvature occurring in the center portion of the plate under load attempts to elongate the in-plane length of the plate. This essentially pulls on the supports and puts the plate fibres into a tensile stress state much like the stresses that develop in a cable stretched between two points and sagging under its own weight. These tensile stresses occur in a radial pattern outward from the plate center. On the other hand, if the plate boundaries are allowed to move towards each other

as the plate deforms, then concentric rings of circumferential compressive stresses develop as the overall plate boundary gets pulled inward from the lateral deflection of the central portion of the plate. The capability of a plate to develop these membrane stresses provides it with greater strength and stiffness than it would have if only bending and torsional stresses could be developed (Salvadori and Levy, 1981).

For a plate with clamped boundary conditions and loaded in both uniaxial in-plane compression and uniform transverse pressure, the following general behaviour can be expected as the loads are increased to the failure point. Under low levels of loading producing relatively small elastic deformations, the membrane stresses can be neglected since their contribution to plate load resistance is small. Most of the plate resistance at this stage comes from the development of bending and torsional stresses (Bleich, 1952). As the loading increases however, lateral deformations in the central region of the plate become more pronounced, and the most highly stressed portions of the plate begin to yield. Tensile membrane stresses develop as the middle surface of the plate stretches from the curvature. These membrane stresses counteract the effect of the in-plane compression, slowing down the rate of increase of lateral deflection and improving plate stability in the distorted shape (Bleich, 1952). As the combined load continues to increase, the plate behaves more like a balloon as the tensile membrane stresses dominate. Finally, enough of the plate section has yielded that an ultimate failure point has been reached, a load point substantially greater than that required to cause first yield at a point in the plate section (Bleich, 1952).

2.5 Summary

The Sandwich Plate System is a relatively new heavy engineering product that has many potential applications for use in the field of maritime engineering. In this chapter, the components and characteristics of SPS material were described, and a typical panel fabrication procedure was explained. Based on the performance of SPS under various testing regimes, it was concluded that SPS panels could be a likely new choice of material for use as ship hull plating, as well as for continued use as a ship decking surface (Brooking and Kennedy, 2003).

The load case and boundary conditions that would be present on a typical section of SPS hull plating were described. From this, it was concluded that testing rectangular panels under uniaxial in-plane compression and uniform transverse pressure would be the most accurate simulation of the worst case load scenario a hull plate would see. Boundary conditions would be clamped edges all around the panel perimeter.

Work done by others on SPS panels with the load case and boundary conditions described is non-existent; however, other relevant tests that present conclusions useful to this report were summarized. In addition, since it will be necessary to have a general understanding of typical plate behaviour, a section on this was also presented. This information will aid in the design of a suitable and effective test setup and procedure.

3.0 Experimental Program

3.1 Overview

This chapter presents an overview of the test program for a series of three tests carried out on sandwich plate system panels. One of the objectives of the test program was to simulate a panel loading condition typical of what a section of ship hull plating below the waterline would see. This required testing the SPS panels under combined in-plane compression and uniform transverse pressure, and to do this properly it was critical to have a test apparatus capable of providing the desired boundary conditions and applying uniform in-plane and out-of-plane loads.

Using a single SPS panel as a test specimen makes it difficult to hold the edges fixed against rotation and out-of-plane translation, and also difficult to apply the transverse pressure uniformly over the entire panel surface. It was therefore determined that for each of the three tests, two identical panels would be tested simultaneously to facilitate the application of the loading and boundary conditions. Two panels placed face to face with a sealed cavity between them permits the application of uniform transverse load by simply pressurizing the cavity with water and controlling the internal pressure as desired. In-plane compression can then be applied to both panels using a hydraulically actuated loading machine. A drawback to this method is that only one face of each panel can be observed throughout the tests, and a test machine with twice the capacity is required.

These tests were performed to collect data that can be used both to characterize the behaviour of SPS panels under various load combinations and to validate a finite element model of SPS plate under similar loading and boundary conditions. In this chapter, the SPS specimens that were tested are first described and the design of the test frame assembly used to apply the loads is then reviewed. The chapter describes the setup of the test frame and its auxiliary support system in a 15 MN universal testing machine and the instrumentation used to measure strains, displacements and rotations under load. Following this is a description of the testing protocol and loading procedures, concluding

with an overview of the ancillary tests carried out to determine specimen material properties.

3.2 Test Specimens

Since there were three sets of SPS specimens tested, with each specimen set containing two SPS panels, a total of six SPS panels were required for the test program. The number of tests carried out in this program was small, thus it was determined that only one parameter would be investigated: the transverse pressure to in-plane load ratio. Each specimen set was tested under different values of transverse pressure, and then the in-plane load was increased until failure. All the SPS specimens were fabricated from one heat of steel, thus eliminating material properties as a variable. Furthermore, all six panels had the same plan dimensions, faceplate thickness and core thickness.

According to the Lloyd's Register Provisional Rules for the Application of Sandwich Panel Construction to Ship Structure (2005), when using SPS for a hull plating application it is recommended that the plate aspect ratio be between 1.2 and 1.7 (Chapter 4 of the Provisional Rules, Section 2.1.1a). The plate aspect ratio is defined as the ratio of the plan dimension of the long side of the plate to the plan dimension of the short side of the plate. In addition, the long side of the panel is not to exceed 3.6 m (Chapter 4 of the Provisional Rules, Section 2.1.1b). Based on this information, an aspect ratio of 1.5 was chosen for all the test specimens, and the dimension of the long side was taken as 1.8 m. These were thus considered to be large scale specimens, with panel plan dimensions as shown in Figure 3.1. Note that the gross panel dimensions are 240 mm longer and 270 mm wider than the 1800 mm x 1200 mm nominal size chosen. This is to accommodate an extended 135 mm wide strip on each of the panel's long edges and a 120 mm extension on each of the short edges, allowing for clamping of the specimens into the test frame assembly.

The thickness of all steel faceplates on the SPS test panels was 5 mm. This is thin enough to keep the load carrying capacity of the specimens below the capacity of the universal testing machine, but of sufficient thickness to allow fabrication using standard procedures

and to maintain good dimensional quality for the finished panels. The elastomer core of all specimens was 32 mm thick, giving a complete SPS thickness of 42 mm. A cross-sectional view of the SPS used is shown in Figure 3.2. A photo of a SPS specimen is shown in Figure 3.3 and a section close-up in Figure 3.4. The faceplate steel used was a mild steel designated as grade J2G3, with a nominal yield strength of 355 MPa, and the elastomer had the same formulation that is used for all SPS applications. The chemical composition of the elastomer is proprietary information. Material properties for the elastomer are provided in Table 3.1, and stress versus strain curves and material properties for the steel are presented in Section 3.6.

Each of the six SPS panel specimens were cut from a larger SPS plate that was fabricated using lengths of square hollow structural sections as perimeter bars to space the plates and contain the elastomer. In addition, small cylindrical plugs of elastomer were used to space the faceplates at intervals over the central region of the panel. Figure 3.5 presents the assembly sequence for one of the test specimens. Steel tension coupons were obtained from each of the top and bottom plates for ancillary testing.

Fabrication of the panels began with the grit blasting and cleaning of the inside (core) face of the steel faceplates. The perimeter bars were then fastened using foam rubber sealing tape to temporarily bond them to the faceplates. The panels were then injected with elastomer and allowed to cure before testing. The required curing time is typically about three to four hours, however since the test specimens were fabricated in Germany and then shipped to Canada, the time between fabrication and testing was at least 60 days.

As shown in Figure 3.5 (f), the faceplates were clamped and held parallel during injection to ensure panel flatness and tight tolerance on the overall thickness of the panels. This clamping was necessary since the elastomer curing process is exothermic, so as the steel plates heat up they have a tendency to bulge outward under the thermal expansion. Once the required three to four hours curing time was complete, the perimeter bars were removed and the edges of the steel faceplates were cut off and milled down to the final

panel dimensions, with each pair of opposite edges being machined perfectly flat, square to the faces, and parallel to each other. This was to ensure that during testing the in-plane load would be distributed evenly over the panel cross-section. The completed panels were then shipped to the test facility.

3.3 Design of Test Frame

3.3.1 Design Overview

Several alternative designs for the panels restraint system were investigated. Ideally the test frame should take the perimeter reactions and moments from the transverse pressure and react them internally. Welding the specimens together using a steel perimeter cap was considered, however this would require delaying the elastomer injection until after the welding was complete, since the weld heat affects the elastomer properties. It would also necessitate extensive fabrication work on each specimen such that they would no longer be considered to be representative SPS panels. In addition, a welded outer frame would not provide an accurate representation of an edge restraint fixed against rotation, and the effects of the welds themselves would also have to be accounted for.

Another alternative consisted of using a gasket spacer material between the two panels and clamping them with closely spaced bolts through the specimens around the perimeter. This had the drawback of having to pre-drill every SPS specimen around its perimeter and then of attempting to accurately account for the effect of the in-plane load in these bolted regions. In addition, the relatively large steel backing bars necessary to prevent the bolt heads from locally deforming the specimen faceplates would also carry a substantial and unknown portion of the in-plane load.

It was determined that the best design option would consist of a type of continuous external C-clamp, where the perimeter bolts used to supply the clamping force would be positioned just outside the perimeter of the test panels. This design has several key advantages, one being the fact that no modifications need to be made to the SPS specimens. The frame allows the application of a uniform in-plane load to the specimens

combined with a uniformly distributed transverse load as it has built-in spreader bars on each of its short sides, and it is set up to ensure that very little of the applied in-plane load goes into the frame itself. It is reusable for all of the test panels, and it is a relatively simple and straightforward procedure to mount a SPS specimen set into the frame. In addition, the frame is rigid enough to enforce a clamped boundary edge all around with no external out-of-plane bracing applied. The following sections describe the test frame design in detail.

3.3.2 Panel Spacer and Gasket Setup

The two SPS panels in a test set were separated around their perimeters by 12.7 mm (1/2 in) thick cold-rolled steel bars. These edge bars were 133 mm (5.25 in.) wide and the top and bottom bars were 120 mm (4.75 in.) wide. Figure 3.6 shows a plan view of the spacer bar layout, with a photo of the spacer bar shown in Figure 3.7. In an assembled panel set, the bars were glued on both sides to the inside faceplates of the two SPS panel specimens, forming a cavity roughly 1200 mm by 1800 mm by 12.7 mm deep. The adhesive bond between the spacer bars and SPS was designed to provided a watertight gasket, allowing the cavity to be pressurized to the required level. The adhesive used to bond the spacer bar to the SPS was a two-part methacrylate manufactured by ITW Plexus, the specifications of which are found in Table 3.2. Water access to the cavity was controlled through 5 mm (3/16 in.) diameter holes drilled through two specially fabricated spacer inserts with threaded attachments shown in Figure 3.8. Shop drawings for the spacer inserts as well as for all test frame components can be found in Appendix A. Fittings for the pump system consisted of 10 mm diameter threaded couplings screwed into the predrilled inlet and outlet holes, allowing straightforward connection of the pump lines. Specifications for the steel spacer bars were obtained from mill certificates provided by the steel supplier, and are found in Table 3.3.

3.3.3 Perimeter Clamping and Loading System

To provide fixed boundary conditions to the plate perimeter, it was necessary to physically clamp the plate perimeter to eliminate edge rotation under transverse load. This was achieved using four separate clamps on each edge of the specimens. A plan

view of the entire test frame assembly is shown in Figure 3.9. Figure 3.10 is a rendered drawing of the test frame and Figure 3.11 is a photo of the assembled frame.

On the top and bottom (short edges) of the specimen, the clamping assembly had to be designed such that it could both resist transverse load and be used to apply in-plane compression parallel to the long axis of the panels. This was achieved using a four piece assembly as shown in cross-section in Figure 3.12. A rendered top clamp section is shown in Figure 3.13. Each of the outer clamp bars were cut to length from 51mm by 305mm (2x12 in.) cold-rolled steel bar and drilled at 150 mm c/c intervals along the bar centerline to accommodate 1.25 in. diameter bolts. The inner in-plane loading bars were cut and milled to size from 51 mm by 203 mm (2x8 in.) cold-rolled steel, then match drilled with the corresponding outer clamp bars to allow the clamping bolts to run smoothly through the entire assembly. To compensate for SPS core shrinkage due to clamping force and allow for additional overall clamp thickness adjustment using shim stock, a 2mm gap was left along each side of the mid-plane between the two halves of each clamp.

On the sides (long edges) of each specimen set, the clamps have to provide out-of-plane restraint only, as no in-plane load is to be applied along these edges. It was critical that the clamps be designed to allow the panel to freely deform in the plane of the plate. Axial force taken by the edge clamp assemblies had to be minimized or eliminated. Therefore, friction on the contact surfaces between the clamps and the test specimens had to be kept as small as possible in the direction of the in-plane load. In addition, a contraction gap must exist between the edge clamps and the top and bottom clamps. Friction between the test specimen and edge clamps was minimized by using roller bearing strips described in Section 3.3.4. A 20 mm gap was created on either end between the edge clamps and top and bottom clamps, thus allowing a reduction of length of the test specimens of 40 mm before the in-plane load gets transferred directly from the end clamps to the edge clamps. A cross-section of an edge clamp is shown in Figure 3.14 and a rendered drawing in Figure 3.15. Figure 3.16 shows a corner of the assembled test frame showing a cross sectional view of both the top clamp and an edge clamp.

A typical edge clamp assembly consisted of five components. The outer bars were cut from 51mm by 305mm (2x12 in.) cold-rolled steel and 33 mm (1-5/16 in.) holes were drilled at 150 mm c/c along the bar centerline to accommodate 1-1/4 in. bolts. The clamp spacer consisted of two 100 mm wide strips of SPS cut from the same material as the test panels, as well as a 100 mm wide steel bar milled to the same thickness as the combined thickness of the two roller bearing assemblies and the 12.7 mm panel spacer bar. Because the SPS elastomer core material has a modulus of elasticity about 250 times smaller than that of the steel, core deformations much larger than those in the steel occur as the material undergoes compressive load normal to the faceplates. By using roughly equal amounts of SPS on both sides of the bolt line, the clamp faces are kept parallel as the bolts are pre-tensioned since equal shrinkage occurs on both sides. This aids in ensuring that a uniformly distributed load is applied to the roller bearing assemblies, while helping to keep time consuming adjustment with shim stock to a minimum.

The bolts used for all of the clamp assemblies were 1-1/4 in. diameter A325, and were 254 mm long for the top and bottom clamps and 305 mm long for the edge clamps. Grade A325 bolts were chosen because they could be reused for all three tests. Proper tightening of the bolts is essential to provide rigid out-of-plane restraint to the panels and prevent separation from occurring between the SPS and the panel spacer bar. As explained in Section 4.2, a slightly different bolt tightening procedure was used for each of the three tests. In addition to the 1-1/4 in. bolts, each of the four clamp assemblies had three 3/4 in. A325 alignment bolts along its outer edge to facilitate alignment of the clamp components during assembly (see Figure 3.9).

3.3.4 Roller Bearing Setup

The roller bearing assemblies helped minimize friction between the edge clamps and the test specimens in the direction parallel to the applied in-plane load. There were a total of four bearing strips, one between each of the edge clamp-to-SPS contact areas. Each strip contained 110 cylindrical rollers spaced at 16 mm c/c and guided parallel to each other using nylon strips connecting the roller end pins. Each roller was 9.5 mm diameter,

78 mm long and was made of case hardened steel with a hardness of Rockwell C58. Two strips of 76 mm wide by 6.4 mm thick hardened steel bearing plates were used to separate the clamp and SPS faceplate from the roller strip on either side. These plates helped guide and support the rollers, and prevented the high contact stresses from deforming the softer steel of the clamp bar and SPS faceplate as the clamp bolts were pre-tensioned. A plan view of a portion of a roller assembly is shown in Figure 3.17 and a cross-section in Figure 3.18. In addition, Figure 3.19 shows rendered cutaway drawing with the location of the roller strips in the test frame, and Figure 3.20 shows a photo of a roller strip during frame assembly prior to the outer bearing plates being applied. Figure 3.21 is a close up of a roller assembly.

Since the purpose of the roller bearing strips was to minimize the in-plane load transferred to material other than the test specimens, the individual rollers were expected to move closer together as the SPS panels were loaded. The nylon retaining strips allowed this for small deformations, since the nylon has a low modulus of elasticity. To further reduce the in-plane load required, each 1760 mm long strip of hardened bearing plates on the specimen side of the rollers was fabricated in ten 173 mm segments. This allowed for nine evenly spaced 3 mm wide contraction joints along each of the specimen edges as shown in Figures 3.17 and 3.18. Specifications for the roller bearings, steel bearing plates and nylon retaining strips are summarized in Table 3.4.

3.3.5 Test Frame Assembly Procedure

Since lab time was very limited during testing, it was critical to develop a rapid assembly procedure for mounting the test specimens into the test frame. To aid in specimen set up, a wooden assembly platform was designed and built to facilitate precise fitting and placement of components without the need for repetitive measuring and alignment. The assembly sequence for the test specimen sets is shown in Figure 3.22 and the assembly sequence for the test frame is shown in the series of photos in Figure 3.23. The timber assembly platform can be seen in Figure 3.23 (a). The assembly procedure for a given test specimen consisting of two SPS panels is described below.

Prior to any assembly taking place, all of the contact surfaces that were to be glued with the Plexus adhesive were prepared using the following procedure. The panel spacer bar components were roughened with a belt sander on all contact faces, then wiped clean, degreased and further wiped until all residue was removed. The SPS panel faceplates did have a very tight mill scale on their outer surfaces. This mill scale was removed from a 75 mm wide strip around the perimeter of the glued face using an air-powered needle scaler. The perimeter was further roughened using a belt sander, then cleaned, degreased and further cleaned until all residue was removed. Once this surface preparation was complete, the assembly process began.

The first of the two SPS panels was laid outside (dry) face down. Adhesive was applied in three parallel beads around the panel perimeter, then each of the four 12.7 mm thick spacer bars and each of the two water inlet ports were positioned one at a time in their respective locations around the panel perimeter flush with the panel edges. In addition, the butt joints between the ends of the edge bars, the bottom bar, the water inlet ports and the top bar were glued together to provide a bond between all components where they joined at the four corners. Once all the bars were positioned, C-clamps were installed at regular intervals around the perimeter to hold the spacer bars in place during the four hours required for the adhesive to cure. After the glue had cured, all clamps were removed and adhesive was applied in three parallel beads to the top face of all bars around the entire panel perimeter. The upper SPS panel specimen was then placed outside (dry) face up onto the bars to form a hollow sandwich. The panel set was again temporarily clamped on all four edges using C-clamps at regular intervals until the glue cured. Care was taken during this stage to ensure that the panel perimeters and the outside faces of all bars lined up exactly flush, especially along the loaded edges. An additional clamping mechanism was fabricated using threaded rod and hollow steel sections for this purpose. The photos showing this entire specimen set assembly sequence are presented in Figure 3.22.

Once the adhesive was cured, the C-clamps were removed from the panel set and the test frame assembly began. One of each of the four outer clamp bars (top, bottom and two

edges) were placed in their proper positions on the assembly platform. The outer bearing plates for the cylindrical rollers were placed on the edge bars, and two sets of roller strips were assembled and positioned on these plates. The inner bearing plates were then positioned on top of the rollers, and the panel set was carefully lowered down onto the clamp bar components and roller assemblies. The edge clamp spacer bars and SPS spacer strips were placed on each edge clamp outer bar and the in-plane loading bars were placed on the top and bottom clamp outer bars with shim stock as necessary to maintain parallel clamp faces as the bolts were tightened. The inner bearing plates were then positioned on the remaining (now upper facing) side of the specimen set. The remaining two roller bearing strips were assembled and placed on the bearing plates and the outer bearing plates were positioned on the rollers. All four remaining outer clamp bars (top, bottom and two edges) were then positioned onto the frame.

Once all the elements of the out-of-plane restraint system were in place, the alignment bolts were installed and snug tightened. The high strength bolts were then installed all around and snug tightened. The bolt pre-tension was then increased in the manner described in Section 4.2 until the frame was fully tightened. Small alignments and shimming were sometimes needed during this stage to ensure proper fit-up of all components. The complete test frame assembly sequence is presented in the photos in Figure 3.23.

The specimen had to be lifted vertically in order to install it in the test machine, and this was achieved using a lifting rig fabricated out of steel angles, rectangular sections and threaded rod. This lifting apparatus was connected to the specimen using the ¾ in. alignment bolts, and two clevises were installed in the top rectangular sections to attach the lifting slings to. Figure 3.24 shows the top of the lifting rig and Figure 3.25 shows the bottom connections.

3.4 Test Setup and Instrumentation

3.4.1 Test Equipment Setup

Because the specimens were tested under combined loading, it was necessary to have two separate pieces of equipment for load application. In-plane compression was applied to the specimens with a 15 MN universal testing machine owned and operated by C-FER Technologies in Edmonton, Alberta. To apply the transverse load by pressurizing the specimen setup with water, a pneumatic powered Haskel water pump was used. During the tests, the output of this water pump was controlled manually by regulating the air pressure supplied to the pump head using a ball valve installed in the air supply line. Relatively precise control of the internal pressure was possible throughout the test, with maximum fluctuations in pressure being generally no greater than about +/- 7 kPa (1 psi). This pump system was also owned and operated by C-FER Technologies in Edmonton.

Prior to installing a specimen set into the testing machine, it was first mounted in the test frame as described in the previous section. Figure 3.26 shows a front view of the test specimen mounted in the testing machine (referred to as the Tubular Testing System (TTS)). Figure 3.27 shows a side view of the specimen in the TTS. The TTS machine applied vertical load using a hydraulically actuated ram located at the base of the machine at the level of the strong floor. The top of the test machine, referred to as the crosshead, was adjustable in its initial height above the loading ram, but once its position was set it was locked in place and did not move throughout the test. Mounting of the test specimen in the test machine required the use of several additional components to help provide a uniformly distributed load to the specimen and to ensure out-of-plane stability during loading. Starting at the base, there was a 1520 mm by 1520 mm by 124 mm thick square machined steel bearing plate that sat directly on the 559 mm diameter loading ram. This plate served as a loading platform as well as an out-of-plane brace to the specimen as it fitted closely between the vertical steel rails of the test machine.

Two solid steel rectangular beams, each 406 mm wide, 1829 mm long and 156 mm thick were placed on top of this square plate. These beams combined with the square plate helped to distribute the in-plane load from the 559 mm wide loading ram to the 1470 mm

wide test specimen, which sat directly on top of these stacked steel beams. When shimming was required for proper load transfer, the shims were positioned between the two rectangular beams, which were separated using a hydraulic flat jack so the shim stock could be inserted. At the top, transferring the in-plane compression from the crosshead to the 1470 mm wide specimen was a 1422 mm wide, 203 mm thick and 914 mm deep steel spreader beam. This "beam" was bolted directly to the TTS crosshead, and sat on the top of the test frame with shims applied as necessary to obtain a uniform load transfer between the two elements.

To ensure that the tests were conducted safely, the Plexiglas blast doors surrounding the test machine enclosure were closed during loading. These prevented any potential leaking water or flying debris from escaping the test area. Any water that did leak out during loading ran directly into the sump located beneath the test machine. In addition, the test machine operator and any observers stood behind the lab strong wall while load was being applied, and the specimen was not approached under any circumstances while it was under load. Photos of the setup at the C-FER test facility are shown in Figures 3.28 to 3.30.

3.4.2 Data Collection and Instrumentation

Data from the tests were collected using several devices. One of the goals of the test program was to record strains in the SPS faceplates under various combinations of in-plane and axial loads. To achieve this, strain gauge rosettes were placed at strategic locations on each outer plate. A total of five strain rosettes were mounted to each of the six panels, with positioning chosen to take advantage of the symmetry of the setup, but to also provide at least two readings for every location in case of gauge malfunction or error. The strain gauge layout used for all specimens is shown in Figure 3.31. This particular arrangement was chosen to obtain principal strains at the points of potential first yield in the plate. These points were located at the clamped support at the midpoint of the short edge of the plate under most load combinations. For the cases where the level of lateral pressure is high enough to cause yield with minimal in-plane load, the point of

first yield would be at the midpoint of the long edge of the plate. Figure 3.32 shows the strain gauge layout for both east and west panels in a specimen set with the corresponding channel numbers used to record the strain data during the test, and Figure 3.33 shows an assembled specimen set with the strain gauge locations marked.

Linear variable differential transducers (LVDT's) were used to record deformations during testing at a total of 21 different locations. The LVDT layout is shown in Figure 3.34, with the channel numbers corresponding to each LVDT position on the west and east faces of the test specimens shown in Figure 3.35. The three LVDT's located at the midpoint and quarter points of each side of the SPS panel were used to measure displacements normal to the panel surface. These SPS panel LVDT's are labelled as channels 24 to 29 in Figure 3.35. A typical mounting bracket for LVDT's is shown in Figure 3.36. The bases of the LVDT's were mounted in wooden support frames that were anchored to the vertical rails of the test machine. A fine steel wire was then spot welded to the desired point on the SPS faceplate and attached to the LVDT shaft.

Four additional LVDT's, two on each side of the specimen, were used to measure overall change in length of the panel. These additional LVDT's, labelled as channels 36 to 39 in Figure 3.35, were necessary since machine stroke only provided deformation data for the overall height of the entire test setup. This included the specimen deformation as well as deformations in the top and bottom clamps, the spreader beams, the vertical machine rails and any slack that may have been present in the various connection points between these members. These in-plane LVDT's were also used to keep track of any relative rotation of the top and bottom clamps as loading progressed, rotation that could occur as a result of one SPS specimen failing before the other, for example. Each in-plane LVDT was mounted to the bottom clamp with a magnetic base and attached to the top clamp using steel wire. Figure 3.37 shows a typical in-plane LVDT setup.

To monitor out-of-plane deflections of the test frame clamps, a LVDT was mounted at the midpoint of the inside edge of each of the four clamp bars on each face of the specimen set. The locations of these LVDT's are shown in Figure 3.34 and correspond to

channel numbers 20 to 23 and 30 to 33 on Figure 3.35. Like the SPS panel out-of-plane LVDT's, these clamp LVDT's were also mounted on wooden support frames anchored to the vertical rails of the test machine and attached to the clamp face using steel wires. To monitor the compression of the outer face of each of the two edge clamps, an LVDT was mounted on each edge clamp using magnetic bases as shown in the photo in Figure 3.38. These LVDT's correspond to channels 34 and 35 on Figure 3.35. Finally, a single LVDT was mounted to the distributing beam at the top of the specimen using a magnetic base and was attached at the mid height of the SPS panel using steel wire. This was installed as a check to ensure that the strain remained relatively uniform over the panel height during loading.

3.5 Test Protocol – Loading Procedures

3.5.1 Test Phase 1: Elastic Loading Range

In this portion of the testing regime, the test specimens were loaded elastically under different load combinations. The purpose of this was to characterize deflections and strain patterns in SPS panels under service load conditions, compare the data results from test to test, and then compare these strain and deflection values taken from the test data with those generated from finite element analyses. Since all test specimens had identical geometry and material properties, the loading sequence was applied in the same manner for each specimen set. Due to strain gauge positioning and the use of symmetry, each SPS panel had two gauges for each monitored point on the panel edges, and one at each point at the panel center. This resulted in a total of between 6 and 12 readings for each strain point, making it possible to obtain an estimate of the precision of the data obtained.

To determine specimen behaviour under a broad range of loads, there were five elastic combinations of in-plane compression and out-of-plane pressure applied to each specimen set. The loading sequence used for all three specimen sets in this phase of the tests is shown in Figure 3.39. However, prior to any of the load steps a seating load of 2000 kN was applied to each specimen to ensure proper seating of the test specimen in the test frame and check the uniformity of the load distribution using the vertical strain

gauges. Shims were inserted as required to ensure a uniform load transfer to the SPS panels.

The first elastic load case involved in-plane load only. This in-plane load was applied to each specimen set to a level of 7200 kN, calculated to be approximately 60% of the in-plane load required to yield the cross-section of the entire specimen set. This in-plane load was then removed, and the specimen was subjected to the second elastic load case of transverse pressure only. The pressure used for this was 276 kPa (40 psi), which was roughly 60% of the calculated lateral pressure required to cause first yield in the panel. This was followed by three intermediate load cases, each one at a different combination of in-plane load and lateral pressure. For the first intermediate case, pressure was reduced to 207 kPa (30 psi) and in-plane load was increased to 1800 kN. For the second intermediate case, pressure was further reduced to 138 kPa (20 psi) and in-plane load increased to 3600 kN. For the third and final intermediate case, pressure was reduced to 69 kPa (10 psi) and the in-plane load increased to 5400 kN. As shown in Figure 3.39, these five load combinations plot a straight line on a graph of in-plane load versus lateral pressure and provide a relatively broad array of load cases in the elastic range of SPS panel behaviour.

3.5.2 Test Phase 2: Loading to the Ultimate Capacity of the Test Specimens

Unlike the elastic tests outlined above, this loading phase was different for each of the three test specimens. Specimen set SPS-1 was first pressurized to 207 kPa, equivalent to 13% of the calculated plastic collapse capacity of the panels. This transverse load level was then held constant while in-plane load was increased to the point of specimen failure. Specimens SPS-2 and SPS-3 were loaded in exactly the same manner, however the lateral pressure on SPS-2 was 415 kPa and was 690 kPa for SPS-3. This was equivalent to 27% of the plastic collapse pressure for specimen 2 and 45% for specimen 3. A description of each of the three ultimate tests is presented in Section 4.2.

3.6 Ancillary Tests

Ancillary tests were performed to determine the material properties of the steel faceplates of the SPS test specimens. The steel plates for the six SPS panels tested were all cut from one heat of steel, hence all faceplate material for all specimens was assumed to have the same material properties. Extra steel plate material was provided by the supplier, and four ancillary coupons were machined. All coupons were milled to the dimensions stated in the ASTM A370-05 (2005) standard for 50 mm gauge length, and are shown in Figure 3.40. Tension coupon tests were conducted in accordance to ASTM A370-05 (2005) in a MTS 1000 universal testing machine. Each coupon was instrumented with an extensometer to measure overall elongation over the gauge length. The stress versus strain curves from the tension coupon tests are presented in Appendix B, and the results from all four coupon tests are listed in Table 3.5. Figure 3.41 is a photo of a typical failed coupon cross section.

The chemical composition and hence the material properties of the polyurethane elastomer core are tightly controlled, and extensive previous testing of these properties by others has been well documented (Brooking and Kennedy, 2003). In addition, the strength of the bond between the faceplates and the core is also well understood. As a result, data from previous testing programs (Brooking and Kennedy, 2003) was used for the elastomer properties, and the bond was not investigated in this project. No ancillary tests were performed to determine either the elastomer properties or the interface bond strength.

Table 3.1: Elastomer Material Properties (Brooking and Kennedy, 2003)

Density	1150 kg/m^3
Compressive Modulus of Elasticity (E) at 23°C	765 MPa
Compressive Yield Stress (σ_Y) at 23°C	18.0 MPa
Shear Modulus (G) at 23°C	285 MPa
Poisson's Ratio	0.36

Table 3.2: Adhesive Properties

Adhesive Type	Plexus MA 560-1 methacrylate
Tensile Strength	17 - 20 MPa
Tensile Elongation	> 130%
Shear Strength	12 - 15 MPa
Working Time	55 - 70 minutes
Curing Time	220 - 240 minutes

Table 3.3: Steel Spacer Bar Material Properties

Steel Type	Cold-rolled flatbar
Modulus of Elasticity (E)	200000 MPa
Yield Strength	386 MPa

Table 3.4: Details of the Roller Bearing Assembly Components

Roller Bearing Dimensions	9.53 mm (3/8 in.) diameter x 78.5 mm (3.09 in.) length
Roller Bearing Steel Hardness	Rockwell C 58 (HRC)
Load Capacity per Roller	115000 N
Inner (SPS side) Steel Bearing Plate Dimensions	6.4 mm thick x 76 mm wide x 173 mm long
Outer (Clamp side) Steel Bearing Plate Dimensions	6.4 mm thick x 76 mm wide x 350.8 mm long
Bearing Plate Steel Type and Hardness	01 Tool Steel Quenched and Tempered to Rockwell C 60 (HRC)
Nylon Retaining Strip Dimensions	6.4 mm thick x 12.7 mm wide x 350.8 mm long
Nylon Retaining Strip Yield Strength	95 MPa
Nylon Retaining Strip Modulus of Elasticity (E)	2800 MPa

Table 3.5: SPS Plate Steel Tension Coupon Test Results

	Coupon 1	Coupon 2	Coupon 3	Coupon 4	Average
E (MPa)	187.2	187.5	189.7	188.2	188
σ_Y dynamic (MPa)	382	383	378	379	380
σ_Y static (MPa)	352	356	349	350	352
$\sigma_{ultimate}$ dynamic (MPa)	630	618	609	622	620
$\sigma_{ultimate}$ static (MPa)	590	570	562	580	575

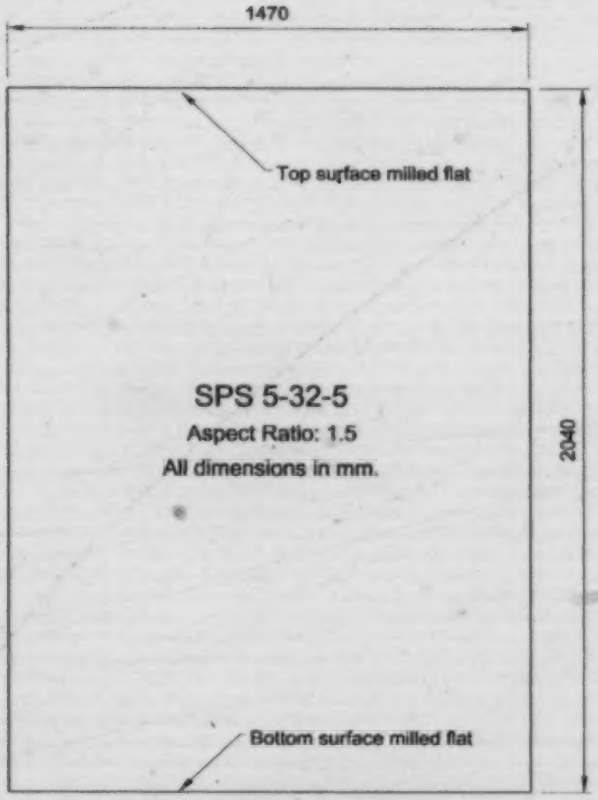

Figure 3.1: Plan View of SPS Specimen

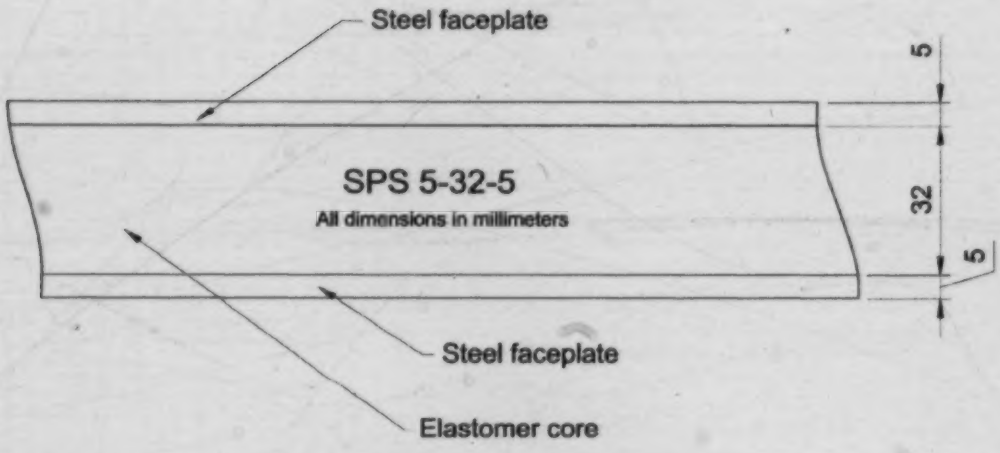

Figure 3.2: SPS Specimen Section

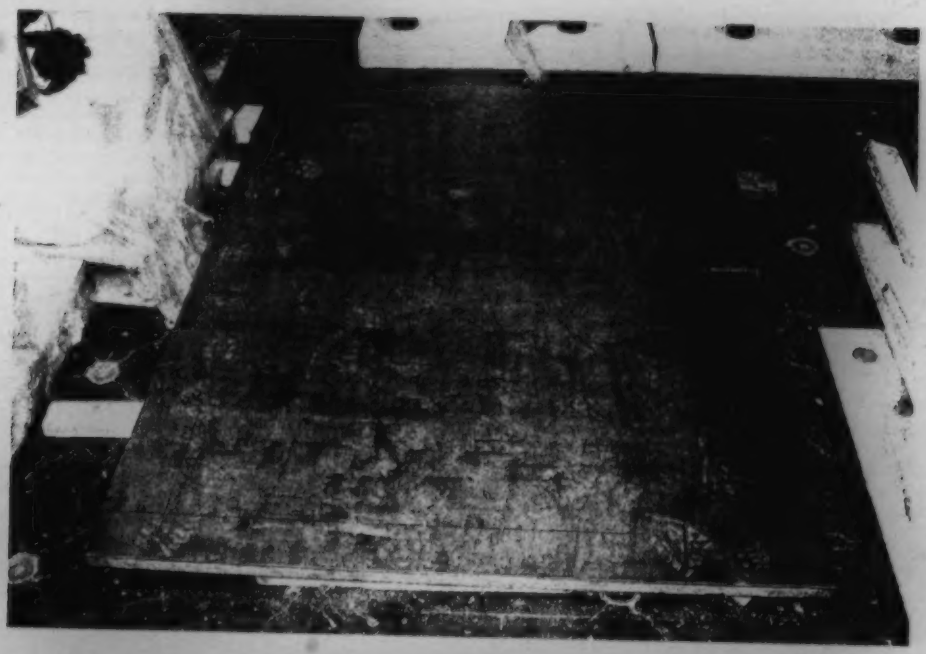

Figure 3.3: SPS Panel Specimen

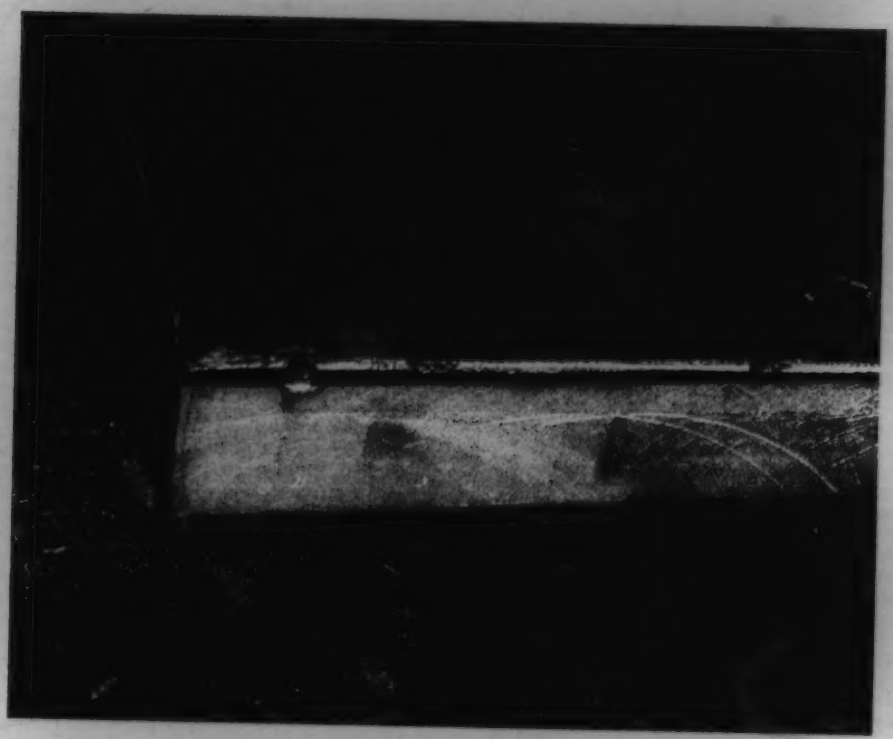

Figure 3.4: SPS Specimen Section

(a): Bottom Steel Plate on Out-of-plane Restraint Beams – Sand Blasted Face Up

(b): Perimeter Bar Positioned on Bottom Steel Plate

(c): Elastomer Spacer Blocks Placed at Intervals on Plate Mid Region

(d): Top Steel Plate Positioned on Perimeter Bar – Sand Blasted Face Down

(e): Upper Out-of-plane Restraint Beams Placed on Top Steel Plate

(f): Entire Assembly Clamped and Elastomer Injected Through Orange Funnel Ports

Figure 3.5: Fabrication Sequence for SPS Test Specimen

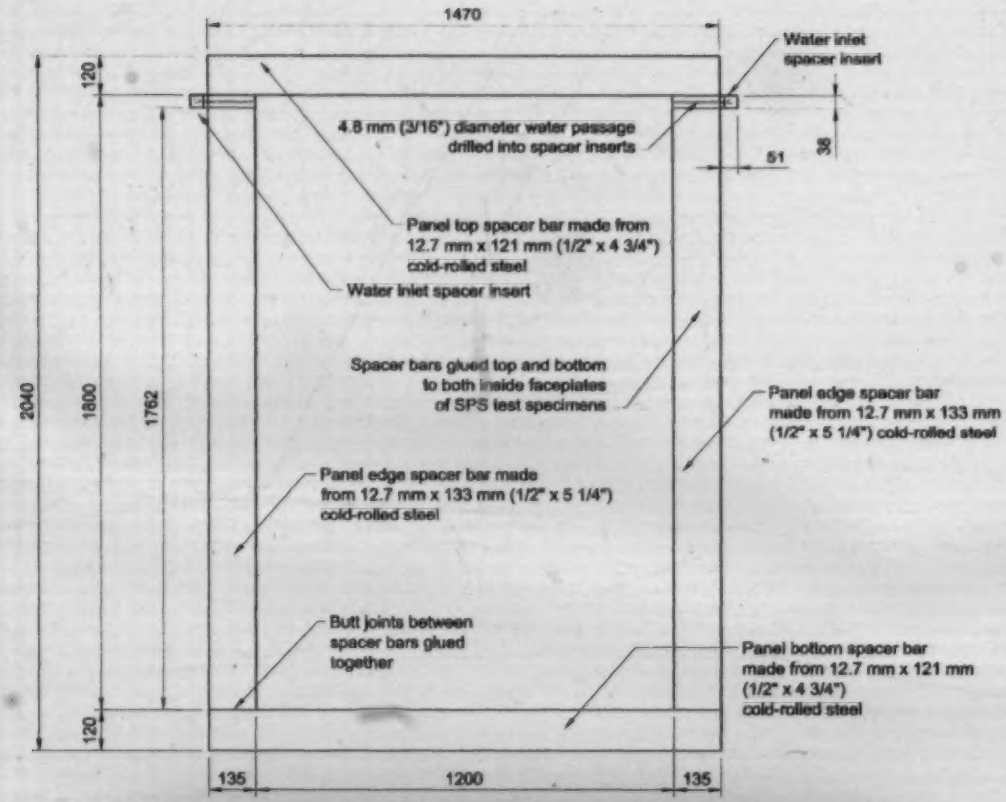
1470
Water inlet spacer insert
120
4.8 mm (3/16") diameter water passage drilled into spacer inserts
51
32
Panel top spacer bar made from 12.7 mm x 121 mm (1/2" x 4 3/4") cold-rolled steel
Water inlet spacer insert
Spacer bars glued top and bottom to both inside faceplates of SPS test specimens
Panel edge spacer bar made from 12.7 mm x 133 mm (1/2" x 5 1/4") cold-rolled steel
2040
1800
1762
Panel edge spacer bar made from 12.7 mm x 133 mm (1/2" x 5 1/4") cold-rolled steel
Butt joints between spacer bars glued together
Panel bottom spacer bar made from 12.7 mm x 121 mm (1/2" x 4 3/4") cold-rolled steel
120
135
1200
135

Figure 3.6: Panel Spacer Bar Layout

Figure 3.7: Spacer Bar Layout

Figure 3.8: Water Inlet Spacer Insert

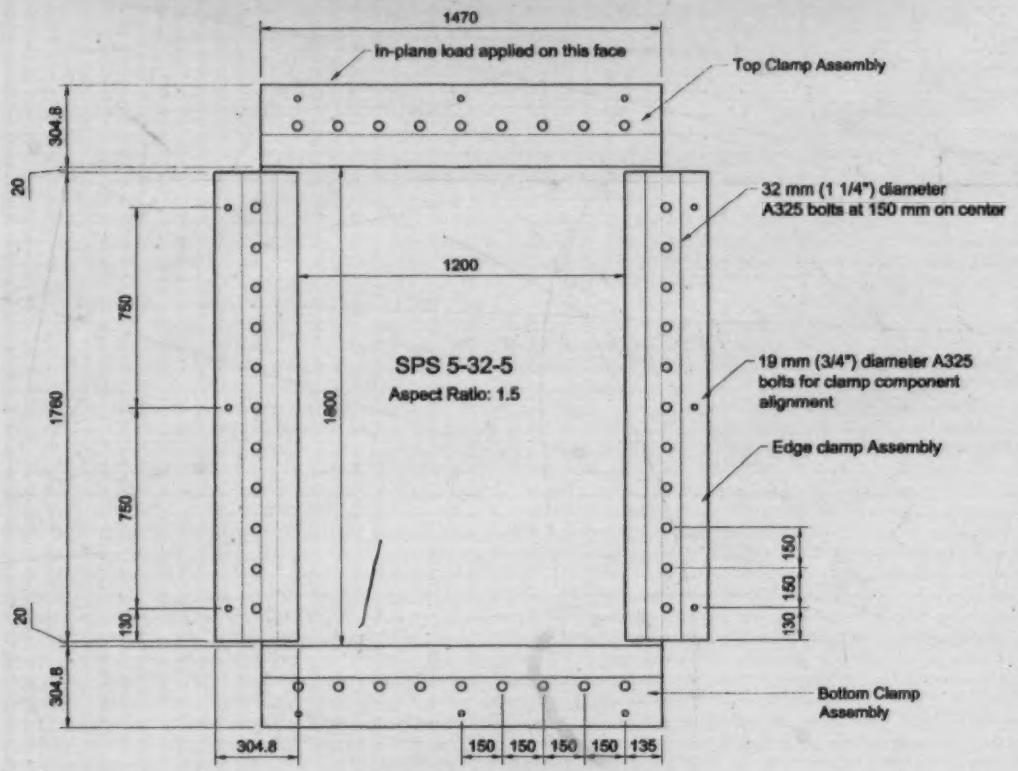

Figure 3.9: Plan View of Test Frame

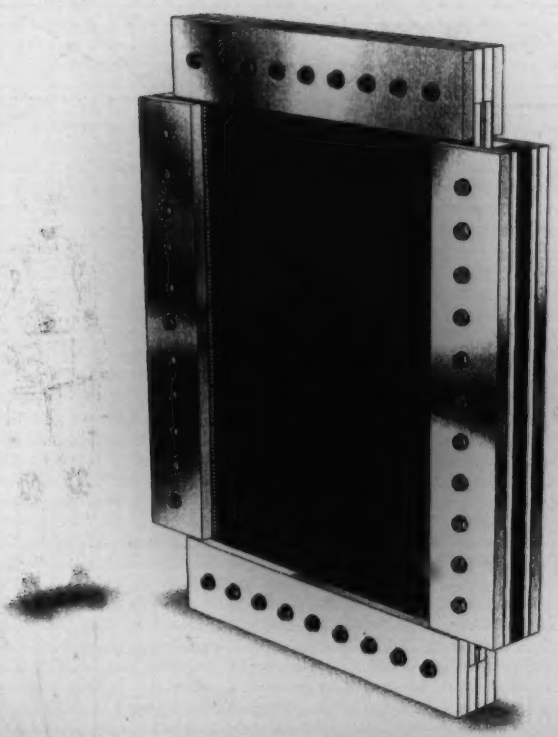

Figure 3.10: Rendered Test Frame

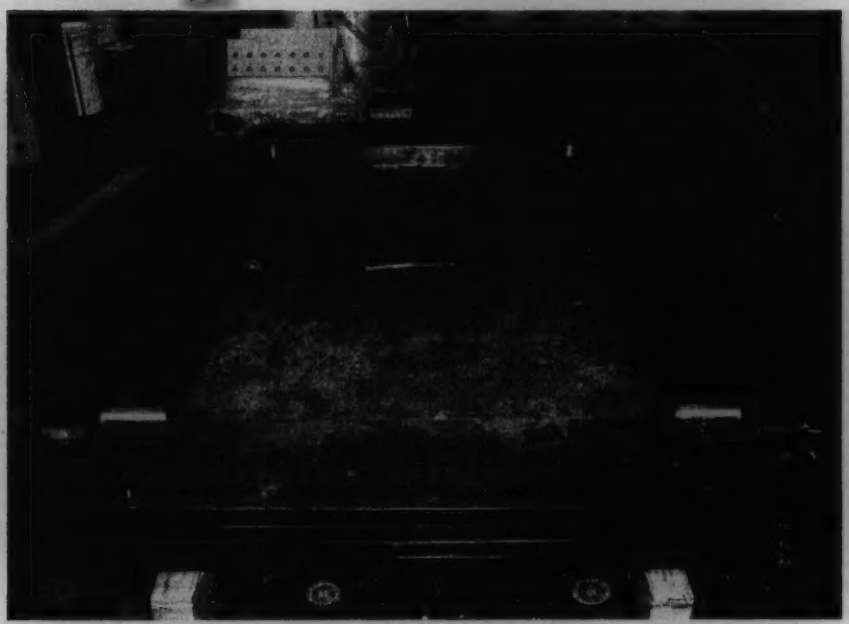

Figure 3.11: Assembled Test Frame

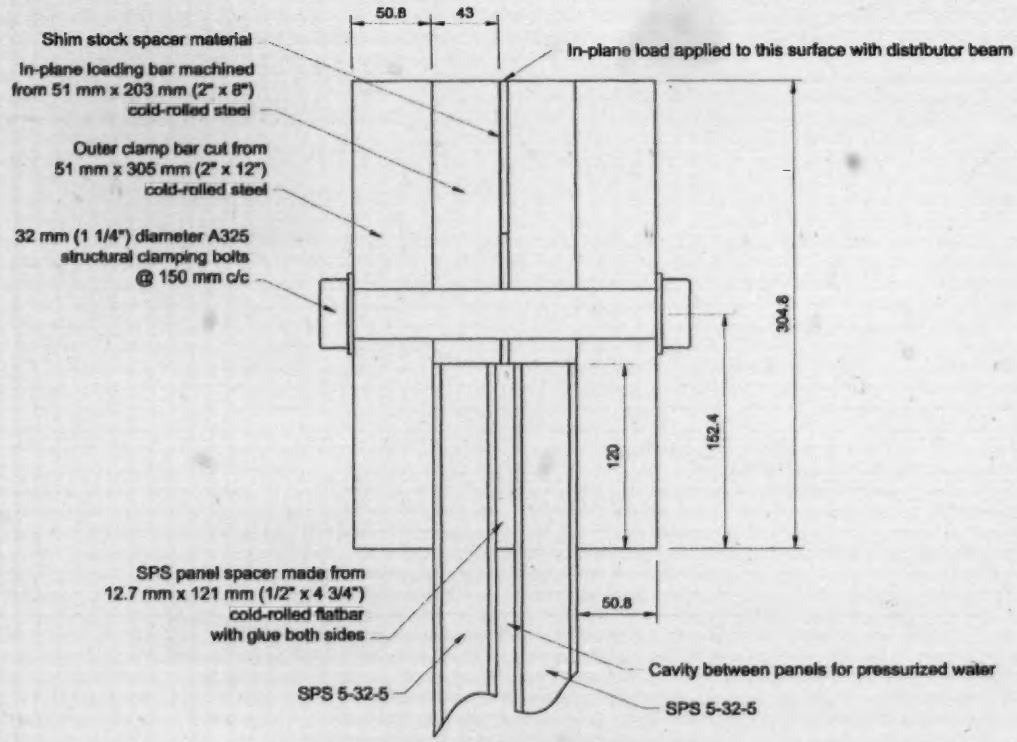
50.8
43
Shim stock spacer material
In-plane loading bar machined from 51 mm x 203 mm (2" x 8") cold-rolled steel
Outer clamp bar cut from 51 mm x 305 mm (2" x 12") cold-rolled steel
32 mm (1 1/4") diameter A325 structural clamping bolts @ 150 mm c/c
In-plane load applied to this surface with distributor beam
304.8
162.4
120
SPS panel spacer made from 12.7 mm x 121 mm (1/2" x 4 3/4") cold-rolled flatbar with glue both sides
50.8
Cavity between panels for pressurized water
SPS 5-32-5
SPS 5-32-5

Figure 3.12: Top Clamp Section

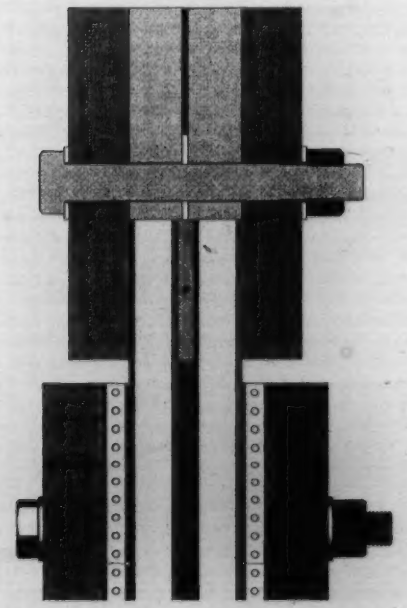

Figure 3.13: Rendered Top Clamp Section

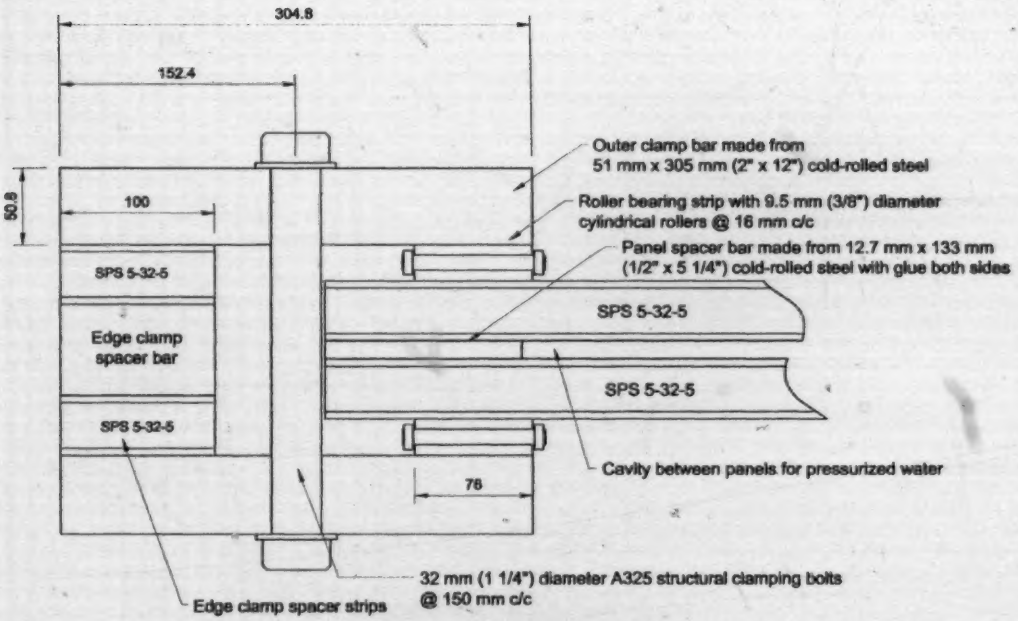
304.8
152.4
50.8
100
SPS 5-32-5
Edge clamp
spacer bar
SPS 5-32-5
Outer clamp bar made from
51 mm x 305 mm (2" x 12") cold-rolled steel
Roller bearing strip with 9.5 mm (3/8") diameter
cylindrical rollers @ 16 mm c/c
Panel spacer bar made from 12.7 mm x 133 mm
(1/2" x 5 1/4") cold-rolled steel with glue both sides
SPS 5-32-5
SPS 5-32-5
Cavity between panels for pressurized water
78
32 mm (1 1/4") diameter A325 structural clamping bolts
@ 150 mm c/c
Edge clamp spacer strips

Figure 3.14: Edge Clamp Section

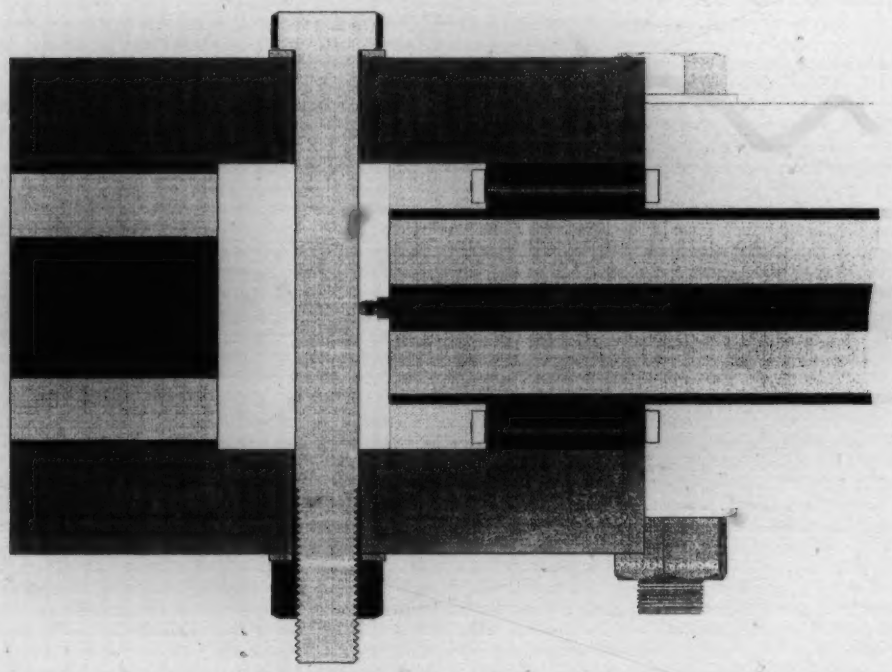

Figure 3.15: Rendered Edge Clamp Section

Figure 3.16: Top and Edge Clamp Sections

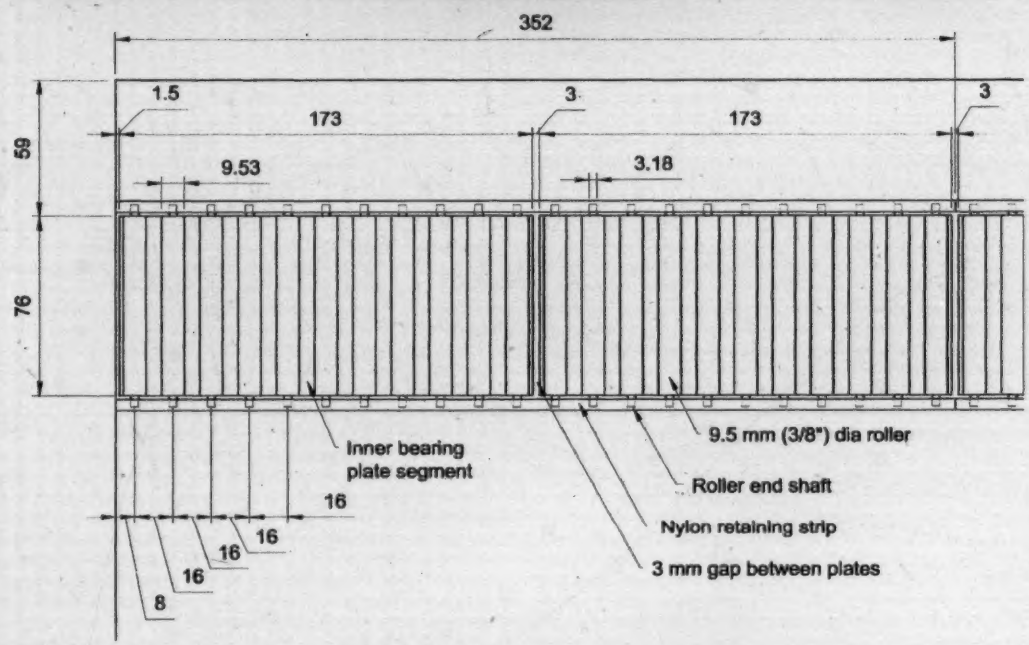

Figure 3.17: Plan View of Portion of Roller Bearing Assembly

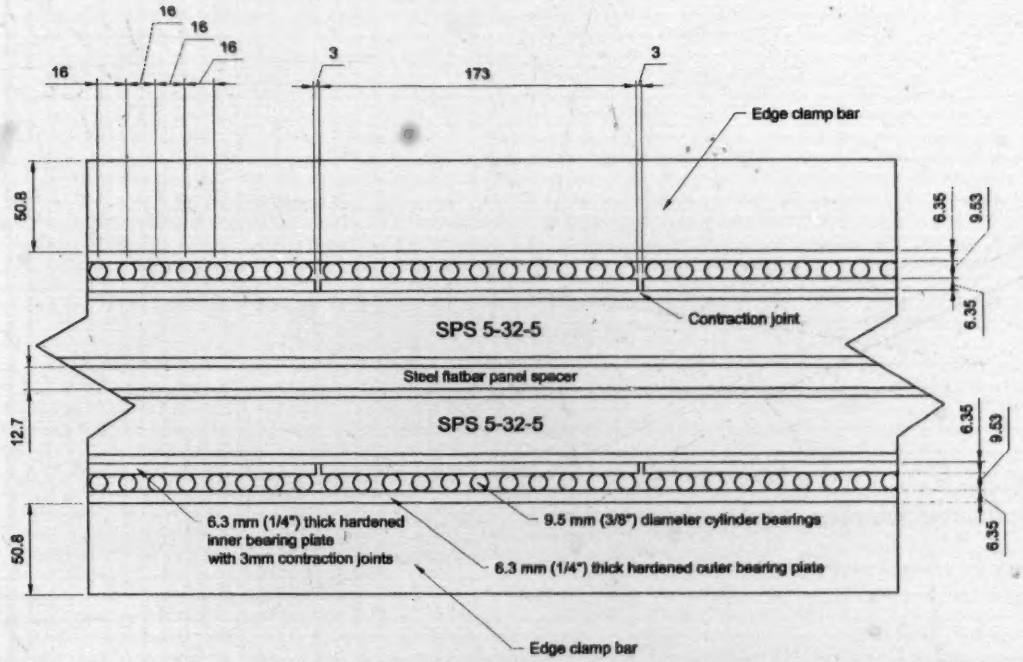

Figure 3.18: Section of Portion of Roller Bearing Assembly

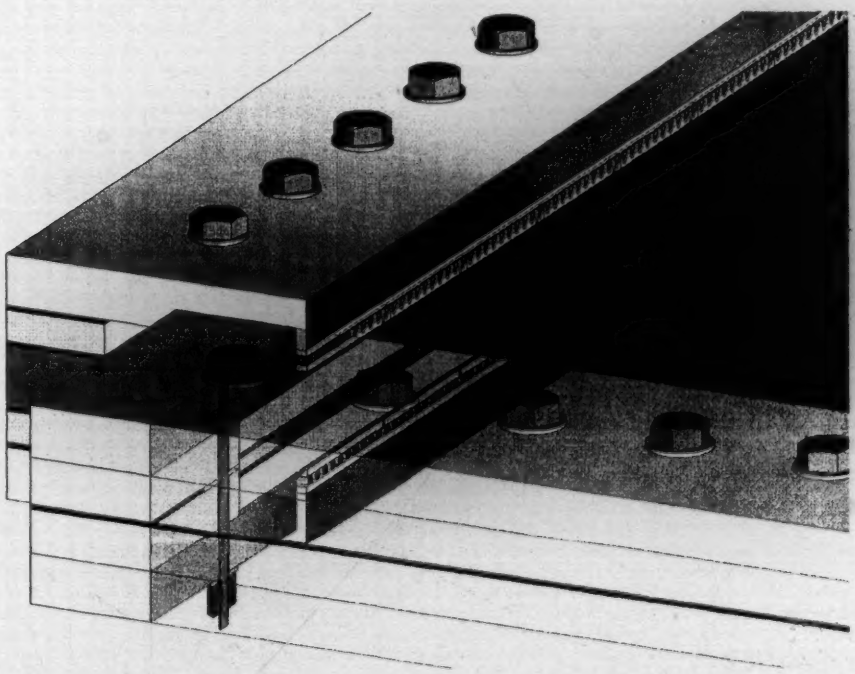

Figure 3.19: Rendered Cutaway View of Portion of Roller Bearing Assembly

Figure 3.20: Roller Strip – Outer Bearing Plates Removed

Figure 3.21:Close-up of Roller Bearing Strip

(a) First SPS Panel with Spacer Bar Components

(b) Three Glue Beads for First Spacer Bar Component (Glue pattern same for all bars)

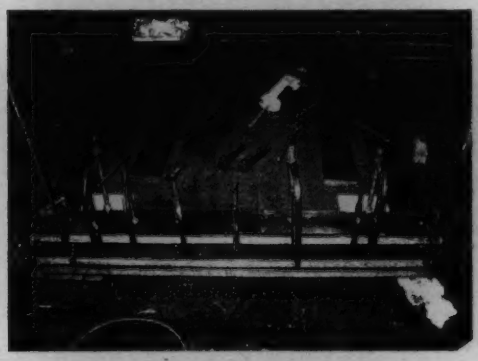

(c) Bottom Spacer Bar Positioned and Clamped with C-clamps

(d) Three Glue Beads for First Edge Spacer Bar Component

(e) First Edge Spacer Bar Positioned and Clamped with C-clamps

(f) Close-up of Typical Water Inlet / Venting Port Insert

Figure 3.22: Specimen Set Assembly

(g) Close-up of Typical Butt Joint Between Top / Bottom and Edge Spacer Bars

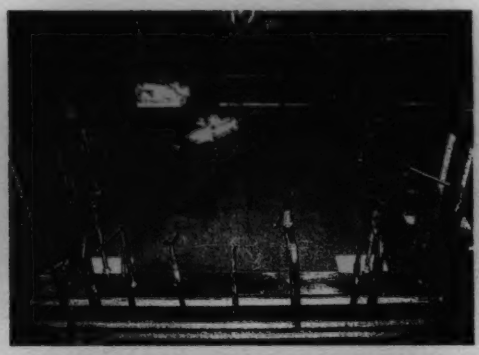

(h) Second Edge Spacer Bar Glued and Clamped in Position Similar to First

(i) Three Glue Beads for Top Spacer Bar Component

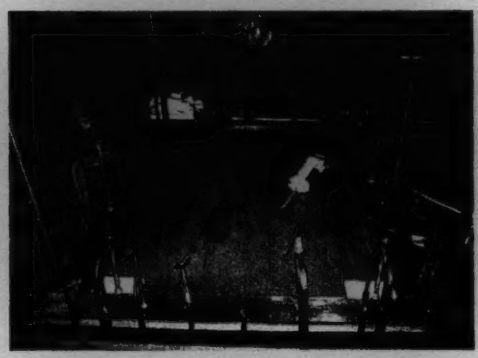

(j) Top Spacer Bar Positioned and Clamped with C-clamps

(k) All C-clamps Removed once Glue Cures – Top Surface of Spacer Bar Sanded and Glued

(l) Second SPS Panel Lowered into Position with Crane and Clamped Until Cure

Figure 3.22: Specimen Set Assembly (Cont'd)

(a) Four Outer Clamp Bars Placed on Wood Assembly Platform

(b) Strip of Outer Bearing Plates and Cylindrical Roller Bearings Placed

(c) Inner Bearing Plates Placed on Each Strip of Roller Bearings

(d) Close-up of a Typical Roller Bearing Strip

(e) SPS Specimen Set (Assembly Sequence Shown in Figure 3.19) Placed on Top and Bottom Clamp Bars and Roller Bearing Strips

(f) In-plane Loading Bars Placed on Top and Bottom Outer Clamp Bars

Figure 3.23: Test Frame Assembly Sequence

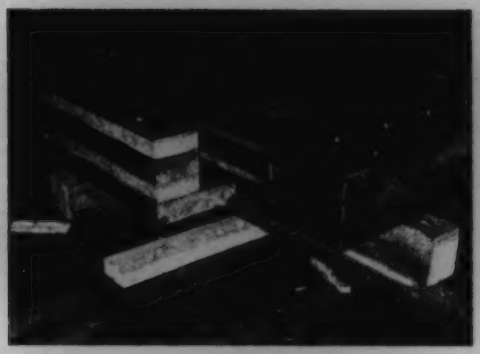

(g) Edge Clamp Spacer Strips (Each with Two SPS 5-32-5 Strips and One Steel bar) Positioned on Outer Edge Clamp Bars

(h) Inner Bearing Plate Strips Positioned on SPS Panel Face

(i) Cylindrical Roller Bearing Strips Placed on Inner Bearing Plates

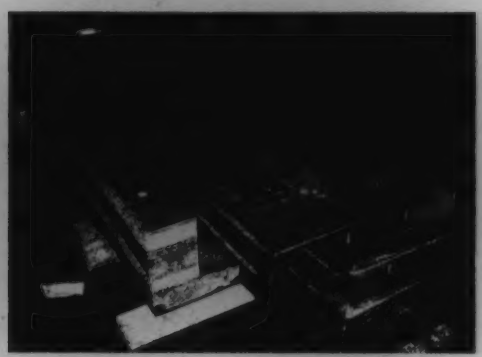

(j) Outer Bearing Plates Placed on Roller Bearing Strips

(k) Four Remaining Outer Clamp Bars Positioned

(l) Rectangular Ring of 1 ¼" Diameter Bolts Inserted and Tightened all Around Frame

Figure 3.23: Test Frame Assembly Sequence (Cont'd)

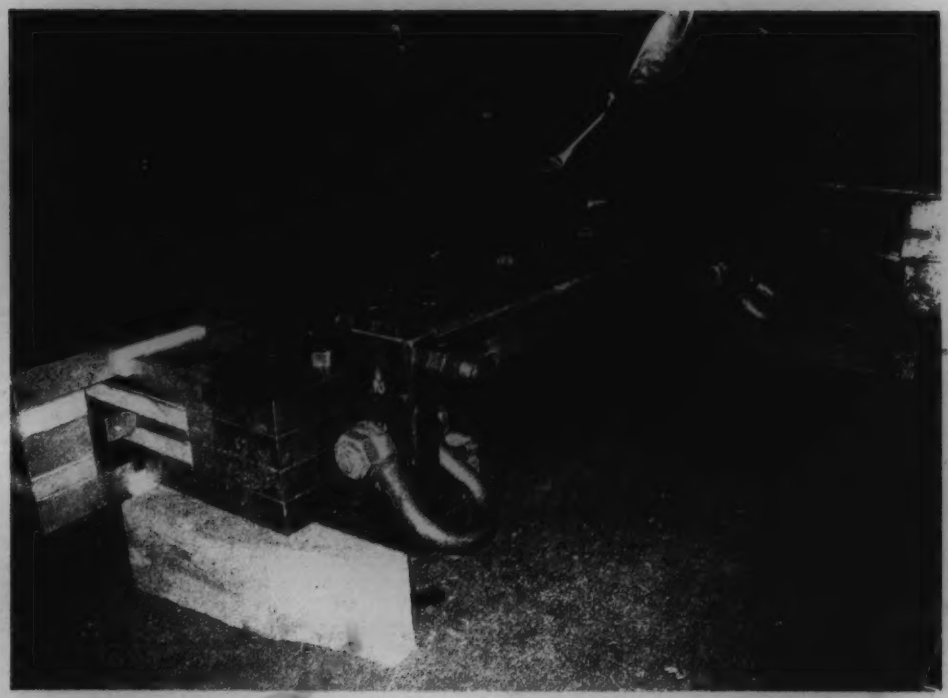

Figure 3.24: Specimen Vertical Lifting Assembly – Top Brackets and Links

Figure 3.25: Specimen Vertical Lifting Assembly – Bottom Brackets and Rods

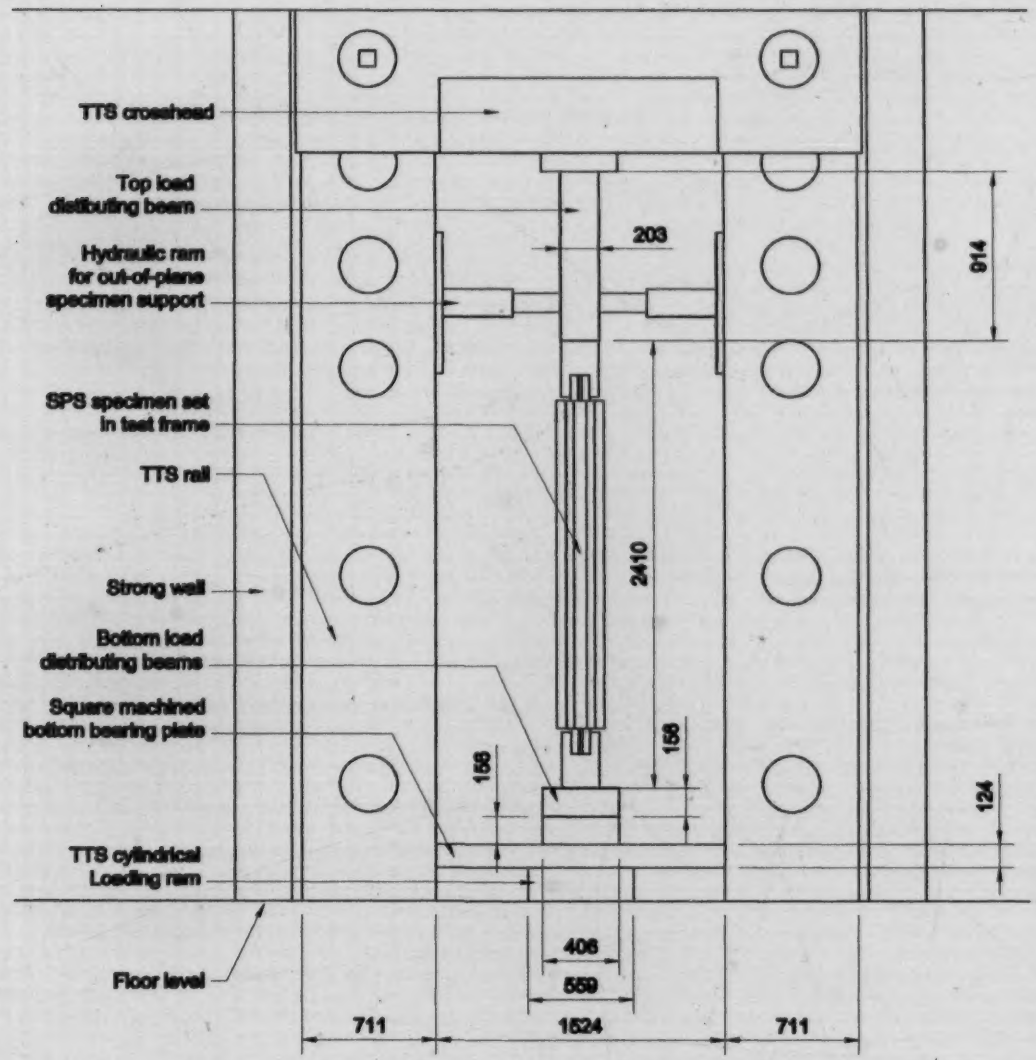

Figure 3.26: Specimen Mounted in the Testing Machine – Front View

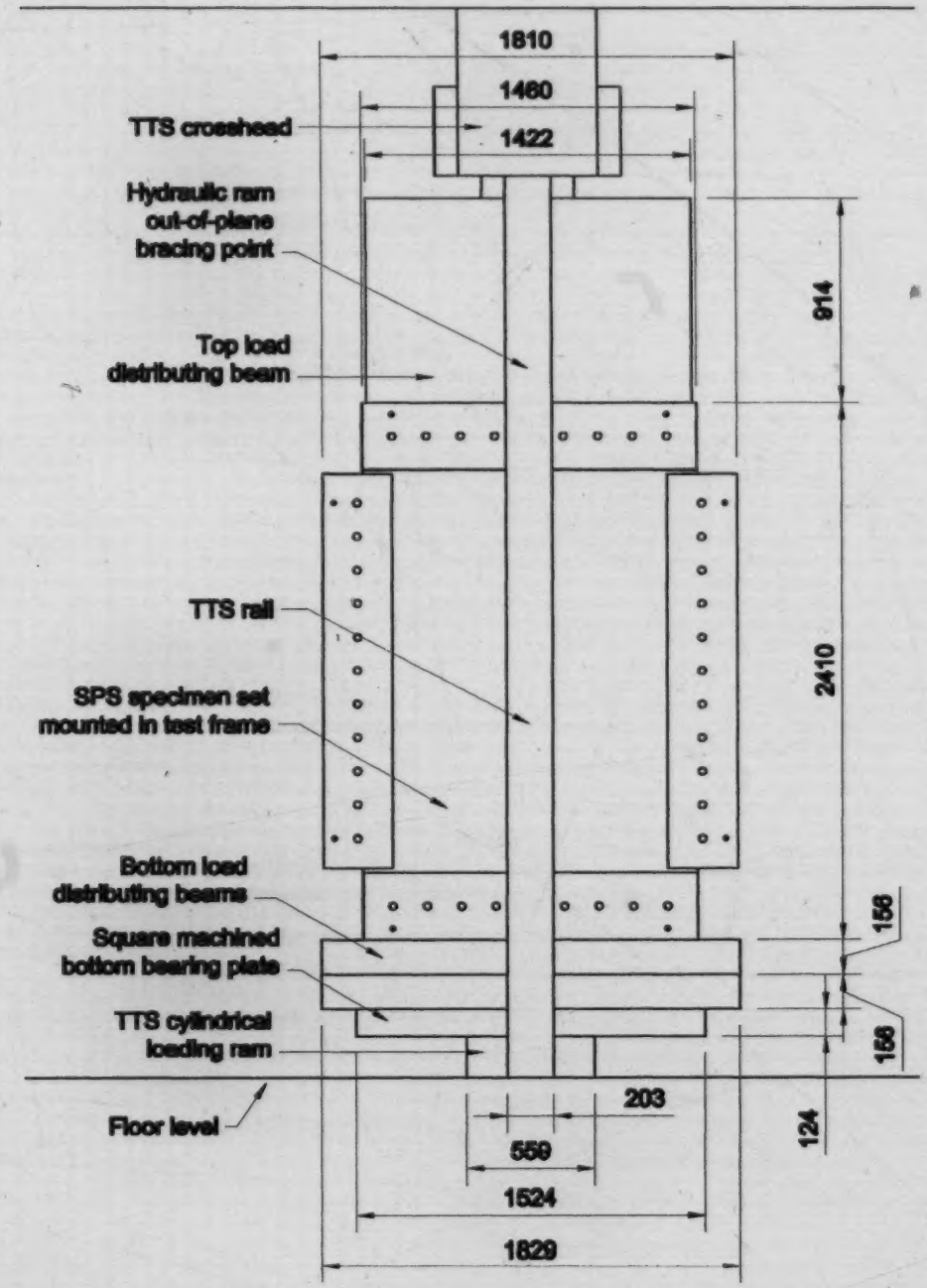

Figure 3.27: Specimen Mounted in the Testing Machine – Side View with Strong Wall Removed for Clarity

Figure 3.28: Specimen Mounted in the Testing Machine – Front View

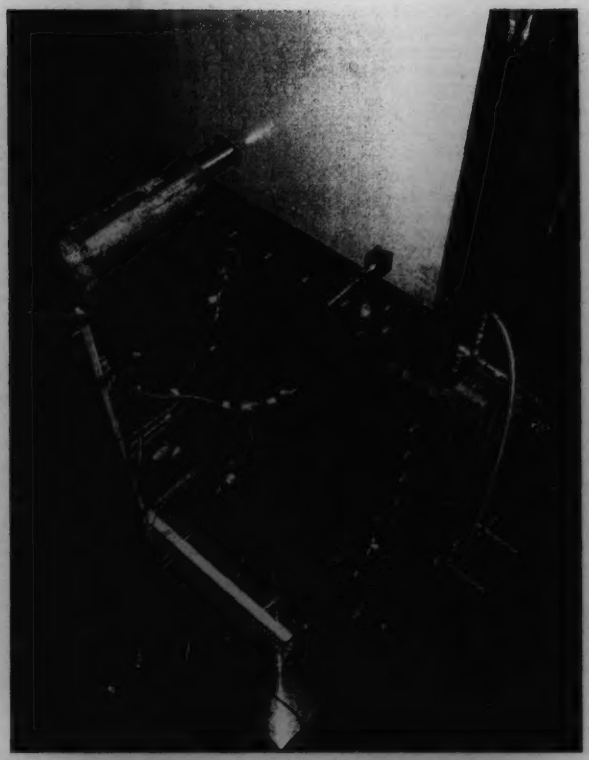

Figure 3.29: Specimen Mounted in the Testing Machine – View from Above

Figure 3.30: Specimen Mounted in the Testing Machine – Bottom Loading Beams

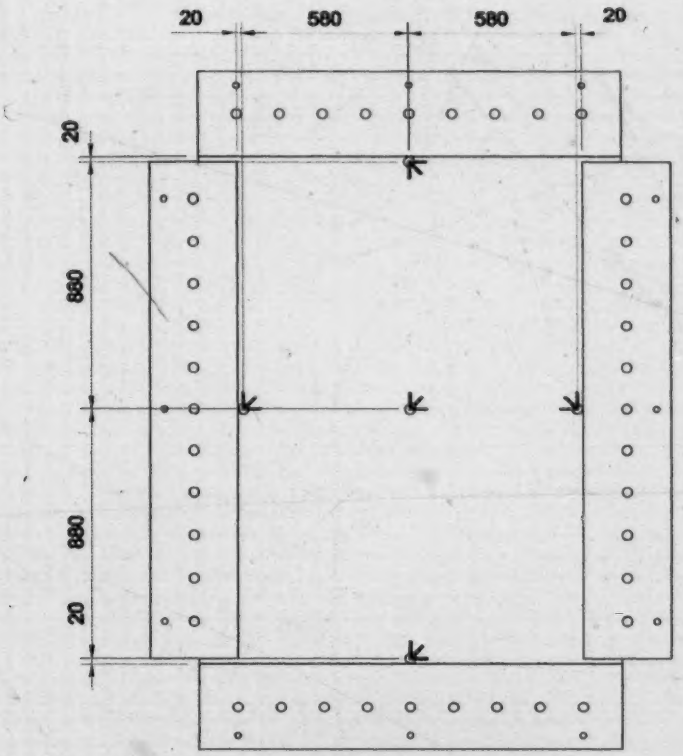

Figure 3.31: Strain Rosette Layout

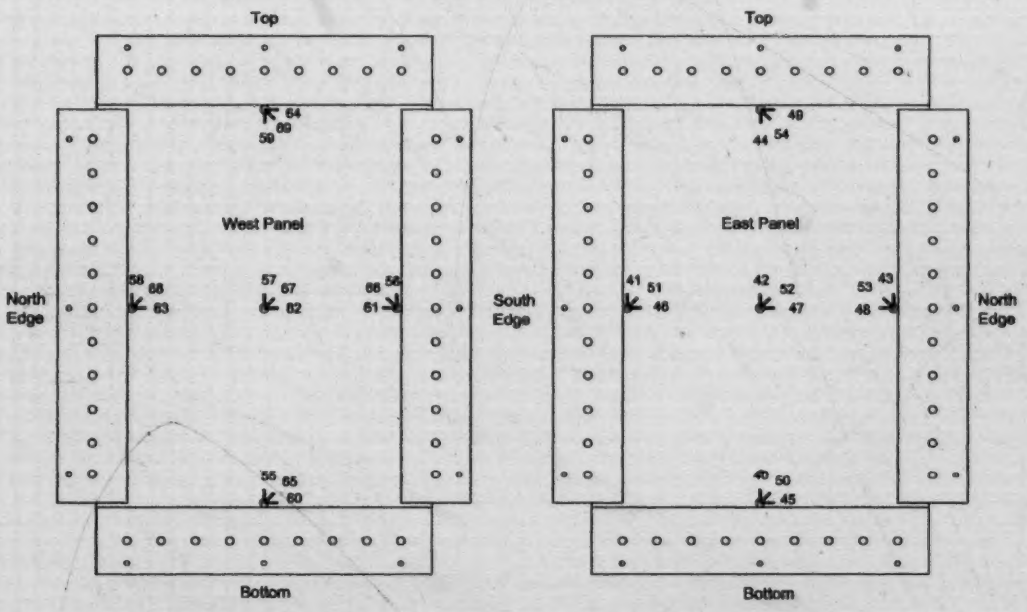

Figure 3.32: Channel Numbers Corresponding to Strain Rosette Components

Figure 3.33: Strain Rosette Locations on One SPS Panel Face

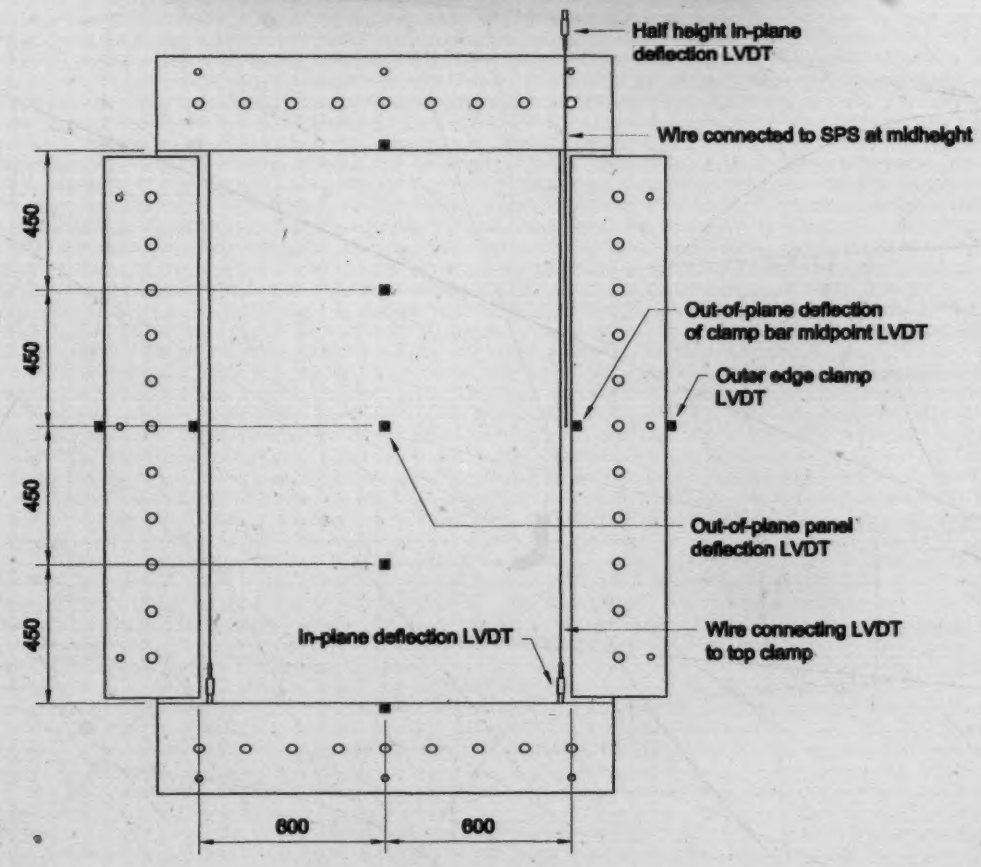

Figure 3.34: LVDT Layout on Specimen Set

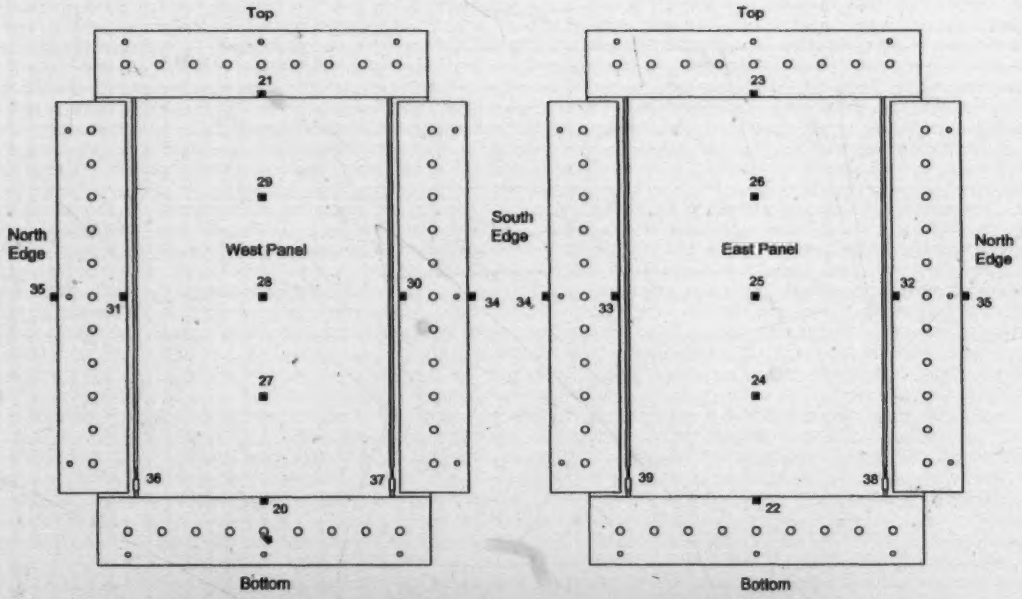

Figure 3.35: Channel Numbers Corresponding to LVDT Positions

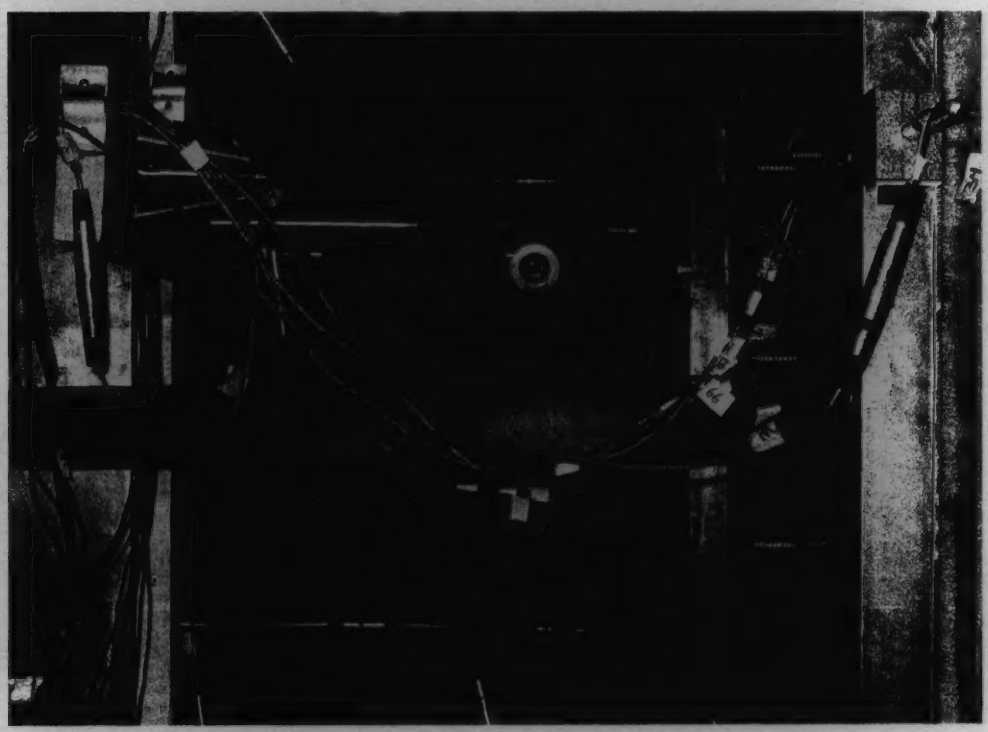

Figure 3.36: Typical Out-of-plane LVDT Setup

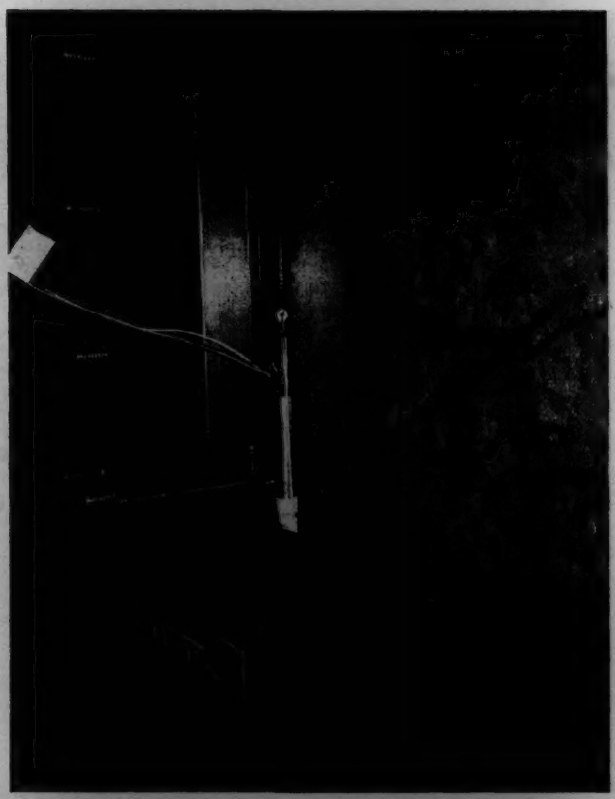

Figure 3.37: Typical In-plane LVDT Setup

Figure 3.38: Typical Outer Edge Clamp LVDT Setup (Channels 34 and 35)

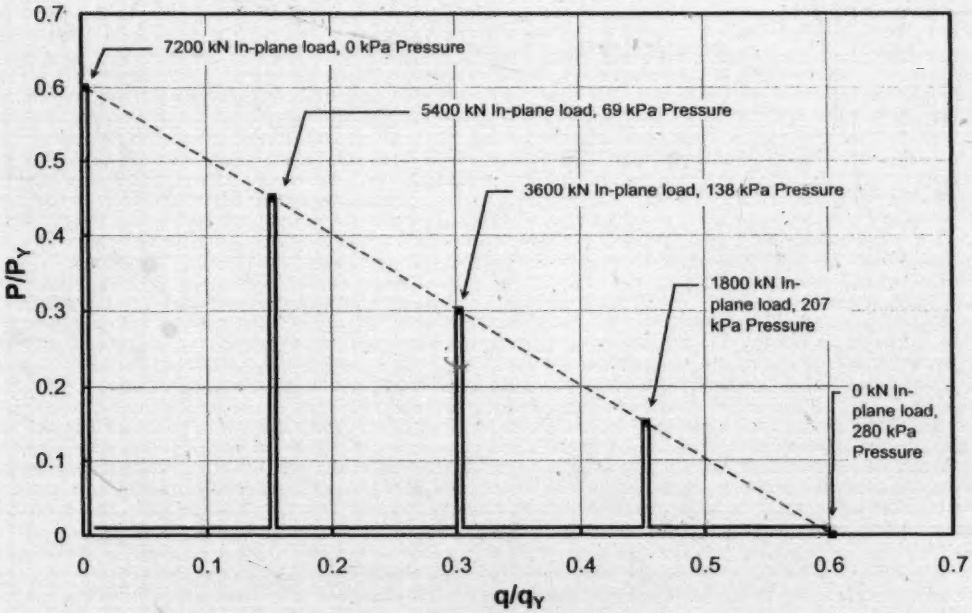

Figure 3.39: Load Combinations Applied to Each Specimen Set in the Elastic Range

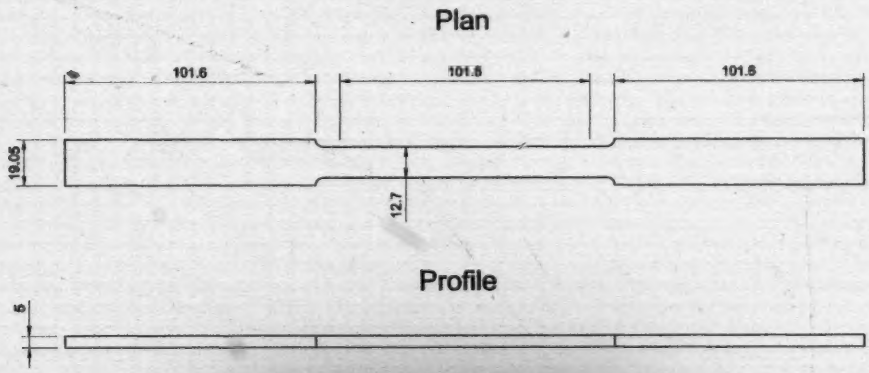

Figure 3.40: Dimensions of Tension Coupon

Figure 3.41: Failed Section of Typical Tension Coupon

4.0 Experimental Results and Analysis

Three SPS specimen sets were tested, with each set loaded in two phases. The first load phase involved loading only in the elastic range, while the second phase involved loading each of the panel sets to the maximum value of in-plane deflection the setup could accommodate, which is referred to as "ultimate". Results from the elastic loading phase will be presented first, followed by results from the ultimate loading phase. Throughout the following Chapters, the specimen sets are numbered in ascending order of the transverse pressure that they were tested at during the ultimate phase of loading. During the ultimate loading phase, SPS-1 was tested at transverse pressure of 207 kPa, SPS-2 at 415 kPa and SPS-3 at 690 kPa of internal pressure.

4.1 Elastic Loading Phase

There were five combinations of in-plane compression and transverse pressure applied to each of the three specimen sets in this phase of the loading procedure. The loading sequence and targeted values used are shown in Figure 3.35. Data generated during this elastic loading phase serves two purposes: 1) a comparison between the three specimen sets since all were subjected to the same loading pattern and values; 2) a comparison with results obtained from a finite element analysis. This section compares the behaviour between the three specimen sets, while the comparison between test results and finite element work is presented in Chapter 5.

The following presents results from each load combination in the order in which the load combinations were applied during the tests.

4.1.1 In-plane Load of 7200 kN and No Lateral Pressure

The first load combination applied consisted of an in-plane force of 7200 kN and no lateral pressure. The vent valve at the water inlet port at the top of the specimen set was left open during the in-plane load application to ensure that the internal pressure remained at zero. Figure 4.1 shows the applied in-plane load versus axial deformation for

each test specimen. On this plot, the value of axial deformation for each test represents the average of the four in-plane LVDT's, channels 36 to 39 shown in Figure 3.35.

Figure 4.1 indicates that SPS-2 had a higher axial stiffness than SPS-1 and SPS-3. The curve for SPS-3 indicates a slight decrease in axial stiffness at an in-plane load level of about 2000 kN, and a 0.1 mm slip in axial displacement at 4800 kN. Table 4.1(a) provides a comparison of the axial deflections of all three specimen sets at 7200 kN of in-plane load. It provides the average and the coefficient of variation (COV) values for each of the three tests as well as for the east panel readings only, west panel readings only and all specimen in-plane deflection readings. SPS-3 had the highest in-plane deflection of 3.2 mm, 11% greater than SPS-1 and 27% greater than SPS-2. Comparing between east and west panels, Table 4.1(a) indicates the west panel average deflection was only 2% greater than the east panel. This suggests that the panels were subjected to the same in-plane deformation, an important requirement for proper test behaviour. The variation in the in-plane deflection data for all tests is represented by the COV for all results of 13%.

Figure 4.2 presents the in-plane load versus average vertical strain in the outer panel faceplates for all three test specimens. This vertical strain value plotted is the average of all the vertical strains recorded with the 10 strain rosettes in the panel set. The vertical strain gauges from the strain rosettes correspond to channels 40-44 and 55-59 shown in Figure 3.32. Figure 4.2 indicates virtually identical average vertical strain behaviour for all three specimen sets as they are loaded to 7200 kN. Table 4.1(b) presents the vertical strain data at the 7200 kN in-plane load level. Average and COV values are presented for the panels' centre readings, the edge readings, the east panel readings, west panel readings and all specimen vertical strain readings. Table 4.1(b) shows that the east and west panels share strain quite equally, with the average west panel vertical strain being only 3% higher than the east panel. Since the two panels also had the same in-plane deformation and all steel plates were from the same heat, this suggests equal load sharing between the panels. The relatively large COV's for the strain data come partly from the variation in strains between the centre portion of the panel and the panel edges. Table 4.1(b) shows that in general the vertical strain in the central region of the panel was 30%

higher than the vertical strains at the panel edges. The central strains were taken as the average of gauge channels 40, 42, 44, 55, 57 and 59 and the edge strains the average of gauge channels 41, 43, 56 and 58, all of which are shown in Figure 3.32.

Figures 4.3 to 4.5 compare the von Mises stresses at three points in the panels, with the von Mises stresses and strains (used in Chapter 5) calculated from the strain rosette data using the following equations (Dally and Riley, 1978). The principal strains are obtained from:

$$\varepsilon_1 = \frac{1}{2}(\varepsilon_A + \varepsilon_C) + \frac{1}{2}\sqrt{(\varepsilon_A - \varepsilon_C)^2 + (2\varepsilon_B - \varepsilon_A - \varepsilon_C)^2} \tag{4.1a}$$

$$\varepsilon_2 = \frac{1}{2}(\varepsilon_A + \varepsilon_C) - \frac{1}{2}\sqrt{(\varepsilon_A - \varepsilon_C)^2 + (2\varepsilon_B - \varepsilon_A - \varepsilon_C)^2}$$

The principal stresses are obtaine from:

$$\sigma_1 = E\left[\frac{(\varepsilon_A + \varepsilon_C)}{2(1-\upsilon)} + \frac{1}{2(1+\upsilon)}\sqrt{(\varepsilon_A - \varepsilon_C)^2 + (2\varepsilon_B - \varepsilon_A - \varepsilon_C)^2}\right] \tag{4.1b}$$

$$\sigma_2 = E\left[\frac{(\varepsilon_A + \varepsilon_C)}{2(1-\upsilon)} - \frac{1}{2(1+\upsilon)}\sqrt{(\varepsilon_A - \varepsilon_C)^2 + (2\varepsilon_B - \varepsilon_A - \varepsilon_C)^2}\right]$$

The von Mises stress is obtained from:

$$\sigma_{VM} = \sqrt{\sigma_1^2 - \sigma_1\sigma_2 + \sigma_2^2} \tag{4.1c}$$

The von Mises equivalent strain is obtained from:

$$\varepsilon_{VM} = \sqrt{\varepsilon_1^2 - \varepsilon_1\varepsilon_2 + \varepsilon_2^2} \tag{4.1d}$$

where,

ε_A = horizontal strain component
ε_B = diagonal (45°) strain component
ε_C = vertical strain component

Figure 4.3 presents the average von Mises stress from the strain rosettes at the top and at the bottom of each panel, corresponding to channels (40,45,50), (44,49,54), (55,60,65) and (59,64,69) as shown on Figure 3.32. Each set of brackets encloses the three channels for each of the four top and bottom rosettes for each panel of a test specimen. Figure 4.4 presents the average von Mises stress for the rosettes mounted along the edge boundaries, namely, channels (41,46,51), (43,48,53), (56,61,66) and (58,63,68) on Figure 3.32. Likewise, Figure 4.5 presents the average von Mises stress for the rosettes at the panels' midpoints and corresponds to channels (42,47,52) and (57,62,67) for the east and west panels, respectively. Symmetry was assumed about a vertical line through the panel mid width and a horizontal line through the panel mid height. Thus for each test, the edge gauge reading used in the plots is the average of all four edge gauges (two gauges on each of the two panels) and the top and bottom gauge reading is the average of the two top and two bottom gauges. Average and COV values are presented in Table 4.1 (c) for the top and bottom von Mises stress readings, edge readings and mid panel readings. All readings were taken at the 7200 kN in-plane load level.

The similarity of behaviour between the three tests is apparent from the von Mises stress plots shown in Figures 4.3 to 4.5. The most variability between tests occurs in the stresses calculated from the panel top and bottom rosettes, the plots of which are shown in Figure 4.3. Table 4.1 (c) reinforces this, as the COV of the top and bottom stress readings is 27%. The COV for the von Mises stresses at the panel edges and midpoints however, is 7% for the edges and 9% for mid panel. This lower level of variability is displayed graphically in Figure 4.4, where the load versus stress plots for the panel edges lie almost on top of one another for all three specimen sets. The same is true for von Mises stress at the panel midpoints, shown in Figure 4.5.

4.1.2 Internal Pressure of 276 kPa and No In-plane Load

The next step in the elastic loading phase involved reducing the 7200 kN in-plane load down to approximately 20 kN, which was enough to retain the specimen in position in the test machine, yet small enough to be considered as zero in-plane load. From here on, this 20 kN retaining load is referred to as the "initial in-plane load point". After in-plane load

was reduced to this initial point, the internal pressure of the specimen was then increased from zero to 40 psi, equivalent to a uniform transverse load of 276 kPa.

A plot of applied pressure versus average mid-panel out-of-plane deflection can be found in Figure 4.6, with the deflection being the average of channels 25 and 28 as shown in Figure 3.35. Similarly, a plot of applied pressure versus panel quarter point out-of-plane deflection can be found in Figure 4.7 with the deflection being the average of channels 24, 26, 27 and 29. This again uses symmetry about the panel mid height so the plotted quarter point deflection for each test is the average of all four quarter point readings taken for that test. The out-of-plane deflection versus transverse pressure behaviour of all three test specimens was very similar, both at the panel midpoints presented in Figure 4.6 and at the panel quarter points, presented in Figure 4.7. Table 4.2 (a) presents the average out-of-plane deflections at 276 kPa of transverse pressure. The average deflection of the panel midpoint at this pressure was 35% greater than the panel quarter point. The similarity of the plotted values is reflected in the low COV of the deflection data: a variation of only 4% in the panel midpoint readings and also 4% in the quarter point readings.

Plots of applied pressure versus average von Mises stresses are found in Figure 4.8 for the panel tops and bottoms, Figure 4.9 for the panel edges and Figure 4.10 for the panel midpoints. The von Mises stresses for the top and bottom points are calculated from the average of the strain rosette data from channels (40,45,50), (44,49,54), (55,60,65) and (59,64,69) on Figure 3.32. The von Mises stresses for the edge points are calculated from the average of the strain rosette data from channels (41,46,51), (43,48,53), (56,61,66) and (58,63,68). Likewise, the von Mises stresses for the panel midpoints are calculated from the average of the strain rosette data from channels (42,47,52) and (57,62,67). All Von Mises stresses are calculated from the strain rosette data using equation set 4.1 presented in the previous section.

Figure 4.8 indicates that the response of the von Mises stresses at the panel top and bottom to the application of transverse pressure for SPS-2 and SPS-3 were very similar.

The plot of SPS-1 however, has a steeper slope which translates into about 20% less top and bottom stress than in SPS-2 and SPS-3 at 276 kPa of transverse pressure. Stress at the panel edges, presented in Figure 4.9, is in general the highest in SPS-1 at any given pressure level. The curve for SPS-3 parallels that of SPS-1 and SPS-2 up until about 100 kPa of pressure. Beyond this, SPS-3 has a continually increasing slope such that at 276 kPa of lateral pressure, the average von Mises stress in the edges of SPS-3 is 30% less than in SPS-1. Mid panel von Mises stress behaviour is plotted in Figure 4.10, and is very similar for SPS-1 and SPS-3. Mid panel stresses in SPS-2 do not initially increase as quickly as in the other 2 specimen sets, however beyond a pressure level of 150 kPa, the slopes of all three specimens' curves are the virtually identical. Average stresses at mid panel of SPS-2 are about 15% lower than in SPS-1 and SPS-3 at 276 kPa of lateral pressure.

Table 4.2 (b) provides a summary of the average von Mises stress values at the panel tops and bottoms, edges and midpoints at 276 kPa of lateral pressure. The variation seen in the plots of Figures 4.8 to 4.10 is reflected in the relatively high COV values of the data collected. The COV is 20% for the top and bottom data points, 31% for the edge data points and 16% for the mid panel data points.

4.1.3 Intermediate Load Combinations: Load Case 1: (207 kPa, 1800 kN); Load Case 2: (138 kPa, 3600 kN); Load Case 3: (69 kPa, 5400 kN)

In this final portion of the elastic loading phase, pressure was reduced from 276 kPa to 207 kPa (30 psi) and held constant at this value while in-plane load was taken from the initial point to 1800 kN. This was the first intermediate load combination referred to as intermediate load case 1. Pressure was then reduced to 138 kPa (20 psi) and held while in-plane load was increased to 3600 kN, producing the second intermediate load combination: intermediate load case 2. Finally, pressure was further reduced to 69 kPa (10 psi) and held constant while the in-plane load was taken to 5400 kN. This was intermediate load case 3, the third and final intermediate elastic load combination.

Figure 4.11 presents a plot of applied in-plane load versus average vertical panel deflection as measured by the in-plane LVDT's for the entire range of intermediate load combinations. The LVDT's used are shown in Figure 3.35 as channels 36, 37, 38 and 39. In-plane loading of the test specimen starts at the far left, where pressure is at 207 kPa, and progresses to the right. As the in-plane load increases, SPS-3 exhibits a slight change in stiffness much like it did under axial load only as presented in Section 4.1.1. Here the change appears to occur at about 2400 kN of in-plane load. At all three intermediate load combinations, the lateral pressure changes have virtually no effect on the in-plane displacement of the panel.

Table 4.3 (a) summarizes the in-plane deflections at all three intermediate load combinations. The relative variation in the deflection data decreases as the in-plane load level increases. The COV of the deflection data at 1800 kN of in-plane load is 45%. It decreases to 24% at 3600 kN and further decreases to 15% at 5400 kN. Recall from Section 4.1.1 that the COV was 13% at 7200 kN of in-plane load. This suggests that panel in-plane deflection values are susceptible to small initial movements that are the result of seating of the panels in the test frame under relatively low loads. These small seating deflection values become less significant as the values of panel in-plane deflection due to loading become larger.

Figure 4.12 presents a plot of in-plane load versus average out-of-plane deflection of the panel midpoints for the entire range of intermediate load combinations for each of the three tests. Likewise, Figure 4.13 shows a plot of in-plane load versus average out-of-plane deflection of the panel quarter points for all intermediate load combinations. The average of the readings from LVDT's on channels 25 and 28 (shown in Figure 3.35) were used for mid panel deflection and from channels 24, 26, 27 and 29 for the quarter point deflections. The loading sequence starts at the far right end, where pressure is at 276 kPa and in-plane load is at the initial point of 20 kN. Regions of change in pressure are as shown in the plot.

Although the exact out-of-plane displacement values varied slightly from test to test at each load combination, the load versus deflection trend of all three tests was the same both for the panel midpoint deflections presented in Figure 4.12 and the panel quarter point deflections presented in Figure 4.13. Out-of-plane displacement was a maximum at 276 kPa, and decreased in every case as the pressure was reduced. As in-plane load was applied from the zero level to 1800 kN, there was very little response in the out-of-plane deflections aside from a small dip as the load started to build. On the other hand, at in-plane load from 1800 kN to 3600 kN and again from 3600 kN to 5400 kN, increasing in-plane load levels caused corresponding small decreases in the out-of-plane displacements.

Table 4.3 (b) presents the out-of-plane deflections for all three intermediate load combinations. Much like with the in-plane deflections, the variation in the out-of-plane deflection data decreases as the lateral pressure increases. The COV of the deflection data at 69 kPa of pressure is 35% for mid panel and 41% at the quarter point. It decreases to 15% and 18% for the mid and quarter points respectively at 138 kPa, and further decreases to 10% and 11% at 207 kPa. Recall from Section 4.1.2 that the COV was only 4% for both mid panel and quarter panel points at 276 kPa of lateral pressure. This suggests that panel out-of-plane deflection values are also susceptible to small initial movements that are the result of seating of the panels in the test frame under relatively low pressures. These small seating deflection values become less significant as the values of panel out-of-plane deflection due to pressure become larger.

Plots of applied in-plane load versus von Mises stresses at various locations are presented in Figures 4.14 to 4.16. Each plot shows all three intermediate load combinations and provides data from each of the three tests. Figure 4.14 plots top and bottom von Mises stresses, calculated from the average of the strain rosette data from channels (40,45,50), (44,49,54), (55,60,65) and (59,64,69) on Figure 3.32. Figure 4.15 plots edge von Mises stresses, calculated from the average of the strain rosette data from channels (41,46,51), (43,48,53), (56,61,66) and (58,63,68) on Figure 3.32. Finally, Figure 4.16 is a plot of mid panel von Mises stresses, calculated from the average of the strain rosette data from

channels (42,47,52) and (57,62,67). All of the von Mises stress values were calculated from the strain rosette data using equation set 4.1 presented in the previous section. Regions of pressure change for all plots are again as shown on the Figures, and the loading sequence begins at the very bottom on the right where the pressure is at 276 kPa and in-plane load is at the initial point of 20 kN.

Much like the out-of-plane deflections, the exact values of von Mises stress at each load combination varied from test to test, but the general behaviour of all tests was very similar. Figure 4.14 plots in-plane load versus average von Mises stresses at the panel top and bottom points. Starting at 276 kPa, each of the three 69 kPa decreases in lateral pressure shown on Figure 4.14 caused a corresponding decrease in the von Mises stress level of roughly 30 MPa. Increasing in-plane load caused a corresponding increase in the stress level in a relatively linear fashion.

Figure 4.15 plots average von Mises stresses at the panel edges. In this case, at no in-plane load the initial pressure decrease from 276 kPa down to 207 kPa caused a corresponding decrease in stress of 18 to 25 MPa depending on the specimen. At 1800 kN of in-plane load the pressure decrease from 207 kPa to 138 kPa caused a corresponding stress decrease of between 10 to 18 MPa depending on the specimen, and the further pressure decrease from 138 kPa to 69 kPa at 3600 kN of in-plane load caused a stress decrease of only about 5 MPa for SPS-1 and 1.5 MPa for SPS-3. Thus as the in-plane load level increased, the effect of the pressure change on the edge stress became less significant. Increasing in-plane load on the other hand, had a more significant effect on edge panel von Mises stress at higher levels of in-plane load. In general, a given increment of in-plane load applied when the in-plane load was already at a high level produced a greater increase in stress than the same in-plane load increment applied when the in-plane load was at a lower level. This same behaviour is apparent for von Mises stress at the panel midpoint, plotted in Figure 4.16.

Table 4.3 (c) provides a summary of the values of von Mises stress at each of the three intermediate load combinations for the panel top and bottom, edge and midpoints. The

variation in the data for the top and bottom stress is fairly constant, with a COV of 18% for intermediate load case 1, 18% for load case 2 and 21% for load case 3. The variation in the data for the edge panel stress decreases as the pressure level drops and the values of in-plane load increase. At intermediate load case 1, the COV for the edge stress data is 33%. The COV for load case 2 is 15% and for load case 3 is 7%. The stress at the panel midpoint follows the same trend with COV values of 10%, 4% and 3% for load case 1, 2 and 3 respectively. This compares well with the variation seen in the load versus strain curves of Figures 4.14 to 4.16. The variation between tests stays relatively constant for the panel top and bottom von Mises stress. On the other hand, the variation for the panel edge and midpoint stress is relatively large at high pressures and low in-plane load, and becomes smaller as the pressure is reduced and the in-plane load increased.

4.2 Loading to Ultimate Panel Failure

In this portion of the test program, each of the three SPS panel specimen sets was taken to ultimate at a different combination of transverse pressure and in-plane compression. Each test began by increasing the internal pressure from zero to the predetermined level, with in-plane load held at the initial point, previously defined as approximately 20 kN. Once the test pressure was reached, it was maintained at this level while in-plane loading was increased until specimen failure. Internal pressure had to be controlled manually, so fluctuations about the specified value did occur throughout the in-plane loading phase, but were always well within +/- 5% of the specified pressure value. The following is an overview of the test setup and procedure for each of the three specimen sets, SPS-1, SPS-2 and SPS-3, after which is a presentation and analysis of the results.

4.2.1 SPS-2: 415 kPa Internal Pressure

This first specimen set to be tested, SPS-2, was initially going to be tested with an internal pressure of 500 kPa (72.5 psi). Unfortunately, problems developed with the glue seal between the inside face of the SPS panels and the steel panel spacer bar. The loading of the panel set began with the application of the internal water pressure. As the pressure was increased, several small leaks began to develop at about 300 kPa. Fortunately, these leaks were small enough that the water pump was able to maintain the pressure. At this

point, the bolts on the frame in the vicinity of the leaks were further tightened, and it was decided that the pressure would be increased to a level as close as possible to the target 500 kPa. At about 415 kPa (60 psi), it was evident that the water loss from the specimen set was increasing. The pressure was therefore held at this level, and the in-plane loading begun.

Based on visual observations, the panel leaking was relatively constant as the in-plane load increased to about 10 MN. At this point, it was evident from the load versus axial displacement curve that the panel set was beginning to lose axial stiffness. From about 10 MN to 12 MN, the leaking increased as the panel set deformed noticeably. As the load increased above 12 MN, panel deformations became more pronounced and both axial and out-of-plane deflections increased rapidly with relatively small load increases. Beyond the 13 MN point, the pump had to work at full speed to maintain the pressure, and at roughly 13.4 MN it became impossible to maintain the target internal pressure. The test was therefore stopped even though the test specimen had not yet reached its peak capacity.

During the assembly of specimen SPS-2 into the test frame, the bolts on the frame were tightened by hand to a torque of 1000 ft-lb using a torque wrench and a torque multiplier with a 4:1 ratio. This torque level equated to roughly 200 kN of pretension per bolt, the maximum that could be applied with the hand tools available. It was evident from the leaking during testing that if possible, more initial preload was required in the frame bolts.

4.2.2 SPS-1: 207 kPa Internal Pressure

Based on the outcome of the test on SPS-2, it was apparent that the glue seals were not as strong as initially anticipated and it was decided that the test frame bolts on the second and third specimen sets would be tightened to a higher pretension value than those on the first specimen. For SPS-1 and SPS-3, an air-powered impact wrench was used, capable of applying up to 3000 ft-lbs of torque. The amount of pretension in the bolts was controlled and monitored by correlating the applied torque to the amount of turn the nut underwent

during tightening. For SPS-1, the 1000 ft-lbs of initial torque applied with hand tools equated to approximately 1/2 turn past the snug tight position. Snug tight was defined as the point where all bolts in the frame were manually tightened with a wrench to remove all "slack" present between the various layers of SPS, spacers, steel plates, roller bearings and shims. Using the impact wrench, all bolts on SPS-1 and SPS-3 were tightened an additional 1/4 to 1/3 turn past the 1000 ft-lb point, for a total of 3/4 turn per bolt past the snug tight position.

An initial low pressure leak test of SPS-1 prior to mounting the test specimen in the test frame revealed a leak in the adhesive seal along one edge. The leak was located at the butt joint between one of the water inlet spacer inserts and the adjacent edge spacer bar. Unfortunately, during the leak test, the initial leak in the seal propagated into a crack in the adhesive down the edge of the specimen set. To fix the initial leak point, the butt joint was drilled out with a 1/8 in. diameter drill bit at the point of leakage, and Plexus MA560-1 adhesive was injected into the hole. The edge crack was repaired by injecting more adhesive along the entire edge where the panel had separated from the panel spacer bar, and was then clamped in a manner similar to that used in the initial panel assembly phase.

Because of the uncertainty surrounding the success of the leak repair, it was decided that SPS-1 would be tested at 207 kPa, the lowest of the three values of internal pressure. Loading proceeded in exactly the same manner as for SPS-2, with the internal pressure taken to 207 kPa, and then the in-plane load increased from the zero point up to failure. Throughout the entire test, leaking from the specimen was virtually nonexistent. This confirmed that the leak repair had been successful and that the combination of lower pressure and extra clamping force from the increased bolt preload had indeed caused a significant improvement in the seal performance.

The ultimate failure point of the panel set, defined as the peak of the in-plane load versus axial displacement curve, was not actually reached during this test. The test was stopped

at an axial deformation of 40 mm, the limit of the restraining frame. Beyond this point, the load started to be carried by the restraining frame rather than by the test specimen.

4.2.3 SPS-3: 690 kPa Internal Pressure

Specimen SPS-3 was tested at an internal pressure of 690 kPa (100 psi). Even though it appeared from the test on SPS-1 that the extra bolt pretension helped solve the leak problem, it was still decided that additional measures should be taken. These additional measures consisted of welding of the specimen corners, sealing the top and bottom of the panel set by placing gasket material between the in-plane loading bars and the SPS/spacer bar, and fastening gasket material and a steel backing strip to the two vertical panel edges. These measures are explained in more detail in the text and photos that follow.

The joints between the panel spacer bar and the inside faceplate of each SPS panel were welded from each corner point to approximately 50 mm away from the corner point in each direction. The exception was the vertical leg of the two top corners, which were welded all the way down to and around the water inlet spacer inserts. Figure 4.17 shows a bottom corner weld and Figure 4.18 shows a top corner weld. All welds were done using a TIG welder with filler metal. The heat generated caused localized vaporization of the elastomer in the steel-elastomer contact regions. It was concluded however, that the effects of this on panel performance were negligible, since the de-bonding was present only in the corners of the panel, which were embedded deep within the clamps and well away from the actual test portion of the specimen.

To provide an additional water seal to the top and bottom edges of the specimen set, a 1.6 mm thick nylon reinforced neoprene rubber gasket was used. This gasket was placed over the full width of the test specimen at the top and bottom edges and covered the entire width of the panel set cross-section. It was sandwiched in place by the in-plane loading bars on the specimen top and bottom, providing a face seal on the joints between the SPS inside faceplates and panel spacer bar. Figure 4.19 shows the position of this gasket material. To reinforce the water seals on the vertical panel edges, a 3 mm thick by 50 mm wide strip of neoprene rubber was again used as a face seal to cover the joins

between the SPS inside faceplates and panel spacer bar. This makeshift gasket was held in place using a 6 mm thick by 32 mm wide steel strip that was tapped and screwed at 150 mm o/c to the edge panel spacer bars up each edge of the specimen set. Figure 4.20 is a photo of a portion of one of these edge gasket assemblies.

As a result of these seal add-ons, the SPS-3 specimen set ended up with slightly larger nominal panel dimensions between the clamps than the first two sets. The edge clamps had to be moved outward from the panel centerline by about 6 mm on each side to allow the structural bolts to clear the additional edge gaskets and bars, and the overall panel height between the top and bottom clamps increased by roughly 3 mm as a result of the additional gaskets between the specimen and the in-plane loading bars. Prior to loading, the steel strips used to fasten the edge gaskets were vertically supported from their bottom face down to the distributing beam at the base of the specimen using steel blocks with a roughly 25 mm x 75 mm cross section. These are shown in the photo in Figure 4.21. These blocks were to prevent the screws in the edge strips from shearing off as the specimen set compressed vertically under the in-plane load. It forced the strips to compress by the same overall amount as the specimen by pinning them between the underside of the water inlets and the bottom distributing beam.

The loading procedure for SPS-3 was very similar to that used for the first two specimens. The lateral pressure was applied first, with the initial in-plane load point of roughly 20 kN held constant until the pressure reached about 300 kPa. At this point the in-plane load was increased to about 150 kN in an attempt to seat the extra top and bottom nylon reinforced rubber gaskets by compressing the in-plane loading bars against them. Pressure was then steadily increased up until the 690 kPa test level, with no sign of water leaks. After a brief visual inspection of the specimen, in-plane loading began at a loading rate of 1 mm/min. In a manner very similar to SPS-2, the in-plane loading had to be stopped prior to the specimen reaching ultimate load carrying capacity. The test frame again ran out of axial displacement and in addition, out-of-plane displacement of the panel mid points was so large that the LVDT's at these points had exceeded their 76 mm travel range and were no longer taking accurate readings.

Test specimen SPS-3 showed virtually no leaks throughout the entire loading range aside from a slight dampness that was present around the base of the test frame at the end of the test. The much-improved leak resistance was attributed mainly to the higher clamping force, as the steel strips holding the extra edge gaskets had buckled under the in-plane deformation. This buckling fractured some of the screw heads and left portions of the rubber strips uncompressed against the joins between the SPS and panel spacer bar.

4.2.4 Test Results

Test results that represent overall specimen behaviour are presented here, consisting primarily of plots showing the various measured deflections under loading. Von Mises strain data are presented in Chapter 5 where they are compared to the finite element analysis results. Figure 4.22 shows a plot of in-plane load versus vertical deflection for all three specimen sets. The value of in-plane deflection was taken as the average of all four in-plane LVDT's for that particular specimen. These LVDT's are shown as channels 36 through 39 in Figure 3.35. This plot shows all of the data readings taken during the test, thus the dynamic curve is shown as well as the static readings taken at regular intervals during the plastic deformation phase of loading. It is apparent from this plot that greater transverse pressure causes the specimen to lose stiffness at lower levels of in-plane load, although the initial in-plane stiffness of all three specimen sets is very similar at low axial loads. The ductility of the specimens in all three cases is apparent, as they undergo large vertical displacements without a reduction in their in-plane load carrying capacity. Note that the curve for SPS-2 ends at a lower level of deflection than that of the other two tests, a result of the premature test stop due to the specimen leaking mentioned in Section 4.2.1. SPS-2 also appears to be increasing in stiffness as the in-plane deflections increase beyond about 18 mm. This is likely due to the fact that the specimen was losing internal pressure in this range because the water pump could not keep up to the leaking.

Figures 4.23 through 4.25 graphically depict the progression of the out-of-plane deflection of each panel set, with the deflections measured at five locations along the vertical centreline of each panel. The LVDT's used are channels 20, 27, 28, 29 and 21 for

the west panel and 22, 24, 25, 26 and 23 for the east panel (see Figure 3.35). The top and bottom LVDT's for each side are attached to the edge of the top and bottom clamps as shown in Figure 3.35, while the remaining three LVDT's per side are located at the midpoint and the two quarter points of each panel. Note that the deflected shapes shown on the plots between the actual data points taken by the LVDT's are approximations using a curve fit.

Figure 4.23 shows the deflected shape of specimen SPS-1, tested at 207 kPa of internal pressure. While under lateral pressure only, or under lateral pressure at relatively low levels of in-plane load (the yellow and red lines on the plot), the specimen bulges in a half-sine-wave shape. As the in-plane load increases into the blue region on the plot, the deflection of the panel quarter points begins to exceed that of the midpoint and the panel starts to take on a three half-sine-wave shape. Finally, as the in-plane deflections become large (the brown lines), the panel midpoint starts to buckle back in towards the transverse pressure, and the three half-sine-wave shape becomes very pronounced.

Figure 4.24 is the progression of out-of-plane deflection for SPS-2, tested at 415 kPa of transverse pressure. It starts out much like SPS-1 but with larger initial deflections since the initial pressure of SPS-2 was double that of SPS-1. The one half-sine-wave shape is apparent until about 10 MN (the light blue curve), at which point the deflection of the panel quarter points begins to catch up to the midpoint deflection. At about 13 MN, the quarter point deflections are greater than the midpoint, which is the beginning of a three half-sine-wave shape, however at the maximum load level (dark brown) the panel midpoint does not deflect back toward the transverse pressure like it did in SPS-1. It should be noted that SPS-2 was only tested to 23 mm of in-plane deflection due to specimen leaking, whereas SPS-1 and SPS-3 were taken to approximately 27 mm and 28 mm respectively.

The progression of out-of-plane deflection for SPS-3 is shown in Figure 4.25. The 690 kPa of initial transverse pressure causes a half-sine-wave bulge with a mid panel out-of-plane deflection of 20 mm, almost double that of SPS-2 at 415 kPa. As a result of this

higher pressure, the general half-sine-wave deflected shape continues throughout the loading range, with the exception of at maximum applied in-plane load of 12.24 MN where the quarter point deflections have just started to exceed the mid panel deflection. At this maximum load level, which was at 28.7 mm of in-plane deflection, the bulge at the panel midpoint exceeded 75 mm out-of-plane on each panel.

4.2.5 Points on the Interaction Diagram

One of the primary objectives of this test program was to use the test results to generate points on a diagram showing the interaction between the in-plane load and the transverse pressure. For a given pressure, a plot of in-plane load versus in-plane deflection was used to obtain the level of in-plane load that resulted in panel failure. Ideally it was thought that the point at which the ultimate in-plane load carrying capacity of the panel was reached would be the point chosen as the interaction diagram point. However, both the test data and the finite element analysis indicate that reaching this ultimate in-plane load capacity requires axial deformations far larger than those that could be applied in the test.

As a result of this high ductility, it was decided that a 0.2% offset method would be used on the in-plane load versus in-plane deflection plots to obtain a consistent in-plane load level for all tests that is close to the ultimate. This 0.2% method was taken from ASTM A370-05, "Standard Test Methods and Definitions for the Mechanical Testing of Steel Products", and it involved three steps. First, a line was drawn along the elastic portion of the load versus deflection curve. A parallel line was then drawn at 0.2% strain (2000 microstrain) from this initial elastic line. The intersection of this offset line and the load deflection curve of the panel was then taken as the interaction diagram point. Figure 4.26 shows how this method was used to determine the interaction point for SPS-1. Note that the interaction points are obtained using the static points of the test to determine the in-plane load values. In Chapter 5, the determination of the interaction points is discussed in more details when they are compared to data from finite element analyses, and a second method of obtaining the interaction points is also presented.

Figure 4.27 shows the interaction points for all three test specimens. The diagram has been non-dimensionalized by dividing each of the in-plane load values by the theoretical value of in-plane load required to cause yield over the entire panel cross-section (P_Y). Each pressure has been divided by the theoretical plastic collapse pressure calculated using the upper bound yield line method. The equation for the plastic collapse pressure is as follows:

$$\frac{M_p[24(\frac{a}{b}+1)]}{b^2(1.5\cdot\frac{a}{b}-0.5)} \tag{4.2}$$

where,

M_P = Plastic moment capacity of the panel

a = Panel long dimension

b = Panel short dimension

Figure 4.28 shows the panel yield line pattern that was assumed in the calculation procedure for the upper bound plastic collapse pressure. Comparison of these test interaction diagram points to those generated from FEA work is done in Chapter 5.

4.3 Test Frame Performance

In order to properly assess the test data obtained from the SPS panels, it is necessary to characterize the behaviour of the test frame itself during the loading procedure. This involves determining the effectiveness of the clamps at maintaining a rigid boundary condition on the panel perimeter, as well as investigating the effectiveness of the roller bearing strips at minimizing in-plane load transfer from the SPS panel faceplates to the edge clamp bars.

4.3.1 Frame Behaviour - Elastic Range of Test Specimens

The rigidity of the clamping system during the elastic test phase was not analyzed thoroughly. The out-of plane clamp deflections that occurred in this range of loading were negligible in comparison to those that occurred during the ultimate loading phase, since the applied pressure and in-plane load combinations in the elastic range were substantially smaller in magnitude than those applied in the ultimate loading regime. The out-of-plane rigidity of the clamps is analyzed in the next section for SPS-3, as its internal pressure of 690 kPa placed the greatest demands on the test frame.

To determine the effectiveness of the roller bearing strips, the elastic load case of 7200 kN axial load with zero lateral pressure was used. The average vertical strain in the panel during this load case was multiplied by the modulus of elasticity for the steel plates obtained from the tension coupon tests. This was then multiplied by the cross-sectional area of steel in the panels to obtain an estimate of the load carried by the plates. The contribution of the elastomer to in-plane load resistance is negligible. Figure 4.29 shows a plot of the difference between applied load and calculated panel load divided by the calculated load on the y-axis (expressed as a percentage), versus applied load from zero to 7200 kN on the x-axis. Percentages greater than zero indicate that more in-plane load is being applied to the specimen than can be accounted for in the panels based on the strain data. This discrepancy could be due to some of the applied load going into the edge clamps of the test frame, suggesting that friction is present in the roller bearing assemblies.

Figure 4.29 indicates that all three specimens behave in a similar manner although the values do not match up exactly. At in-plane load below 1200 kN, there is at least 20% more load being applied to the specimens than what is calculated to be in the panels. This is attributed to uneven seating of the panels during this phase, so the load is likely not evenly distributed to all the panel gauges. As the in-plane load increases to 7200 kN, the additional applied load steadily approaches zero, and at 7200 kN it is slightly less than zero for SPS-1 and SPS-2. Based on this data, it appears that the roller bearing assemblies

are effectively preventing in-plane load from being transferred to the edge clamps, especially as the in-plane load becomes large. Note the dips in the curves that occur whenever loading was paused during testing to take visual observations of the specimen.

It was also of interest to determine if the vertical strain in the panel was uniform over the panel height. A LVDT was thus installed to measure the vertical deflection from the mid panel height to the top distributing beam. Figure 4.30 is a plot for SPS-1 of vertical deflection over the top half of the panel calculated from this half-height LVDT. Deflections measured with this half height LVDT are plotted against one-half of the overall average vertical panel deflection taken from the in-plane LVDT's: channels 36 thru 39 as shown in Figure 3.35. The vertical deflections compare relatively well over the loading range, with the half-height LVDT indicating a maximum difference of about 15% less defection than one-half the average of the in-plane LVDT's at 7200 kN. Plots for SPS-2 and SPS-3 showed similar trends.

4.3.1 Frame Behaviour – Loading to Ultimate

During the ultimate loading phase, the effects of combined loading and yielding material made it impractical to estimate the relationship between load in the panel versus applied load, as was done in Figure 4.29. The primary parameter of frame behaviour that was monitored in this ultimate loading range was the out-of-plane motion of the clamp faces. Plots of both pressure and in-plane load versus clamp bar out-of-plane deflection were generated for the top, bottom and both edge clamps for each test throughout the entire loading range. Since all plots had similar characteristics, only those for the highest pressure test (SPS-3) are presented here as the worst case scenario, since the maximum clamp deflections for the other two tests were less than those that occurred in SPS-3.

Figure 4.31 is a plot of transverse pressure versus top and bottom clamp out-of-plane deflection for SPS-3 (690 kPa test). This is the initial pressure-up phase of the test, with no axial load applied aside from 150 kN as a gasket seating load as explained in Section 4.2.3. The LVDT channel numbers shown in the legend in brackets can be related to their

positions on the panels by referring to Figure 3.35. On these plots, out-of-plane motion is taken as positive to the right (east on the actual test setup), thus an opening of the clamp faces corresponds to a separation of the two lines on the plot that correspond to that clamp. On the other hand, two lines for a given clamp that move in parallel correspond to a translation of that clamp but not an opening of the faces. From this, it can be seen that the bottom clamp (blue lines) opened by about 0.28 mm and the top clamp (red) opened 0.22 mm and translated east by 0.15 mm.

Figure 4.32 plots the motion of the top and bottom clamps of SPS-3 during the application of the in-plane load, starting from the point where Figure 4.31 ends. The top clamp continued to separate slightly to a maximum of about 0.5 mm, then closed back up and translated about 0.5 mm west by the time maximum in-plane load had been reached. The bottom clamp behaved similarly, opening to a maximum of 0.6 mm and translating east by about 2 mm as the in-plane load reached its peak. Overall, the clamps maintained exceptional rigidity since the largest separation of 0.6 mm is only 0.6% of the original 96 mm thickness of the clamped specimen set.

Since there was SPS spacer material on the outside edges of the edge clamps (see Figures 3.12 to 3.14), an additional LVDT was added to each edge clamp to measure the relative movement of the outer edge faces of the clamp bars. These two extra LVDT's correspond to channels 34 and 35 on Figure 3.35, and the green lines on the plots in Figures 4.33 and 4.34. Positive motion implies a squashing together of the outer clamp edges resulting from compression of the elastomer in the edge clamp spacer strips that are shown in Figures 3.14 to 3.16. Using all three LVDT's per clamp, it was possibly to roughly calculate the rotation of the clamp faces with respect to their original position.

Figure 4.33 plots the motion of the edge clamps during the application of the initial 690 kPa of pressure on SPS-3. The north clamp (red lines) opened by 0.95 mm on its panel edge and crushed together on its outer edge by about 0.22 mm. The horizontal distance between these measured points was 341 mm. The rotation of each clamp face with respect to its original position was taken as the arctangent of the ratio of one-half of

the total vertical displacement (the total being 0.95 mm + 0.22 mm in this case) to the horizontal distance (341 mm for this clamp). In this case, the clamp face rotation was in the order of 0.1 degree. The south clamp shown by the blue lines in Figure 4.33 behaved similarly, with a clamp face rotation of 0.05 degrees at 690 kPa.

As the in-plane load was applied, edge clamp movement stayed fairly constant as can be seen in Figure 4.34. At very high in-plane loads, it appears that the entire specimen rotated very slightly about a vertical axis, as the south clamp translated east by about 2.5 mm and the north clamp translated slightly west after it had previously moved east at lower levels of in-plane load. Maximum clamp face rotation of 0.25 degrees occurred in the south clamp at the highest value of in-plane load. Overall however, these motions are all very small relative to the specimen size. A further analysis of the effects of these clamp rotations is carried out in Chapter 5 when the test results are compared to those produced from finite element analyses.

Table 4.1: Data for Elastic Load Case of 7200 kN In-plane Load and No Lateral Pressure

(a): In-plane Displacement (mm)

	Average	Coefficient of Variation
All SPS-1 Test In-plane Readings (4)	2.504	6%
All SPS-2 Test In-plane Readings (4)	2.876	7%
All SPS-3 Test In-plane Readings (4)	3.199	12%
All East Panel Readings (6)	2.831	16%
All West Panel Readings (6)	2.888	12%
All In-plane Deflection Readings (12)	2.860	13%

(Number of data point readings for each parameter in brackets ( ))

(b): Vertical Strains (microstrain)

	Average	Coefficient of Variation
All Panel Center Region Readings (18)	-1356	22%
All Panel Edge Region Readings (12)	-1036	7%
All East Panel Readings (15)	-1207	21%
All West Panel Readings (15)	-1248	26%
All Vertical Strain Readings (30)	-1228	23%

(Number of data point readings for each parameter in brackets ( ))

(c): Von Mises Stresses (MPa)

	Average	Coefficient of Variation
All Panel Top and Bottom Point Readings (12)	257.2	27%
All Panel Edge Point Readings (12)	194.8	7%
All Panel Midpoint Readings (6)	228.8	9%

(Number of data point readings for each parameter in brackets ( ))

Table 4.2: Data for Elastic Load Case of 276 kPa Lateral Pressure and No In-plane Load

(a): Out-of-plane Displacement (mm)

	Average	Coefficient of Variation
All Panel Center Point Readings (6)	7.411	0.043
All Panel Quarter Point Readings (12)	5.535	0.037

(Number of data point readings for each parameter in brackets ( ))

(b): Von Mises Stresses (MPa)

	Average	Coefficient of Variation
All Panel Top and Bottom Point Readings (12)	93.5	20%
All Panel Edge Point Readings (12)	78.1	31%
All Panel Midpoint Readings (6)	120.8	16%

(Number of data point readings for each parameter in brackets ( ))

Table 4.3: Data for Three Intermediate Elastic Load Cases

(a): In-plane Displacement (mm)

	Average	Coefficient of Variation
All Panel In-plane Readings (12) - Case 1: 1800 kN, 207 kPa	0.495	45%
All Panel In-plane Readings (12) - Case 2: 3600 kN, 138 kPa	1.049	24%
All Panel In-plane Readings (12) - Case 3: 5400 kN, 69 kPa	1.607	15%

(Number of data point readings for each parameter in brackets ( ))

(b): Out-of-plane Displacement (mm)

	Average	Coefficient of Variation
All Panel Center Points (6) - Case 1: 1800 kN, 207 kPa	6.049	10%
All Panel Center Points (6) - Case 2: 3600 kN, 138 kPa	4.147	15%
All Panel Center Points (6) - Case 3: 5400 kN, 69 kPa	1.926	35%
All Panel Quarter Points (12) - Case 1: 1800 kN, 207 kPa	4.555	11%
All Panel Quarter Points (12) - Case 2: 3600 kN, 138 kPa	3.136	18%
All Panel Quarter Points (12) - Case 3: 5400 kN, 69 kPa	1.497	41%

(Number of data point readings for each parameter in brackets ( ))

(c): Von Mises Stresses (MPa)

	Average	Coefficient of Variation
All Top and bottom Points (12) - Case 1: 1800 kN, 207 kPa	137.8	18%
All Top and bottom Points (12) - Case 2: 3600 kN, 138 kPa	172.5	18%
All Top and bottom Points (12) - Case 3: 5400 kN, 69 kPa	200.6	21%
All Edge Points (12) - Case 1: 1800 kN, 207 kPa	63.1	33%
All Edge Points (12) - Case 2: 3600 kN, 138 kPa	86.0	15%
All Edge Points (12) - Case 3: 5400 kN, 69 kPa	129.0	7%
All Midpanel Points (6) - Case 1: 1800 kN, 207 kPa	100.3	10%
All Midpanel Points (6) - Case 2: 3600 kN, 138 kPa	113.3	4%
All Midpanel Points (6) - Case 3: 5400 kN, 69 kPa	155.5	3%

(Number of data point readings for each parameter in brackets ( ))

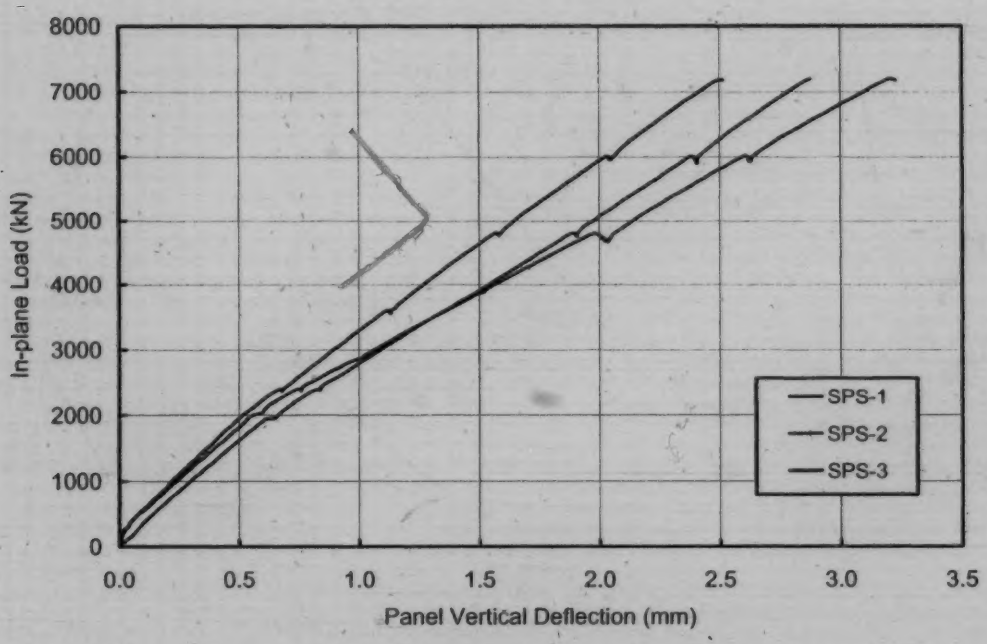

Figure 4.1: In-plane Load versus In-plane Deflection for 7200 kN Axial Load and No Lateral Pressure

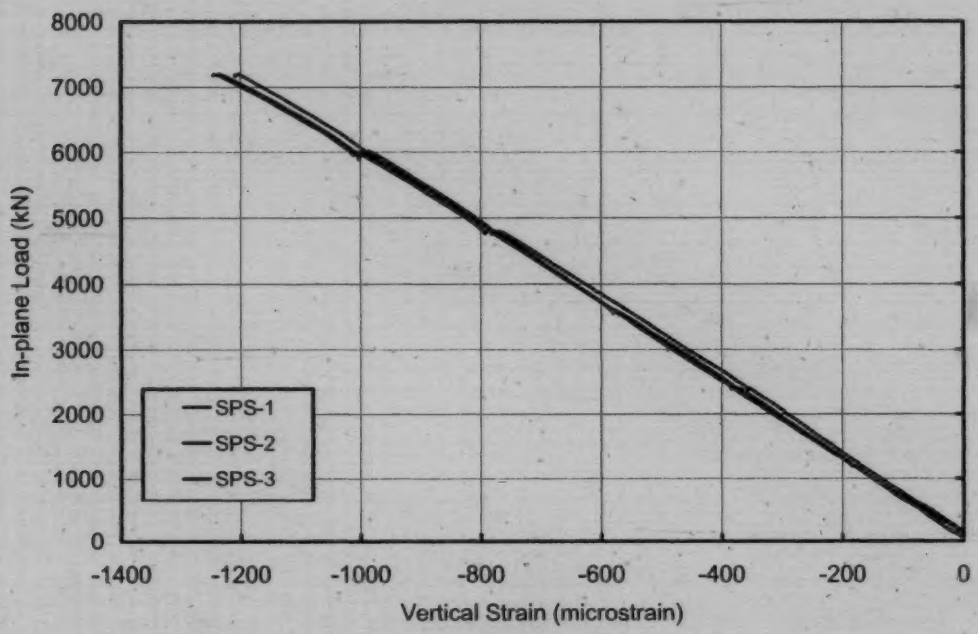

Figure 4.2: In-plane Load versus Average Vertical Panel Strain for Axial Load of 7200 kN and No Lateral Pressure

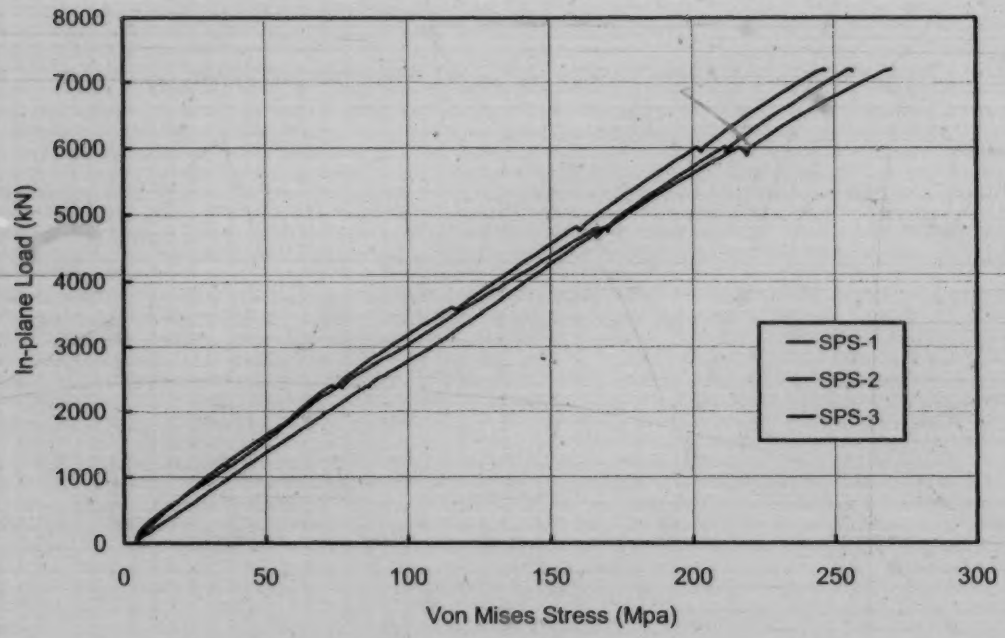

Figure 4.3: In-plane Load versus Average Top and Bottom von Mises Stress

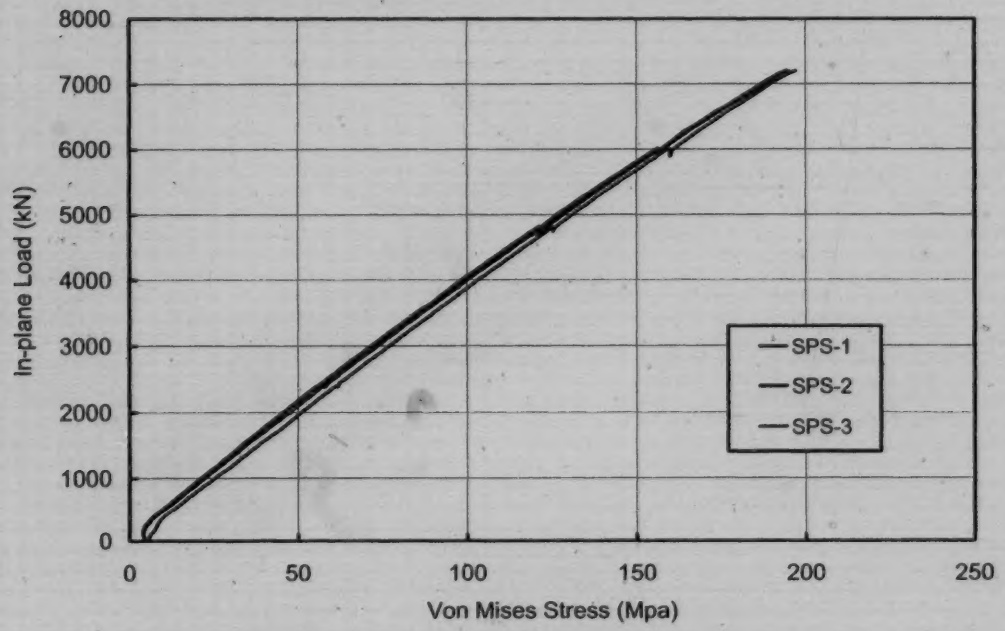

Figure 4.4: In-plane Load versus Average Panel Edge von Mises Stress

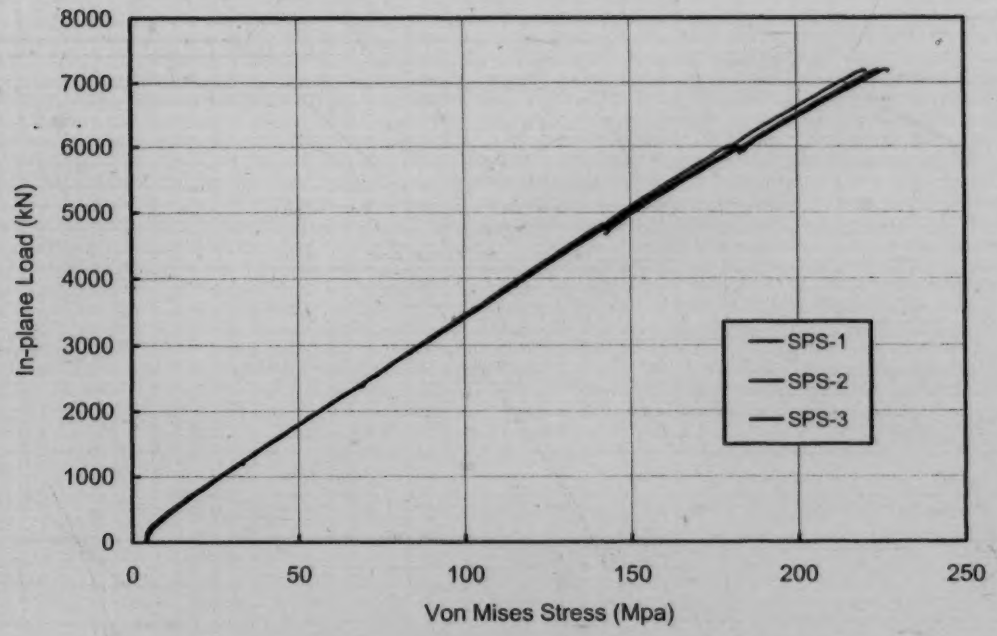

Figure 4.5: In-plane Load versus Average Panel Midpoint von Mises Stress

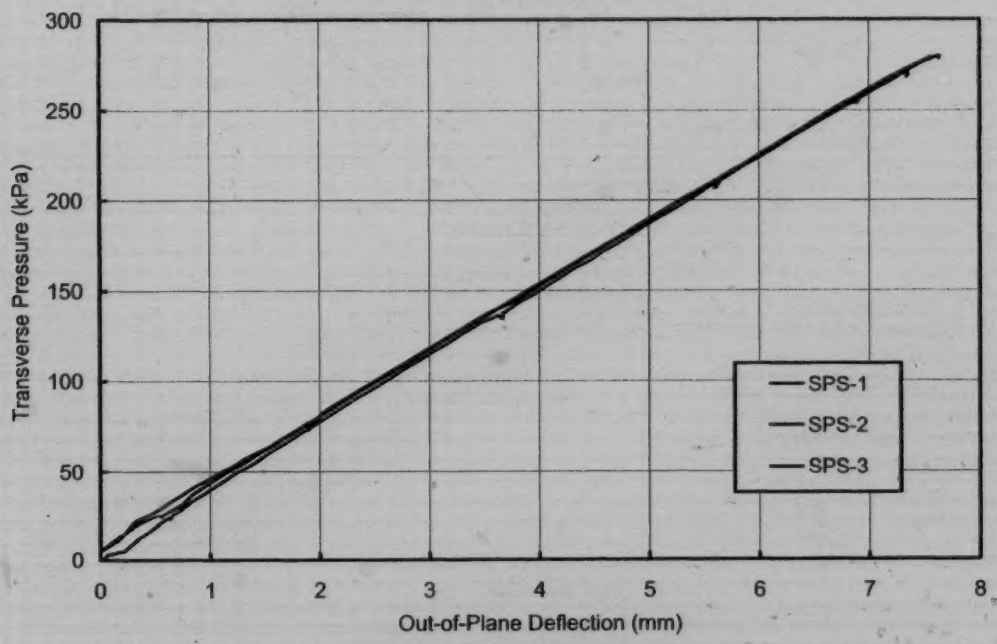

Figure 4.6: Transverse Pressure versus Mid Panel Out-of-plane Deflection for 280 kPa Lateral Pressure and No In-plane Load

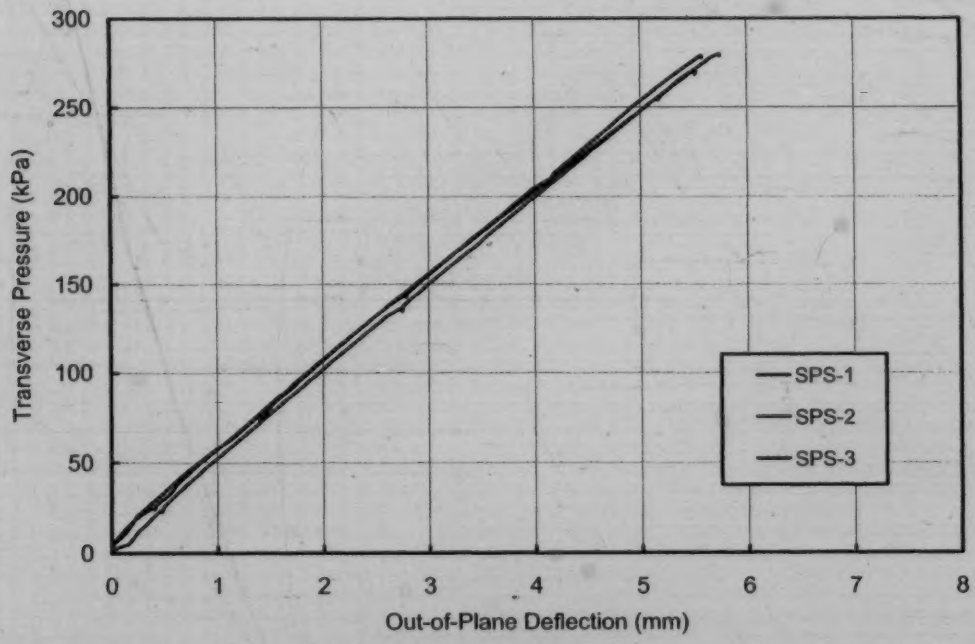

Figure 4.7: Transverse Pressure versus Panel Quarter Point Out-of-plane Deflection for 280 kPa Lateral Pressure and No In-plane Load

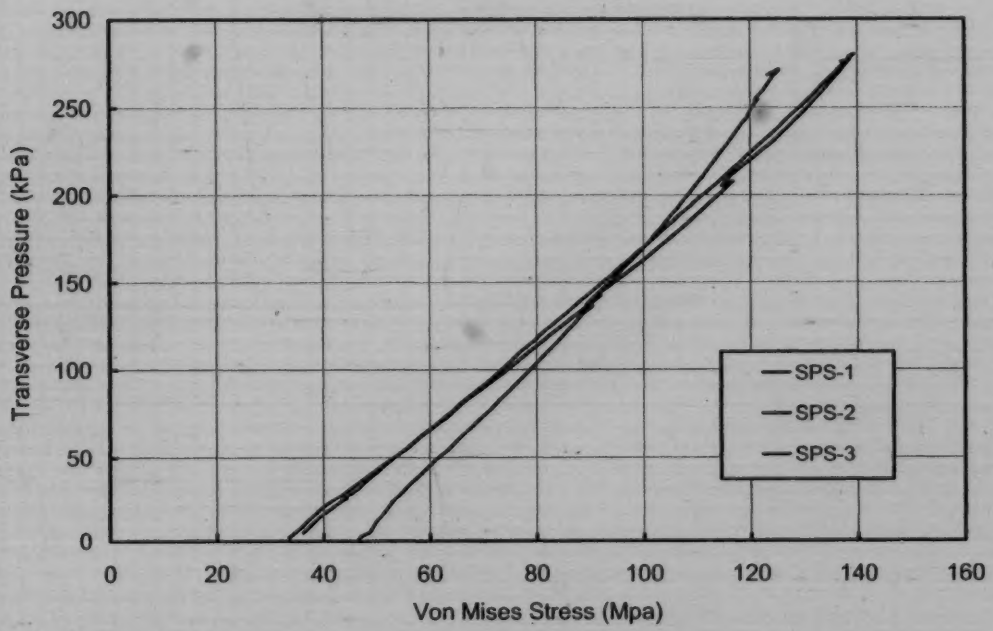

Figure 4.8: Transverse Pressure versus Ayerage Panel Top and Bottom von Mises Stresses

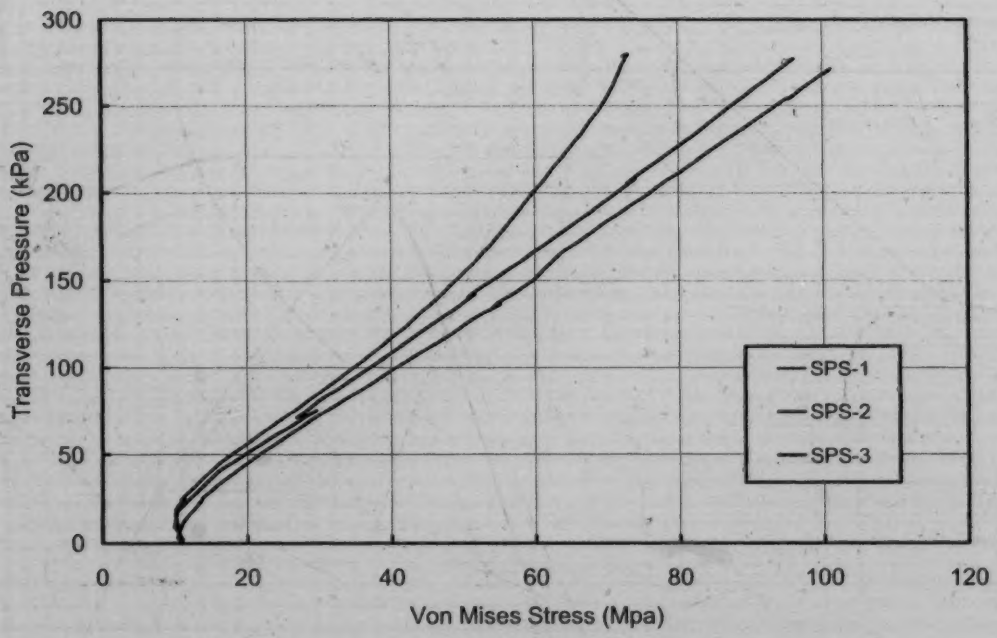

Figure 4.9: Transverse Pressure versus Average Panel Edge von Mises Stresses

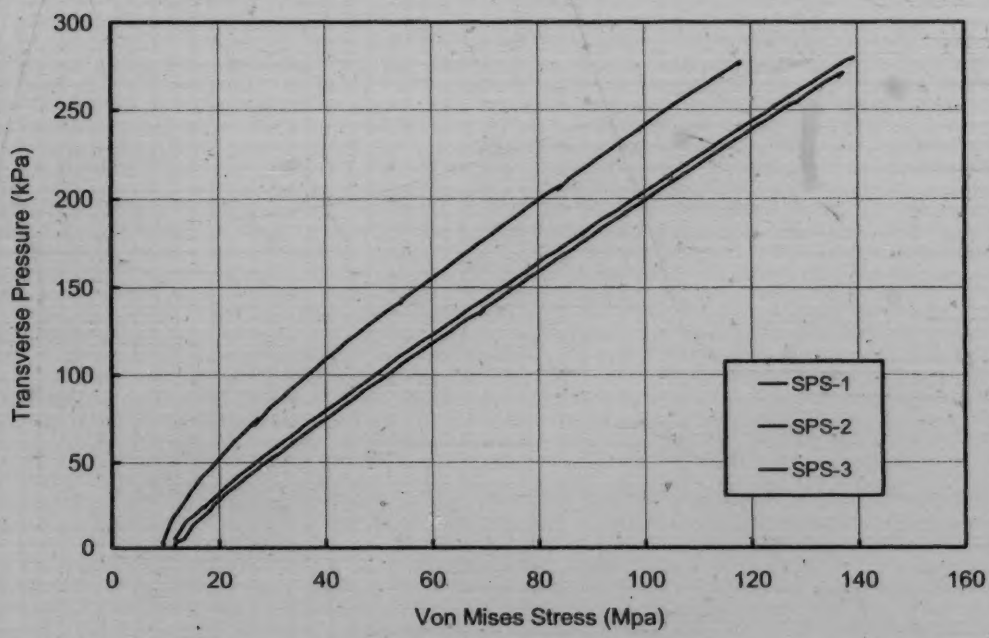

Figure 4.10: Transverse Pressure versus Average Panel Midpoint von Mises Stresses

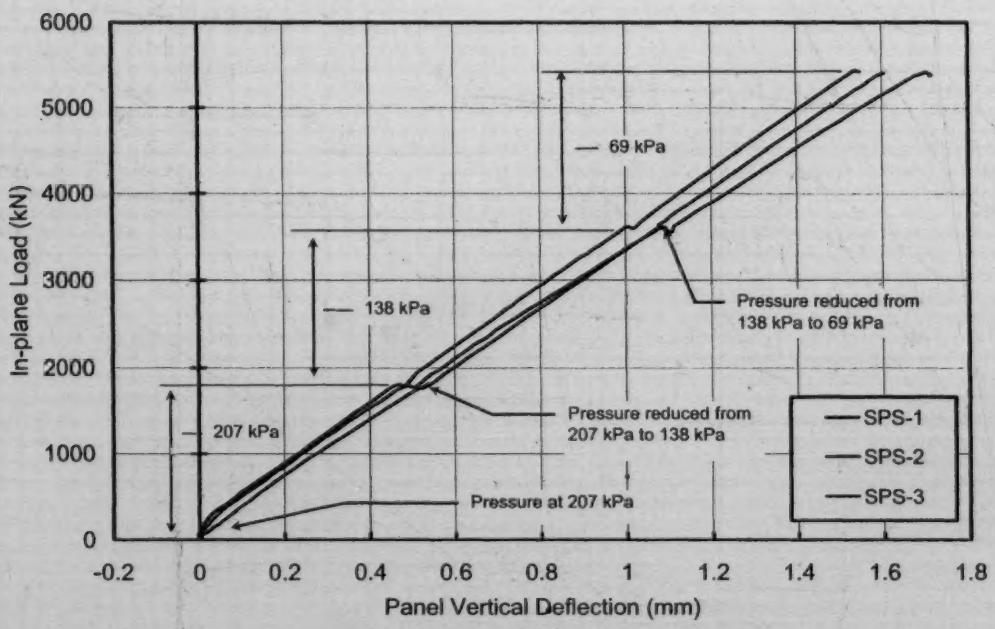

Figure 4.11: In-plane Load versus In-plane Deflection for Three Intermediate Load Cases

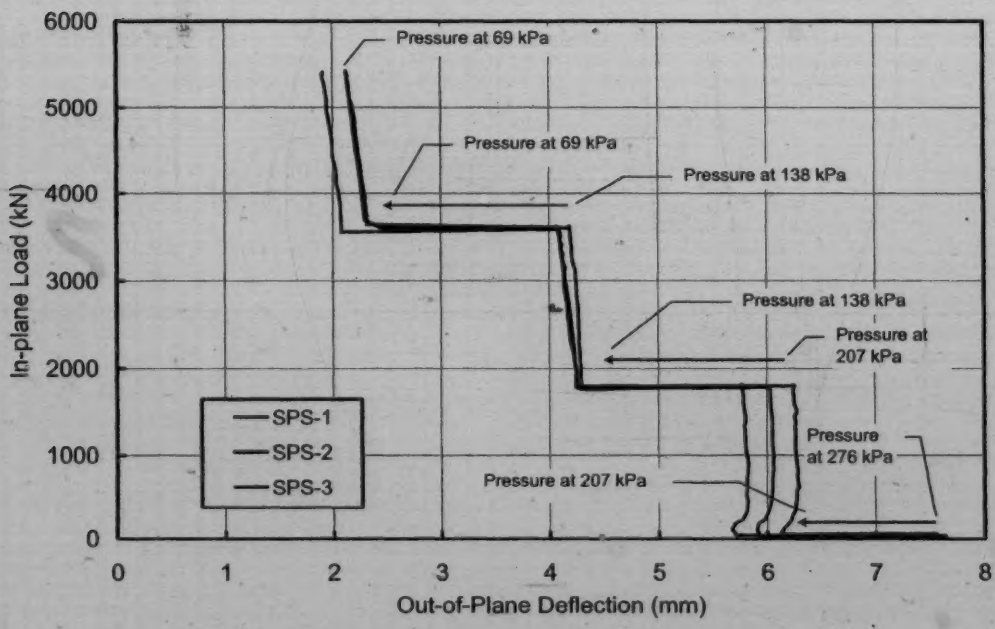

Figure 4.12: In-plane Load versus Panel Midpoint Out-of-plane Deflection

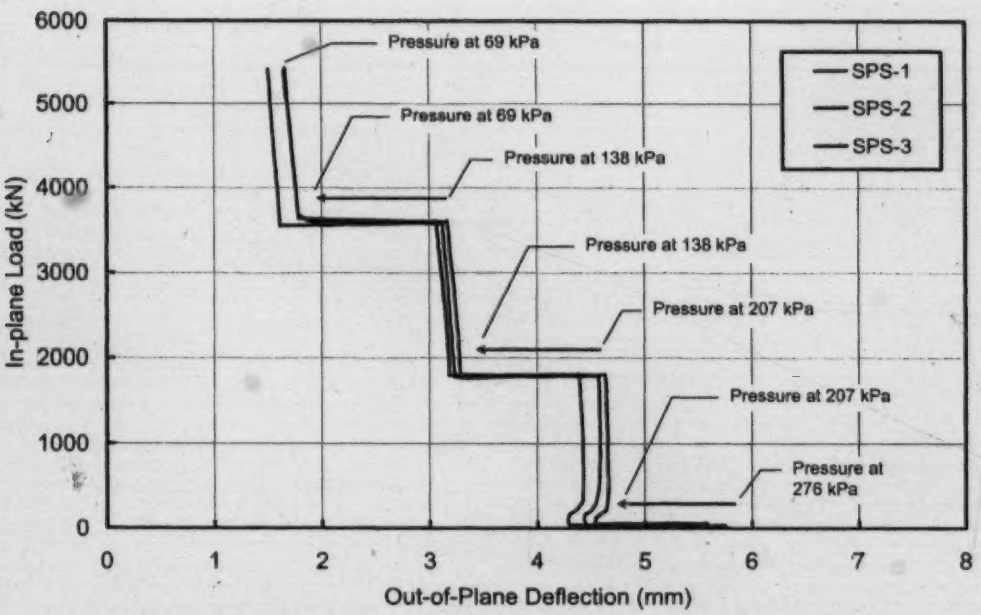

Figure 4.13: In-plane Load versus Panel Quarter Point Out-of-plane Deflection

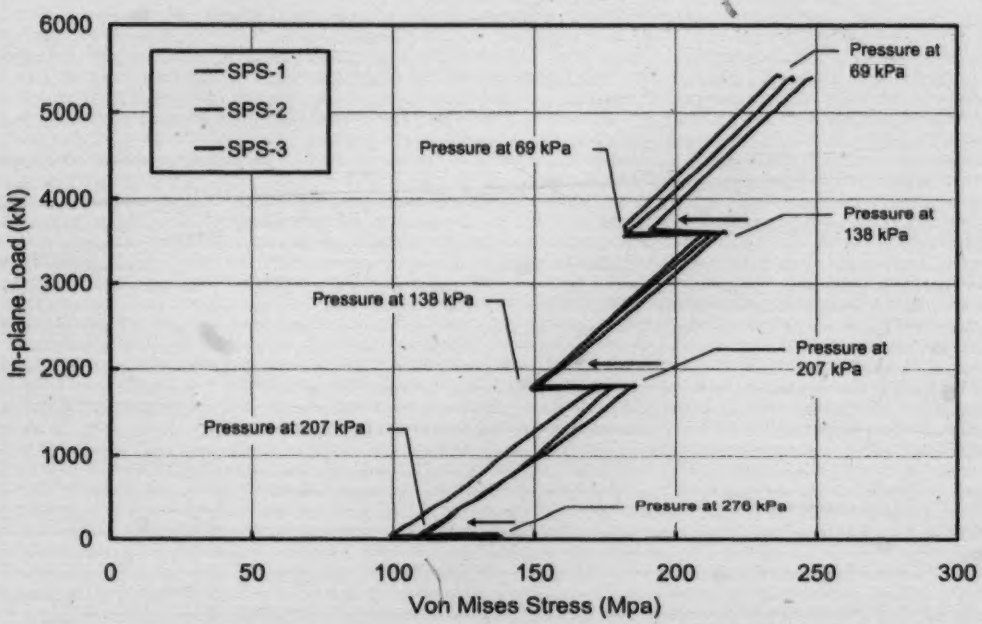

Figure 4.14: In-plane Load versus Average Panel Top and Bottom von Mises Stress

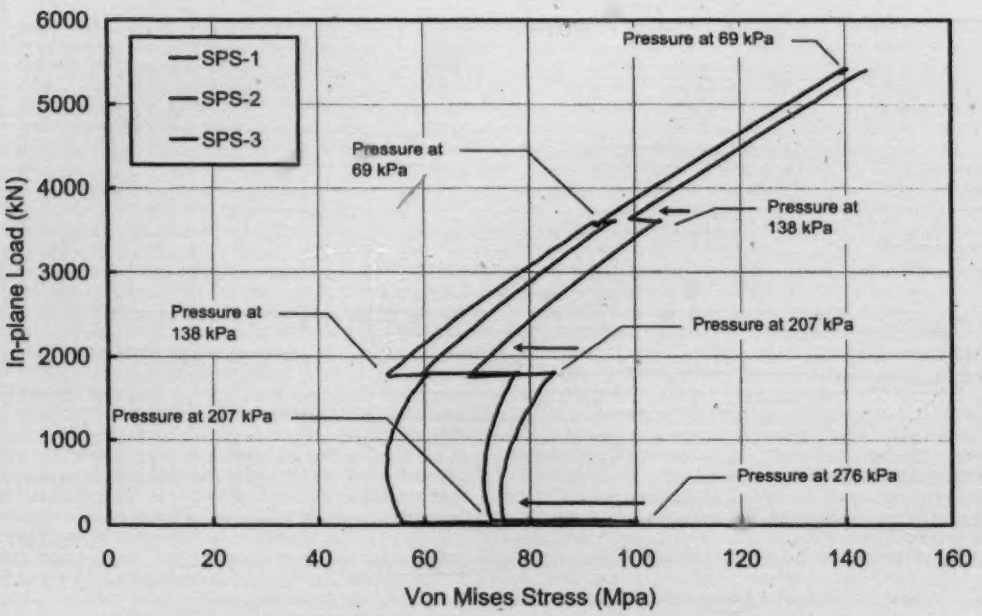

Figure 4.15: In-plane Load versus Average Panel Edge von Mises Stress.

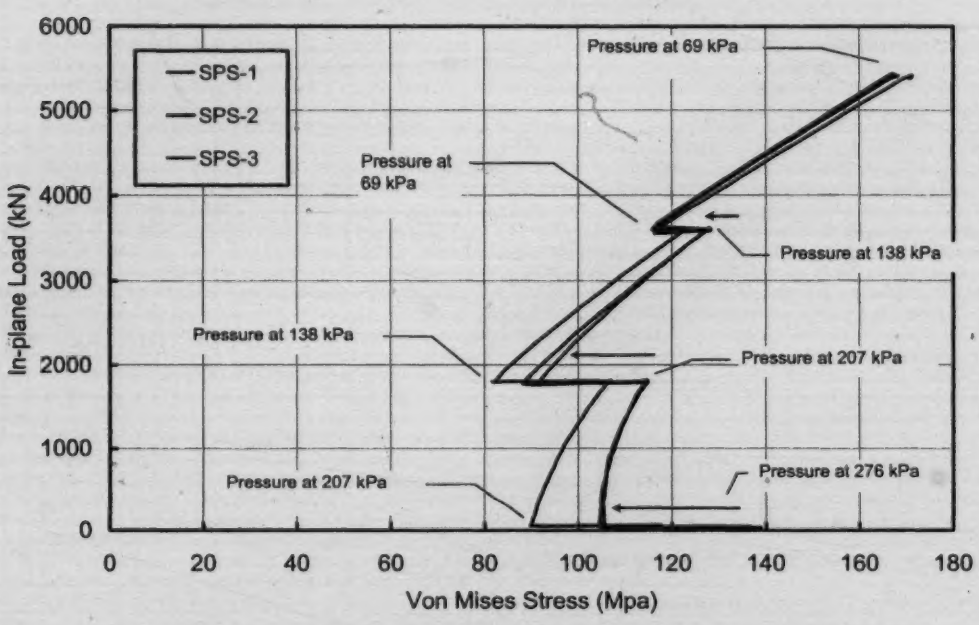

Figure 4.16: In-plane Load versus Average Panel Midpoint von Mises Stress

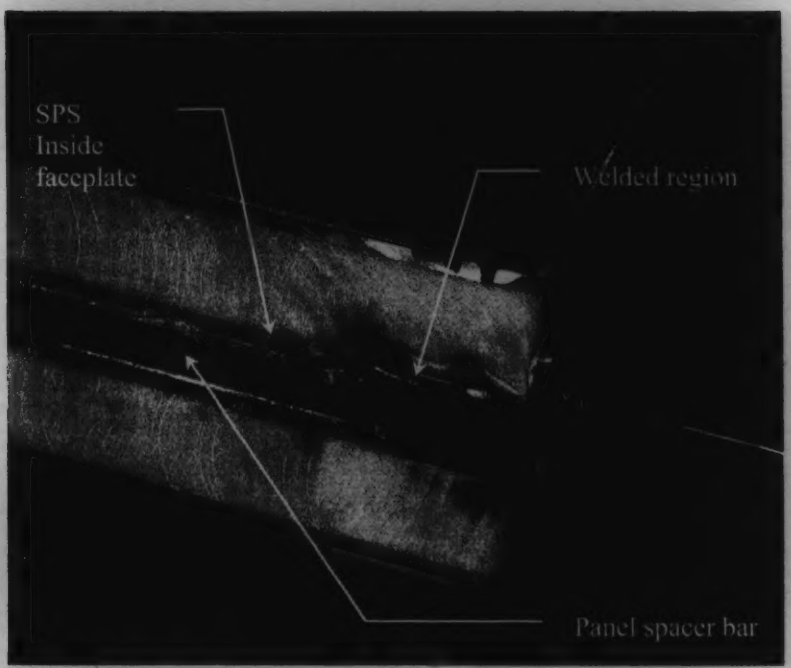

Figure 4.17: Welded and Ground Bottom Corner of SPS-3 Specimen Set

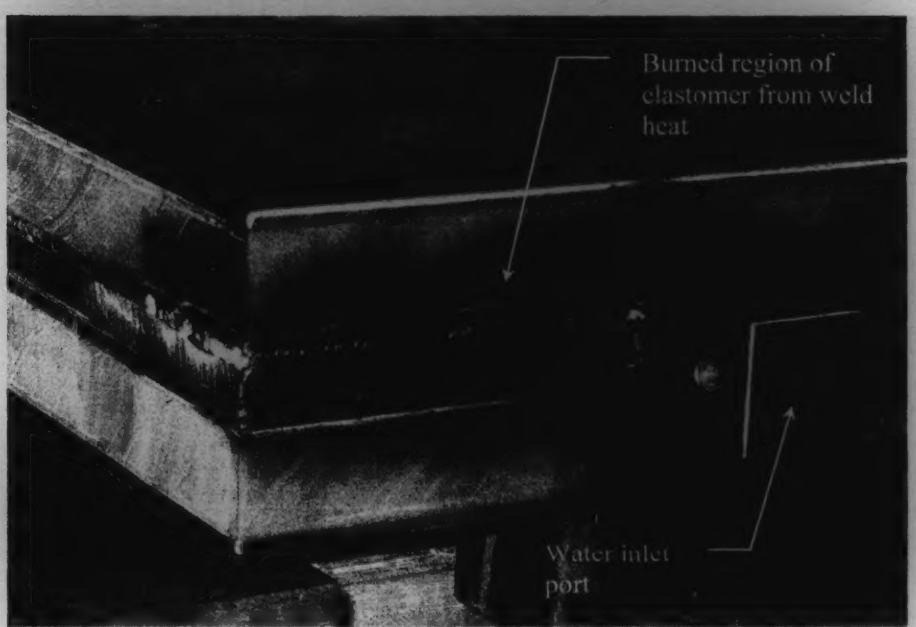

Figure 4.18: Welded Top Corner and Water Inlet Port of SPS-3 Specimen Set

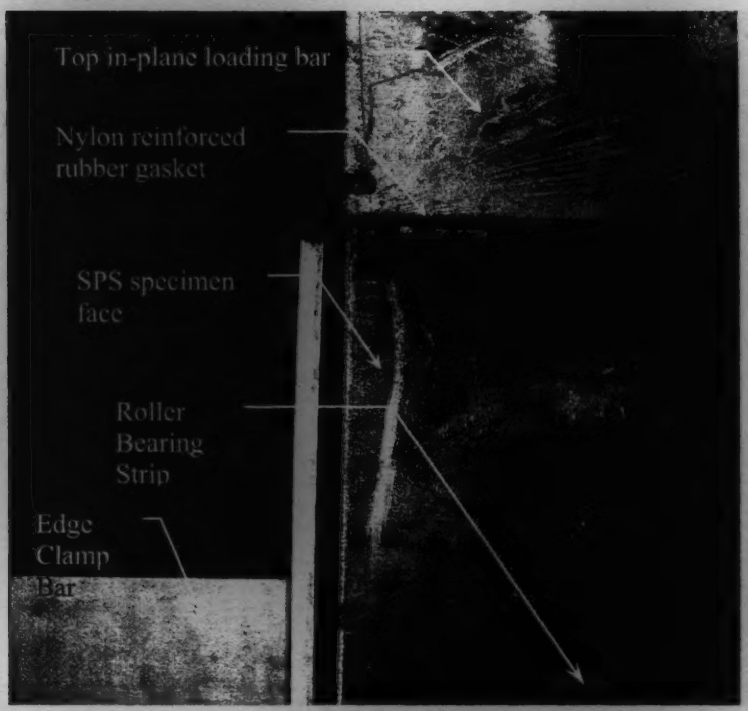

Figure 4.19: Nylon Reinforced Neoprene Rubber Top Gasket Material Added to SPS-3 Specimen Set – Top Corner Close-up with Outer Clamp Bars Removed

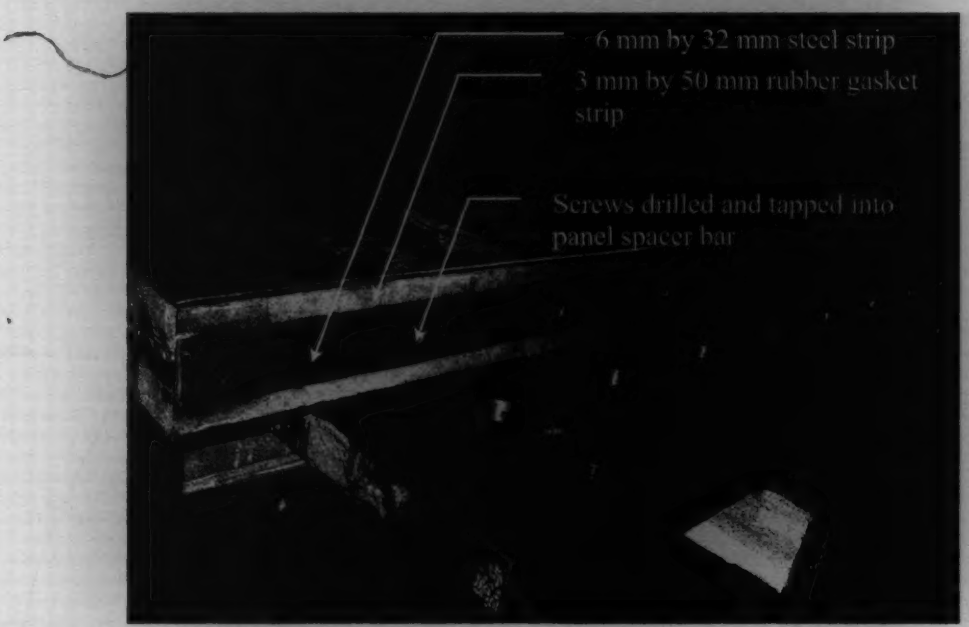

Figure 4.20: Extra Neoprene Edge Gasket and Steel Retaining Strip added to SPS-3 Specimen Set

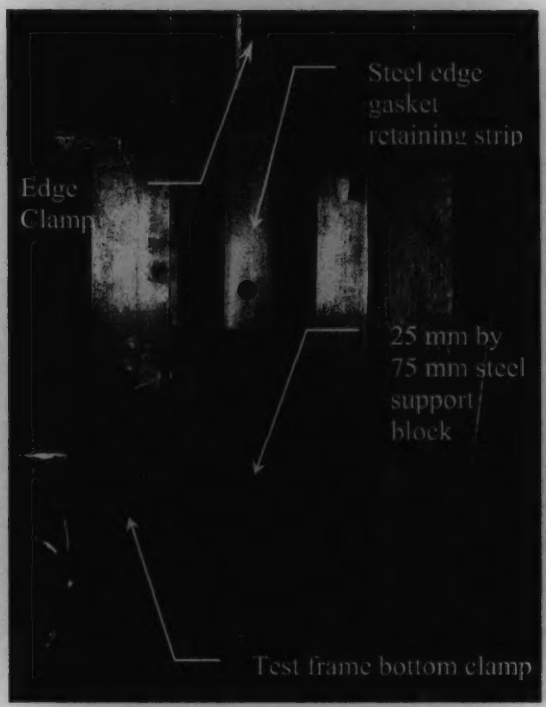

Figure 4.21: Steel Block for Axial Support of Gasket Retaining Strip on SPS-3 Specimen Set

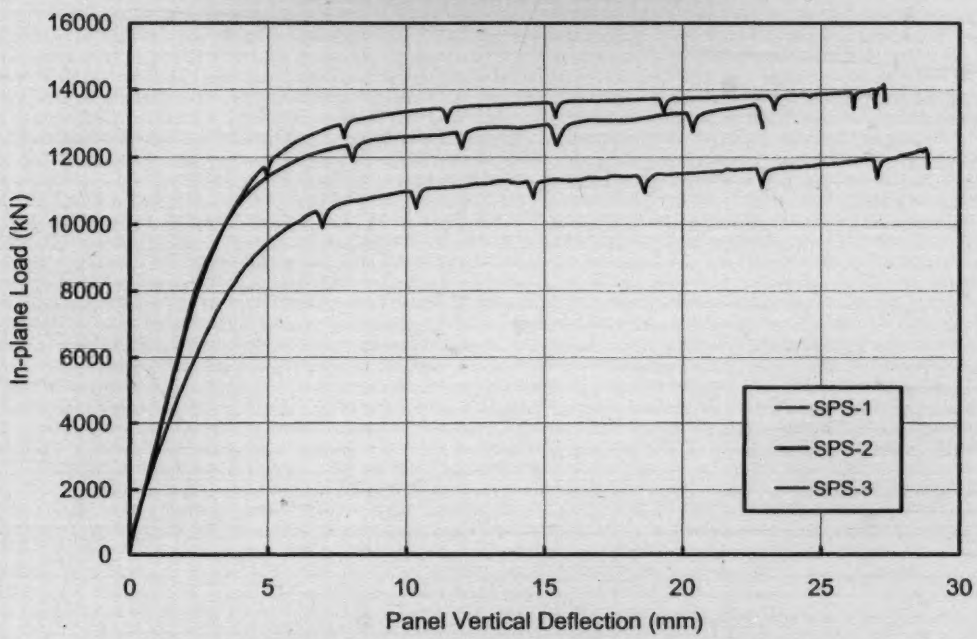

Figure 4.22: In-plane Load versus In-plane Deflection for All Three Tests

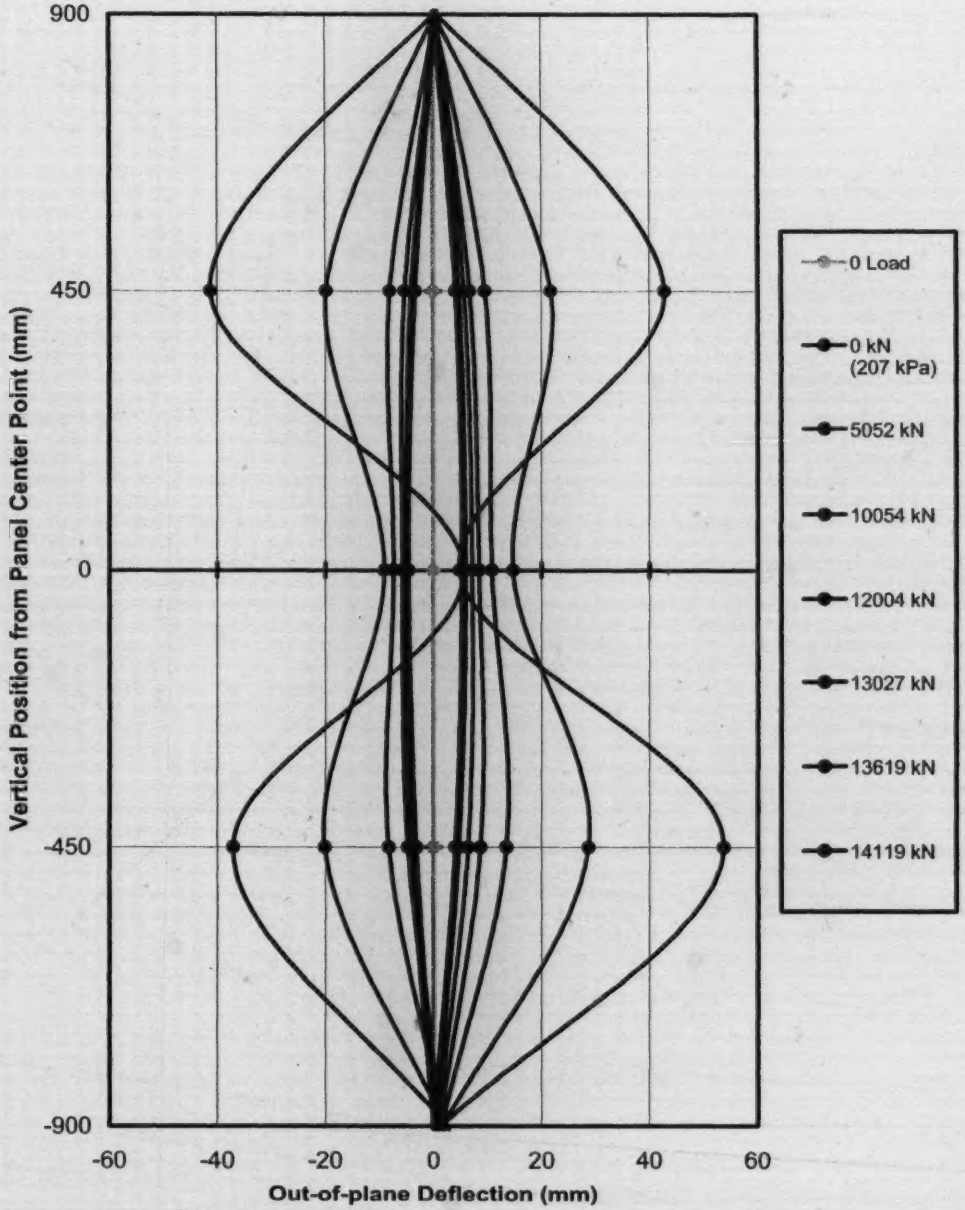

Figure 4.23: Progression of Out-of-plane Deflected Shape During Loading of SPS-1

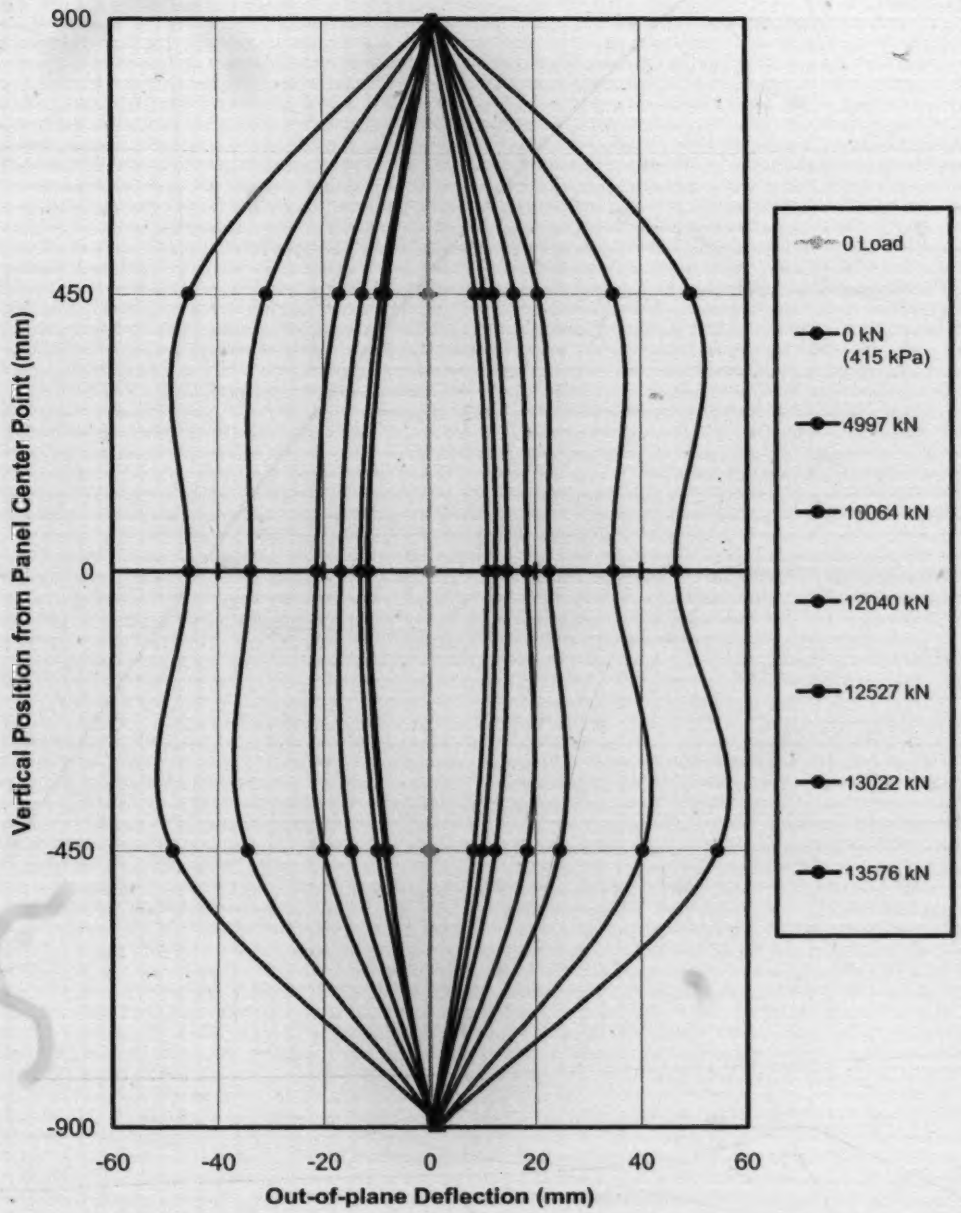

Figure 4.24: Progression of Out-of-plane Deflected Shape During Loading of SPS-2

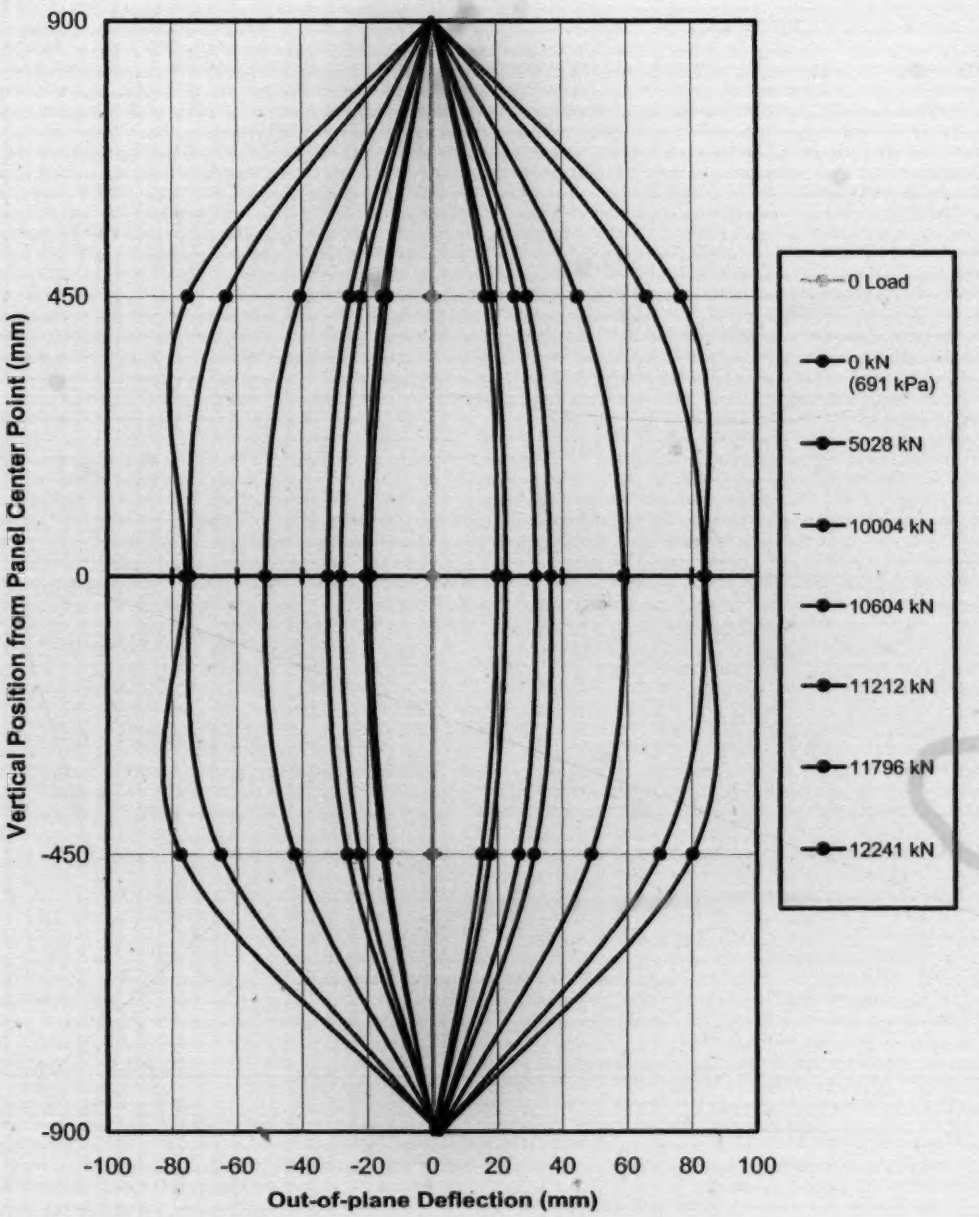

Figure 4.25: Progression of Out-of-plane Deflected Shape During Loading of SPS-3

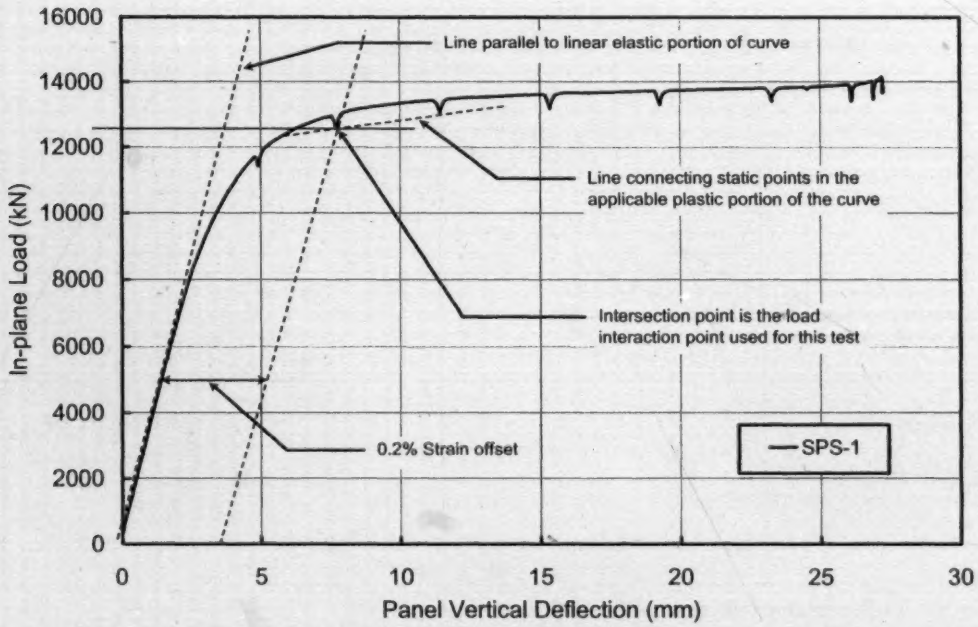

Figure 4.26: Interaction Point from In-plane Load versus In-plane Deflection Curve for SPS-1 Test

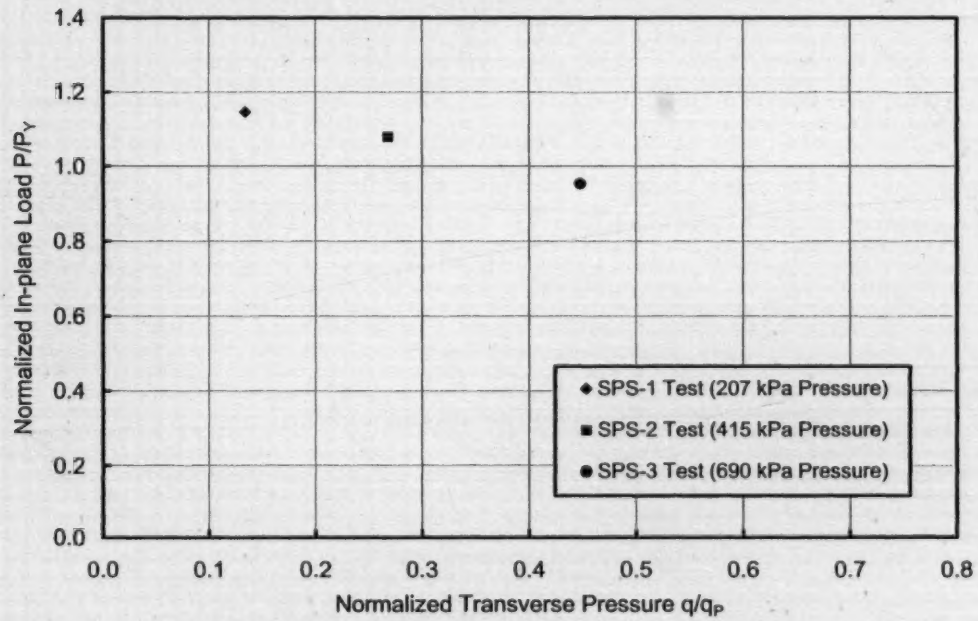

Figure 4.27: Interaction Points Calculated From All Three Test Results

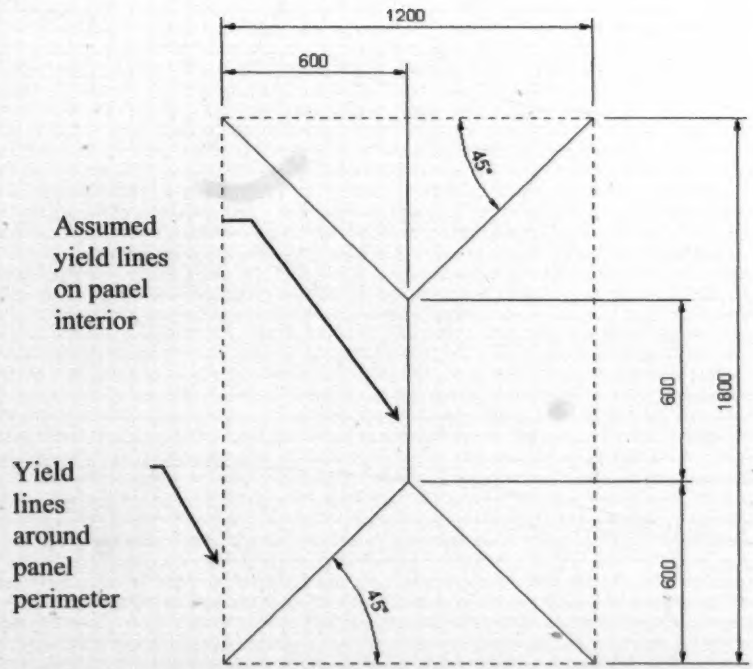

Figure 4.28: Yield Line Pattern Assumed in Calculating Upper Bound Plastic Collapse Pressure

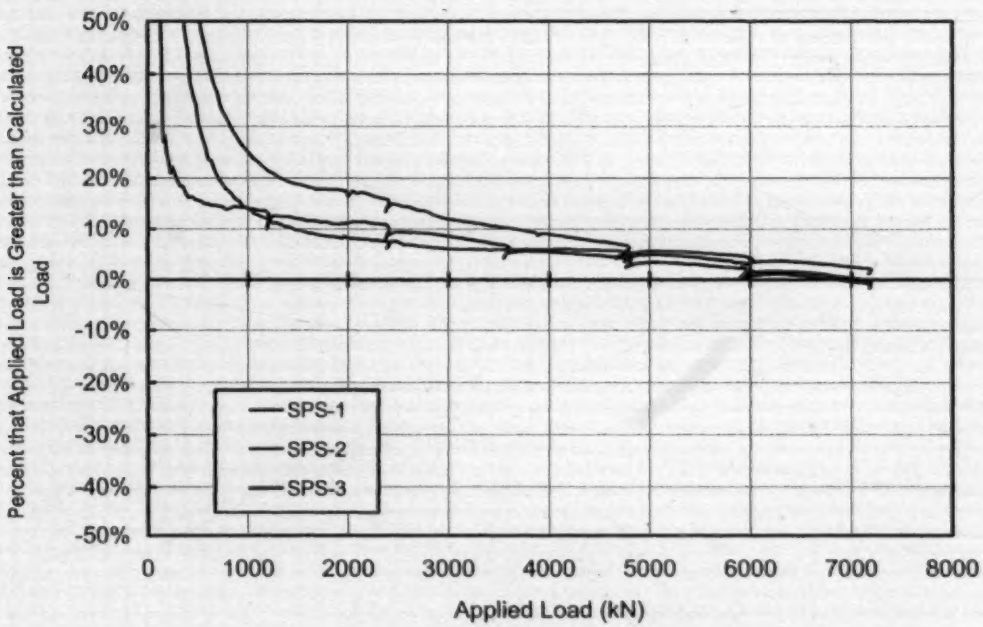

Figure 4.29: Comparison of Applied In-plane Load to Calculated In-plane Load

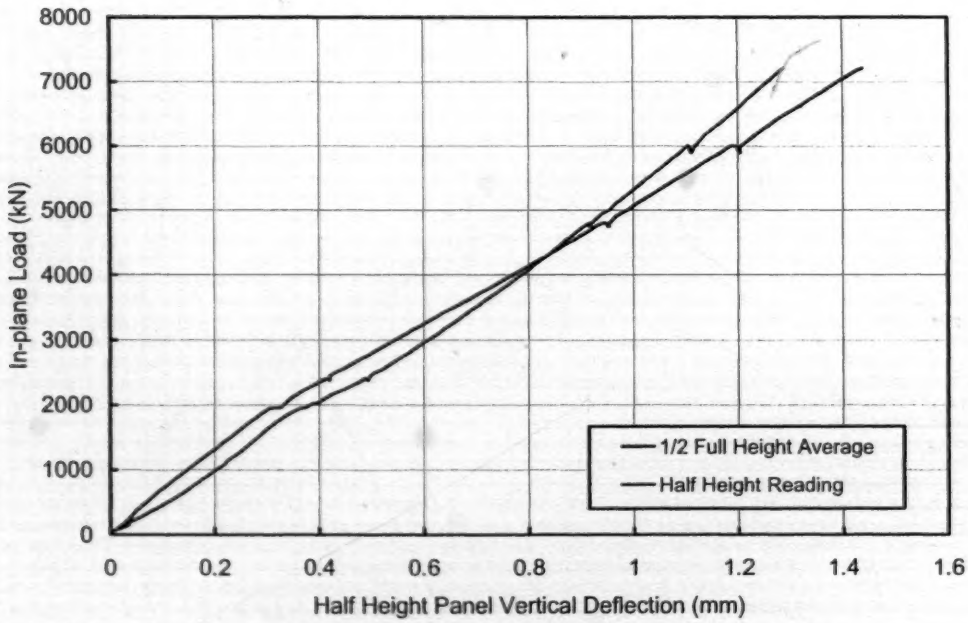

Figure 4.30: Half-height In-plane Deflection of SPS-1

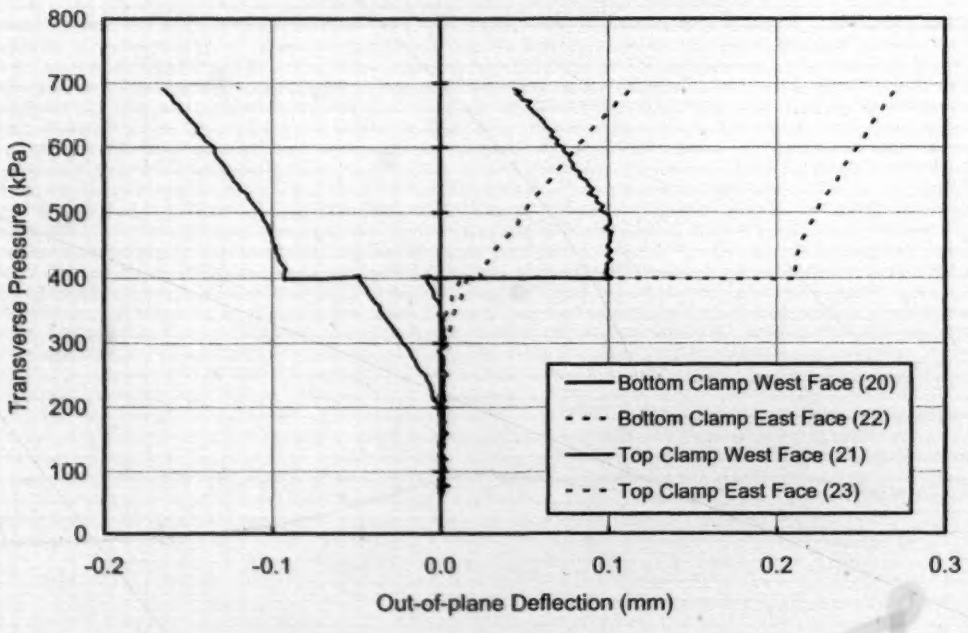

Figure 4.31: Transverse Pressure versus Top and Bottom Clamp Motion for SPS-3

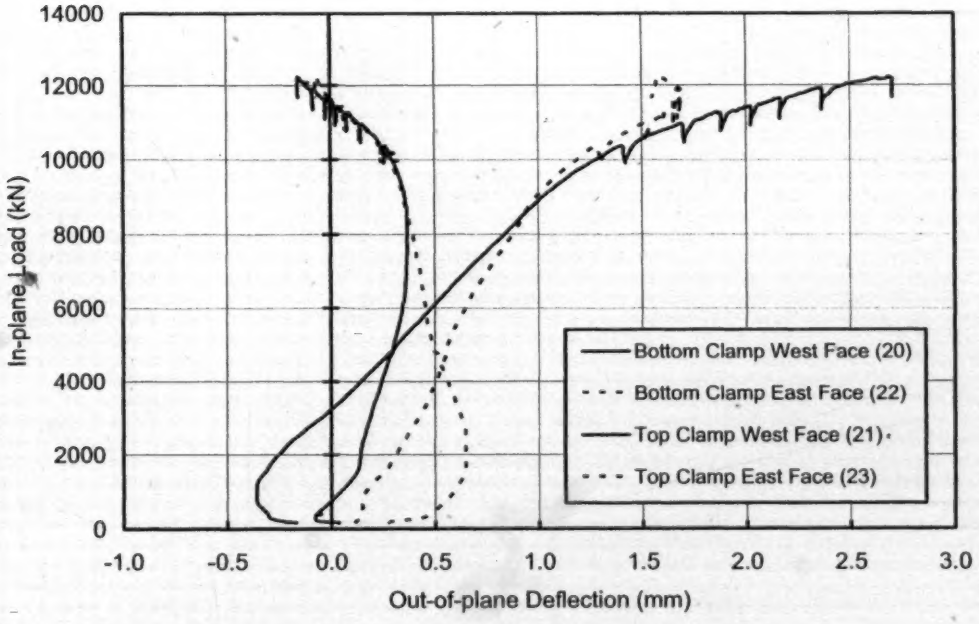

Figure 4.32: In-plane Load versus Top and Bottom Clamp Motion for SPS-3

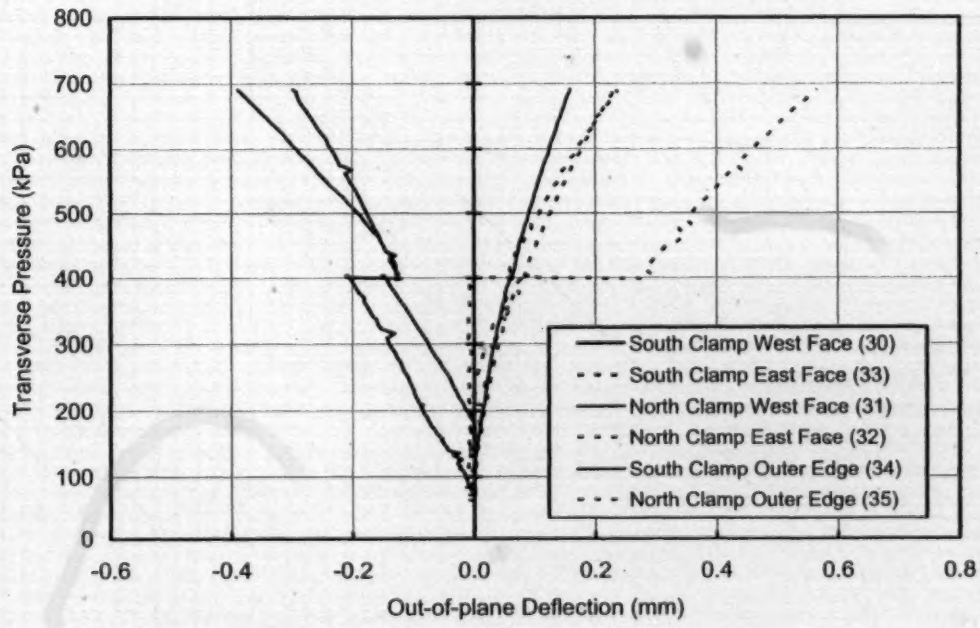

Figure 4.33: Transverse Pressure versus Edge Clamp Motion for SPS-3

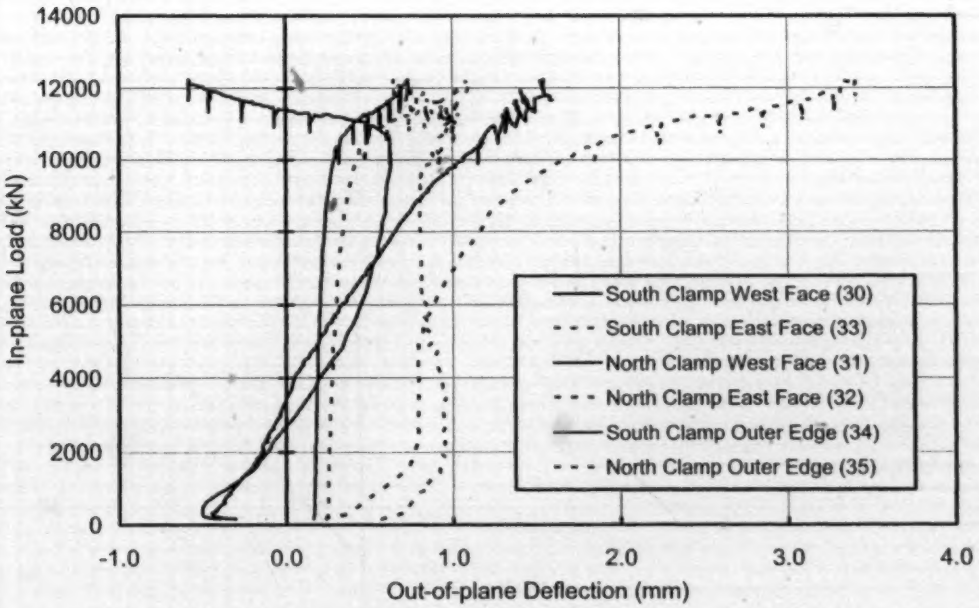

Figure 4.34: In-plane Load versus Edge Clamp Motion for SPS-3

5.0 Finite Element Analysis

A finite element model of the test specimens was developed using the general purpose finite element software ANSYS. The finite element analysis work was done by Intelligent Engineering. The model was developed and validated using the test results so that it can be used to expand the database of test results. This will aid in the development of reliable interaction curves for the design of SPS panels subjected to combined in-plane and out-of-plane loading. This chapter describes the development of the finite element model and presents a comparison of the test data with the finite element results in the elastic and ultimate loading regimes. It finally presents the interaction diagram for the SPS panels tested.

5.1 Finite Element Model Overview

5.1.1 Model Geometry and Material Properties

A finite element model was developed to match the nominal SPS test panel dimensions between the clamps, since the tests attempted to model perfectly fixed boundary conditions around the perimeter of the test panels. The plan dimensions of the finite element model were thus 1200 mm wide by 1800 mm tall, with 5 mm thick steel plates and a 32 mm thick elastomer core. A description of the model parameters used including element types, element layout and material properties is presented in Figure 5.1.

One full SPS panel from a test assembly was discretized using the solid element SOLID45 from ANSYS. A total of 50 elements across the width and 75 across the length were used in each layer. Each steel SPS faceplate was modeled by one layer of elements, and the core was modeled by four layers of elements through its thickness. The interface between the steel and the elastomer layers was assumed to be perfect with no possibility for delamination since delamination was not observed in the tests.

The stress versus strain curves used in the finite element model for the steel and for the elastomer are presented in Figure 5.2. The stress versus strain curve for steel was

obtained from the results of the ancillary tests performed on tension coupons from the actual panel steel used. This is a true stress versus true strain curve; thus, the high stress and strain at steel rupture shown on the plot were calculated by measuring the cross section of a failed coupon and using this area to calculate the rupture stress and strain values. The elastomer properties used for the core were obtained from earlier tests on elastomer conducted by Intelligent Engineering. A multi-linear stress versus strain curve with isotropic hardening model was used for the analysis.

5.1.2 Kinematic Boundary Conditions

The kinematic boundary conditions used in the model are shown in Figure 5.1. Although the geometry, material properties and modeling parameters of all the finite element models were identical, there were two slightly different sets of boundary conditions applied. It was decided that the boundary conditions used for runs to generate the interaction diagram should consist of perfect rotational restraints around the plate perimeter. The model with these boundary conditions was labelled finite element analysis Version 1. For a direct comparison between the finite element analysis and the test results a theoretical case with slightly softer lateral edge restraints was used, labelled as finite element analysis Version 2. The softer edge restraint was modeled to account for the in-plane expansion that might have taken place during the tests because of limited friction between the edge bearings and the test specimens in the lateral direction and the stiffness of the spacer bars. These two versions of kinematic boundary conditions are described below.

The Version 1 finite element model, used to generate the theoretical interaction diagram, had its entire perimeter fixed against translation in the transverse (x-) and out-of-plane (z) directions and restrained against rotation about all x-, y- and z- axes (refer to Figure 5.1). The nodes along the two unloaded (vertical) edges were free to move in the y- direction. All the nodes along the top loaded edge were coupled in the y- direction such that they were allowed to translate in the y- direction, but all by the same amount. The nodes along the bottom edge were fully restrained in the y- direction, which, combined with the top coupling, forced the top and bottom edges to remain straight and parallel during loading.

The Version 2 finite element model, used for comparison with the test results, was identical to Version 1 with the exception of the two vertical 1800 mm long panel edges. The lateral restraints (in the x-direction) in Version 1 were replaced by spring restraints to allow partial lateral movement of the panel edges. This is believed to better represent the actual test specimens, which were restrained in the x-direction by the in-plane bending stiffness of the panel edge spacer bars. Presuming that the roller bearings slip in the lateral direction, then it was the shear stiffness of the adhesive that governed how much load was transferred from the SPS to the panel edge spacer bars, thus this was the factor used to estimate the value for the spring constant. Based on the estimated adhesive shear stiffness and the glued contaet area between the edge spacer bar and the SPS, a spring coefficient of 400 N/mm per millimetre of edge length was obtained.

5.1.3 Loading Conditions

There were a total of 21 different analyses conducted using the finite element models, eight of them using finite element analysis Version 1 boundary conditions and 13 using Version 2. Table 5.1 lists all of the analyses done. The sequence and method in which the loads were applied are described in Figure 5.1. The first load step for each model was the application of the lateral pressure to the SPS faceplate. In the model cases of axial load only, there was still a 2 kPa lateral pressure applied to the SPS faceplate to account for initial imperfections that would be present in the actual test specimens. The second load step for each model consisted of a forced in-plane displacement applied to generate the desired level of in-plane load. This level of applied in-plane displacement is listed in Table 5.1 for all the finite element load cases run.

5.2 Results of Elastic Analysis – Comparison of the Finite Element Analysis Results with the Test Results

A finite element model was analysed for each of the five load combinations in the elastic range and data was obtained from points on the finite element model that corresponded to the locations of the strain rosettes and LVDT's on the test panels. Tables 5.2 through 5.4 summarize the results from the finite element Version 2 model load cases run in the

elastic range, and compare these results directly to the results obtained from the tests. The load levels at which the comparisons are made are listed in the Tables. Because there were a total of six SPS panels tested under the same loading regime in the elastic range, an estimate of the variation in the test data was obtained and is presented for each parameter as the coefficient of variation (COV) of the test results for that parameter. The number of test readings used to determine each test average and COV value are listed in square brackets in the heading for each parameter. The difference between the finite element value and the test average is also taken, then divided by the test average to get a value for the variation between the finite element analysis result and the test average result. This value is presented in the "COV Difference FEA vs Test" column of Tables 5.2 through 5.4. Also presented is the test-to-predicted ratio for all results. The results presented in the Tables are discussed in detail in the following sections.

5.2.1 Load Case 1 – 7200 kN Axial Load and No Lateral Pressure

Table 5.2 compares the finite element analysis results with the data obtained during the elastic test for the load case of in-plane compression only. All the analysis results are within one standard deviation of their respective test results except for the value of in-plane deflection. The average test in-plane deflection was 50% greater than the finite element analysis result, which corresponds to approximately 1 mm greater deflection in the test than in the finite element analysis. This extra 1 mm is attributed to initial seating between the edge restraints and the SPS panels. In-plane deflections for subsequent load cases compare more favourably. The vertical strains were on average 19% higher for the test results than for the finite element model and the von Mises stress at the panel top and bottom points was 30% higher in the test results than in the model. The von Mises stress at the panel edges and midpoint compare more closely between test and model, with test to predicted ratios of 0.95 and 1.06, respectively.

5.2.2 Load Case 2 – 280 kPa Lateral Pressure and No Axial Load

Table 5.3 compares the finite element analysis results with the test results for the pressure only elastic load case. The finite element model shows compressive strains at the top and edge boundaries that are about two times larger than the corresponding strains in the test

specimens. On the other hand, tension strains at the panel midpoint are 60% greater in the test than in the finite element model. The von Mises stresses exhibit a similar trend, with the boundary stresses being much larger in the finite element model than in the test, and the mid panel stress being greater in the test than in the finite element analysis. Out-of-plane deflections of the panel midpoint and quarter point were 50% larger in the test than in the finite element model. From these results, it is apparent that the boundary conditions on the test specimens were less stiff than the finite element model boundary conditions.

When measuring strains at the top and edge boundaries, the perfect fixity of the finite element model against edge rotation and out-of-plane motion creates high strains at the boundaries. Although the clamps remained very rigid during loading as shown in section 4.3 there was still opportunity for some movement and initial seating of the test specimens within the clamps during the application of the transverse pressure. Unlike the finite element model, the edges of the test specimens were not restrained against shear deformation. The overall result of this was a softer boundary response with lower boundary strain in the test than in the finite element model. In addition, the initial edge seating in the test allowed very slight edge rotation of the SPS inside the clamps, resulting in out-of-plane deflections on the test specimens at mid panel being between 2 mm to 2.5 mm larger than those of the finite element model at the maximum elastic range pressure of 276 kPa.

The softer test boundary conditions also explain why the strains and the von Mises stresses at mid panel are lower in the finite element models than in the tests. The extra stiffness in the finite element model boundaries reduces out-of-plane deflection, resulting in a lower curvature in the central region of the finite element model under pressure.

5.2.3 Load Cases of (5400 kN, 70 kPa), (3600 kN, 140 kPa), (1800 kN, 210 kPa)

Table 5.4 presents a comparison of the finite element analysis results with the test results for all three intermediate elastic load cases. It should be noted that as the pressure to in-plane load ratio becomes smaller, the von Mises stresses from the finite element analysis match those of the test results more closely, implying that at low pressures the effect of

the stress concentration near the boundaries is less severe. However, the boundary stresses are still greater in the finite element model than in the test while the mid panel stresses are smaller in the finite element model than in the test.

Out-of-plane displacements are still between 0.5 mm and 2.5 mm larger in the test than in the finite element model, with the difference being smaller as the pressure is reduced. In-plane deflections obtained from the finite element analysis are in good agreement with the test results, with all results falling within one standard deviation of each other.

5.3 Loading to Ultimate – Comparison of Finite Element Analysis with Test Results

5.3.1 In-plane Deflections

A finite element analysis of the Version 2 model (see Figure 5.1) was conducted for each of the load cases tested, as shown in Table 5.1. Figure 5.3 shows a plot of in-plane load versus in-plane deflection for all three tests and their respective finite element models. The in-plane deflection data was taken as the average of the in-plane deflections recorded by LVDT channels 36 through 39 shown in Figure 3.35. The curves plotted for the test results were adjusted to lie on the static points recorded during testing. In addition, the in-plane load values for all curves were normalized by dividing by the in-plane load required to yield the entire cross-section (P_Y) for each case. The value of P_Y for the test specimens was calculated using the cross-sectional area of two SPS panels of 1470 mm width, and included the edge spacer bar steel area. The value of P_Y for the finite element model was calculated using one SPS panel of 1200 mm width.

In all three cases, the finite element models hold their initial axial stiffness to higher levels of in-plane load than the test specimens. The test specimens however, do exhibit slightly higher in-plane resistance in the order of about 3% greater total capacity once the vertical deflection of the panel progresses past the 10 mm point, equivalent to about 0.5% axial strain. Although the finite element analyses were run to 50 mm axial displacement, for comparison purposes the plot only extends to the point where the tests were stopped.

5.3.2 Out-of-plane Deflections

Figure 5.4 presents the out-of-plane deflection at the panel mid points for all three tests and finite element models. The data were recorded for the tests using LVDT channels 25 and 28 shown in Figure 3.35. Note that each test curve starts at a different out-of-plane displacement depending on the test internal pressure. The value of this initial out-of-plane deflection was a result of the lateral pressure prior to application of the in-plane load. This initial out-of-plane deflection value resulting from lateral pressure differed between the tests and the finite element models. The values are presented for both the test results and finite element results in Table 5.5, including test-to-predicted ratios. To make comparing the results between the finite element model and tests easier for the in-plane loading range, each of the out-of-plane displacement curves for the test results were translated horizontally to match the starting points of their respective finite element curves. This horizontal shift was done by simply taking the difference between the initial test deflection value and initial finite element deflection value, and then subtracting this difference from all deflection values in the test curve. No change in shape of the test curves resulted from this shift. Note that this translation is required only for this particular finite element model, and is done only for ease of visual comparison of the load deflection results in the in-plane loading range.

The load versus deflection behaviour of the test specimens and the finite element models is very similar for all three tests throughout the in-plane loading range of the tests. This includes the test for SPS-1 at 207 kPa, in which the panel midpoint buckled back in toward the transverse pressure at about 13 MN of in-plane load. This can be seen in Figure 5.4, as the load-deflection curves for SPS-1 indicate a displacement in the negative direction at load levels beyond 13MN.

The out-of-plane deflection of the panel quarter points is presented in Figure 5.5 for all three tests and finite element models. The test data presented are the average of LVDT channels 24, 26, 27 and 29 shown in Figure 3.35. The test curves were shifted horizontally in the same manner as for Figure 5.4, with the initial deflections under

transverse pressure provided in Table 5.5. Much like at the panel midpoint, the predicted load versus deflection behaviour at the quarter points is very similar between that observed in the tests throughout the in-plane loading range. At both the mid and quarter points of the panel, virtually no out-of-plane motion occurs until the in-plane load reaches the point where the linear elastic portion ends on the respective in-plane load versus in-plane deflection curve (see Figure 5.3).

Although the out-of-plane deflection curves indicate similar behaviour for both the tests and the finite element models in the in-plane loading range, there is a substantial difference in deflections under lateral pressure only. Table 5.5 indicates that in all cases the out-of-plane deflections of the test specimens were from 50% to 65% greater than the corresponding finite element models under lateral pressure only. This is indicative of a softer boundary condition in the tests, likely a result of unrestrained shear deformation of the SPS edges, as well as small opening of the perimeter clamps and seating of the SPS against the roller assemblies and clamp faces as the lateral pressure is applied.

5.3.3 Von Mises Equivalent Strains

Figures 5.6, 5.7 and 5.8 present the relationships between in-plane load and von Mises strains calculated from the recorded strains for the 207 kPa, 415 kPa and 690 kPa tests. Each plot shows the von Mises strains at the strain rosette locations at the panel top, edge and midpoint respectively. The von Mises strain for the test curves in Figure 5.6 is the average of readings from the strain rosettes at the top and bottom panel boundaries, corresponding to channels (40,45,50), (44,49,54), (55,60,65) and (59,64,69) in Figure 3.32. Each set of brackets encloses the three channels for each of the four top and bottom rosettes. The von Mises strains for the rosettes at the edge boundaries plotted in Figure 5.7 correspond to the average of channels (41,46,51), (43,48,53), (56,61,66) and (58,63,68) in Figure 3.32. Likewise, Figure 5.8 plots the average von Mises strain for the rosettes at the panel midpoints and corresponds to channels (42,47,52) and (57,62,67). Symmetry was assumed about a vertical line through the panel mid width and a horizontal line through the panel mid height. Thus for each test, the edge gauge reading used in the plots is the average of all four edge gauges (two gauges on each of the two

panels) and the top and bottom gauge reading is the average of the two top and two bottom gauges.

In the elastic range, the von Mises stresses were compared between the finite element results and the test results. In the ultimate loading range however, the von Mises equivalent strain is the parameter compared. The finite element program ANSYS calculates the von Mises stresses using the elastic portion of the strain present, so for the ultimate loading case, it was necessary to calculate equivalent von Mises strains using Equation set 4.1 presented in Section 4.1.1.

The starting von Mises strain values shown in Figures 5.6 to 5.8 for each test at zero in-plane load are the strains resulting from the application of the initial transverse pressure. These initial von Mises strains, however, differed between the tests and their respective finite element models. Therefore, just as was done for the out-of-plane displacements, the strain curves from the test results were horizontally translated to match the starting strain values of their corresponding finite element model curves. The initial von Mises strains under transverse pressure for all tests and finite element models are provided in Table 5.5.

Based on Figures 5.6 through 5.8, the von Mises strains for the test conducted at a transverse pressure of 207 kPa show the best correlation with the corresponding finite element model strains at all three panel points where data were recorded. As the transverse pressure increases, the top, bottom and edge strains in the finite element model stray from the corresponding test strains at increasingly lower levels of in-plane load. At 690 kPa for a given in-plane load level, the top/bottom and edge strains in the finite element model are higher than in the test results. This effect is most pronounced in the strains present at the top/bottom panel point and is similar to the effect that occurred in the transverse pressure load case from the elastic range of tests described in Section 5.2.2.

Comparing the top and bottom and edge strains in Table 5.5 for the tests and finite element model under lateral pressure only, in all cases the finite element boundary strains

are much higher than the corresponding test boundary strains, with test-to-predicted ratios from 0.72 down to 0.10. Strains at mid panel however, are much closer between the tests and the model, with test-to-predicted ratios of 0.88 to 1.01. This further reinforces that the test specimens had softer boundary conditions than the finite element model, since the perfect rotational stiffness at the boundaries in the finite element model causes regions of very high strain at these locations.

5.4 Interaction Diagram – Comparison of finite element analysis with Test Results

The final step in the finite element investigation was to generate an interaction diagram for SPS panels of the same geometry and material properties as the test specimens. As presented in Table 5.1, eight load combinations were run for each of the Version 1 and Version 2 finite element models. It is recalled that the Version 1 model had the perfectly fixed boundary condition whereas Version 2 had softer lateral edge restraints (see Section 5.1 and Figure 5.1). Note that although all the interaction diagrams presented are normalized, they are still only applicable to SPS specimens of the geometry and material properties similar to that of the test specimens. Panels of different aspect ratios in particular would require further analyses to generate appropriate interaction diagrams.

5.4.1 Methods to Determine Interaction Points

As for the test data, there were two methods used for determining the values of the interaction points from the in-plane load versus in-plane deflection plots generated for each load case. The 0.2% offset method is described in ASTM A370-05, "Standard Test Methods and Definitions for Mechanical Testing of Steel Products". An example of the use of this method is illustrated in Figure 5.9 for the normalized in-plane load versus in-plane deflection plot of SPS-1.

The second method used, also from ASTM A370-05, is described as the "Total Extension under Load Method". For steel yield strengths less than 550 MPa, an allowable extension of 0.5% strain is recommended. Note that for the case of these tests, this 0.5% strain value will be an allowable compressive deflection and not an allowable extension, thus

this method is referred to as the "allowable deflection method" in the following. Figure 5.10 illustrates how this allowable deflection method is used to determine the in-plane load for the interaction point from the normalized in-plane load versus in-plane deflection plot of SPS-1. A vertical line is drawn at a 0.5% strain offset from the point of zero in-plane load. The intersection of this line with the load deflection curve provides the in-plane load used for the interaction point for this model.

5.4.2 Interaction Results for Finite Element Model Version 1

The eight interaction points for the finite element model with the ideal rigid boundary conditions were all determined from the in-plane load versus in-plane deflection plots presented in Figure 5.11. It is apparent from these plots that the panel initial axial stiffness reduces as the transverse pressure level increases at decreasing levels of in-plane load. With no transverse pressure, the model reaches its maximum in-plane capacity at about 9 mm of in-plane deflection. The in-plane load carrying capacity then reduces slightly with increasing in-plane deflection. At the 207 kPa and 415 kPa transverse pressure, the SPS models maintain their initial axial stiffness beyond 10 MN of in-plane load. They reach their in-plane peak load at a deflection of about 5 mm, experience a slight loss of axial capacity over the next 15 mm of in-plane deflection, and then gradually start to regain some capacity as the in-plane deflections increase to 50 mm. For the higher transverse pressures, the models do not exhibit a peak load. The load versus deflection curves show a more gradual decrease in axial stiffness from the initial axial stiffness that occurs below 3 mm of in-plane deflection, to a much lower but still positive stiffness in the plastic deformation range starting at in-plane deflections of about 10 mm. It is interesting to note that at a deflection of 50 mm the panel with a transverse pressure of 207 kPa has only about 25% more in-plane load carrying capacity than does the panel loaded with a transverse pressure of 1700 kPa.

It should also be noted that, as the transverse pressure is increased, the panels develop increasing tensile in-plane stresses before the in-plane loading is applied. This is a result of the in-plane restraint provided to the panels while the transverse pressure is applied. As out-of-plane pressure and resulting out-of-plane deflections increase, membrane

action develops in the panels. Therefore, to obtain the interaction points, the load versus deflection curves were shifted horizontally so that the point of zero in-plane load corresponded to the point of zero in-plane deflection.

Figure 5.12 presents the interaction diagrams obtained for the finite element Version 1 model using the 0.2% offset method and the 0.5% allowable deflection method. The results from the three tests are also plotted for comparison purposes. The interaction diagrams have been non-dimensionalized as in Figure 4.26. The transverse pressure, q, was divided by the plastic collapse pressure calculated using yield line theory, and the in-plane load was divided by the theoretical in-plane load required to yield the entire panel cross-section. This procedure was explained in section 4.2.5.

Both the 0.2% offset and 0.5% allowable deflection methods produce similar interaction curves for normalized pressure values less than about 0.5. As the normalized pressure increases, the interaction curve obtained using the 0.2% offset method becomes more conservative. In-plane load values at a normalized pressure of 1.0 are about 20% less for the 0.2% method than for the 0.5% allowable deflection method. The three test results fall very close to the interaction curves developed using the finite element model. The test-to-predicted ratios for the axial load capacity are 0.99, 1.00 and 0.99 for SPS-1, 2 and 3, respectively. The test results obtained with the 0.2% offset method follow the same trend as observed for the finite element analysis but all show about 5% lower in-plane load capacity than the finite element analysis at the same pressures. Test-to-predicted ratios using the 0.2% offset method are 0.95, 0.96 and 0.93 for SPS-1, 2 and 3 respectively.

5.4.3 Interaction Results for Finite Element Model Version 2

Interaction diagrams derived using the finite element analysis Version 2 model are presented in this section.

Figure 5.13 shows the in-plane load versus in-plane deflection for all eight Version 2 finite element model cases. As for the Version 1 model, these load versus deflection

curves were used to determine points on the interaction curves using the two methods outlined in Section 5.4.1. The trends in the in-plane load versus in-plane deflection response for the Version 2 model are virtually identical to those discussed in the previous section for the Version 1 models. One distinct difference is the load versus deflection response for the zero transverse pressure case. The Version 1 case reached the peak in-plane load at approximately 9 mm of in-plane deflection, whereas the version 2 case does not reach its axial capacity until 25 mm of in-plane deflection. However, the peak in-plane load value for Version 2 is about 2% higher than the peak load obtained from the Version 1 model. The Version 2 models also attain lower values of in-plane load at the end of the initial linear elastic region of their load versus deflection curves than do the Version 1 models for the transverse load cases of 207 kPa and 415 kPa. The load versus deflection curves for both versions are very similar to each other for the higher transverse pressure cases of 690 kPa through 1700 kPa. This is demonstrated clearly in section 5.4.4 where the interaction diagrams of both versions are compared.

Figure 5.14 presents the non-dimensionalized interaction diagrams for the finite element Version 2 model, again using both the 0.2% offset method and the 0.5% allowable deflection method (ASTM A370-05). The results from the three tests are also plotted for comparison. In this case the offset method produces a more conservative diagram than does the 0.5% allowable deflection method. In the normalized transverse pressure region between 0 and 0.2, the 0.2% offset method predicts in-plane load values that are in the range of 1% to 2% lower than those predicted by the allowable deflection method. Between normalized pressures of 0.2 to 0.5 the two methods predict virtually identical load points. Above normalized pressures of 0.5, the in-plane load values predicted by the 0.2% offset method become increasingly smaller than the values from the allowable deflection method, with the offset method values being 32% lower than the allowable method values at the highest plotted normalized pressure case of 1.1.

The finite element results show that the theoretical panels can carry more pressure than the theoretical upper bound collapse pressure calculated using yield line theory. Recall however that this upper bound pressure is based on yield lines forming when the stress in

the steel reaches the yield point of 352 MPa as determined from the tension coupon tests. There is more capacity available however, as these same tension coupon tests indicated an ultimate steel strength of 575 MPa, 63% greater than the yield strength. Thus even though yield lines may have formed in a pattern sufficient to allow collapse, no collapse will occur since the steel still has a vast reserve of capacity prior to reaching ultimate strength and finally rupture.

The interaction points from the test results compare very favourably to the finite element Version 2 model. As for the Version 1 results, the test-to-predicted ratios are closer to 1.0 when the allowable deflection method is used to obtain the interaction points. The ratios using the allowable deflection method are 1.01, 0.99 and 0.99 for SPS-1, 2 and 3, respectively. The test-to-predicted ratios using the 0.2% offset method are 1.00, 0.96 and 0.95 for SPS-1, 2 and 3, respectively.

5.4.4 Comparison of Interaction Results between Finite Element Model Version 1 and Version 2

Figure 5.15 presents the interaction diagrams for both finite element versions and the test results, with all data points obtained using the 0.2% offset method. Between normalized transverse pressures of 0 and 0.25, Version 1 predicts higher strength than does Version 2. The maximum difference occurs at the zero transverse pressure level, where Version 1 predicts 10% higher in-plane load capacity than Version 2. This is primarily due to the nature of the in-plane load versus in-plane deflection plots for the two cases (see Figures 5.11 and 5.13). Recall from the previous section that finite element Version 2 actually predicted 2% more in-plane load capacity than Version 1, but Version 2 peaked at 25 mm of in-plane displacement compared to 9 mm for Version 1. Since the interaction point is taken at about 7 mm of displacement, the Version 1 model has more axial capacity at this deflection point than does the Version 2 model. In the normalized transverse pressure region between 0.25 and 0.8, the Version 1 and Version 2 models predict virtually identical results. As the normalized transverse pressure increases beyond 0.8, Version 1

again predicts in-plane loads that are between 5% and 7% higher than Version 2 for a given transverse pressure level.

Figure 5.16 shows the interaction diagrams for finite element model Version 1, finite element model Version 2 and the test results, with all data points obtained using the 0.5% allowable deflection method. In the normalized transverse pressure region between 0 and 0.25, Version 1 again predicts higher values of in-plane load for a given pressure than does Version 2, with the largest difference of 10% occurring at the zero transverse pressure level. The reasons for this were presented previously. Throughout the rest of the transverse pressure range, the two finite element model versions predict near identical results. Test data is again shown for reference, with the test-to-predicted ratios for both the Version 1 and Version 2 models located in Section 5.4.2 and 5.4.3.

Using the 0.5% allowable deflection method, the test interaction values match both finite element versions very closely, with test-to-predicted values of 0.99, 1.00 and 0.99 using Version 1 results, and ratios of 1.01, 0.99 and 0.99 using Version 2 results. The load deflection behaviour of the test specimens compares better with Version 2 than with Version 1, thus overall it is concluded that the test results most closely match the behaviour of the Version 2 finite element model with the softer lateral edge restraints. Using the 0.2% offset method it is found that the Version 2 model interaction diagram matches the test results slightly better than Version 1. Test-to-predicted values for SPS-1, 2 and 3 using Version 2 are 1.00, 0.96 and 0.95 respectively, and ratios using the 0.2% method and Version 1 are 0.95, 0.96 and 0.93 for SPS-1, 2 and 3, respectively.

Table 5.1: Summary of Finite Element Analyses

Analyses for Comparison with Elastic Loading Range of Tests

{Run using Version 2 FEA model}

FE Model Name	Initial Transverse Pressure	In-plane Deformation Applied
FEA E-1	0 kPa	3.5 mm
FEA E-2	69 kPa	2.5 mm
FEA E-3	138 kPa	1.75 mm
FEA E-4	207 kPa	1.0 mm
FEA E-5	276 kPa	0 mm

Analyses for Comparison with Ultimate Loading Range of Tests

{Run using Version 2 FEA model}

FE Model Name	Initial Transverse Pressure	In-plane Deformation Applied
FEA U-1	207 kPa	50 mm
FEA U-2	415 kPa	50 mm
FEA U-3	690 kPa	50 mm

Analyses for Generating FEA Interaction Diagram using Theoretical Model

{Run using Version 1 FEA model}

FE Model Name	Initial Transverse Pressure	In-plane Deformation Applied
FEA ID-0	0 kPa	50 mm
FEA ID-1	207 kPa	50 mm
FEA ID-2	415 kPa	50 mm
FEA ID-3	690 kPa	50 mm
FEA ID-4	950 kPa	50 mm
FEA ID-5	1200 kPa	50 mm
FEA ID-6	1450 kPa	50 mm
FEA ID-7	1700 kPa	50 mm

Analyses for Filling in FEA Interaction Diagram using Version 2 Model

{Run using Version 2 FEA model}

FE Model Name	Initial Transverse Pressure	In-plane Deformation Applied
FEA U-0	0 kPa	50 mm
FEA U-4	950 kPa	50 mm
FEA U-5	1200 kPa	50 mm
FEA U-6	1450 kPa	50 mm
FEA U-7	1700 kPa	50 mm

Table 5.2: Comparison of Finite Element Analyses with Test Results for Elastic Load Combination of 7200 kN In-plane Load and No Lateral Pressure

	Test Average	FEA Result	Test COV	COV Difference FEA vs Test	Test to Predicted Ratio
In-plane Displacement (mm) [12]	2.860	1.910	13%	33%	1.50
Vertical Strain (microstrain) [30]	-1228	-1031	23%	16%	1.19
Von Mises Top/bottom Stress (MPa) [12]	257.2	197.9	27%	23%	1.30
Von Mises Edge Stress (MPa) [12]	194.8	204.9	7%	5%	0.95
Von Mises Midpanel Stress (MPa) [6]	228.8	215.6	9%	6%	1.06

(Number of test data point readings for each parameter shown in brackets [ ])

Table 5.3: Comparison of Finite Element Analyses with Test Results for Elastic Load Combination of 276 kPa Lateral Pressure and No In-plane Load

	Test Average	FEA Result	Test COV	COV Difference FEA vs Test	Test to Predicted Ratio
Mid Panel Horizontal Strain (microstrain) [6]	649	403	2%	38%	1.61
Mid Panel Vertical Strain (microstrain) [6]	314	196	8%	38%	1.60
Top/bottom Vertical Strain (microstrain) [12]	-558	-1029	18%	84%	0.54
Edge Horizontal Strain (microstrain) [12]	-508	-1109	27%	118%	0.46
Von Mises Top/bottom Stress (MPa) [12]	93.5	204.6	20%	119%	0.46
Von Mises Edge Stress (MPa) [12]	78.1	214.6	31%	175%	0.36
Von Mises Midpanel Stress (MPa) [6]	120.8	89.5	16%	26%	1.35
Mid Panel Out-of-plane Deflection (mm) [6]	7.411	4.937	4%	33%	1.50
Quarter Point Out-of-plane Deflection (mm) [12]	5.535	3.680	4%	34%	1.50

(Number of test data point readings for each parameter shown in brackets [ ])

Table 5.4: Comparison of Finite Element Analyses with Test Results for Three Intermediate Elastic Load Combinations

(a): Intermediate Load Combination 1: 800 kN, 210 kPa

	Test Average	FEA Result	Test COV	COV Difference FEA vs Test	Test to Predicted Ratio
Von Mises Top/bottom Stress (MPa) [12]	137.8	205.2	18%	49%	0.67
Von Mises Edge Stress (MPa) [12]	63.1	203.6	33%	223%	0.31
Von Mises Midpanel Stress (MPa) [6]	100.3	77.9	10%	22%	1.29
Mid Panel Out-of-plane Deflection (mm) [6]	6.049	3.766	10%	38%	1.61
Quarter Point Out-of-plane Deflection (mm) [12]	4.555	2.807	11%	38%	1.62
In-plane Displacement (mm) [12]	0.495	0.479	45%	3%	1.03

(Number of test data point readings for each parameter shown in brackets [ ])

(b): Intermediate Load Combination 2: 1600 kN, 140 kPa

	Test Average	FEA Result	Test COV	COV Difference FEA vs Test	Test to Predicted Ratio
Von Mises Top/bottom Stress (MPa) [12]	172.5	204.1	18%	18%	0.85
Von Mises Edge Stress (MPa) [12]	86.0	160.5	15%	87%	0.54
Von Mises Midpanel Stress (MPa) [6]	113.3	108.2	4%	5%	1.05
Mid Panel Out-of-plane Deflection (mm) [6]	4.147	2.547	15%	39%	1.63
Quarter Point Out-of-plane Deflection (mm) [12]	3.136	1.896	18%	40%	1.65
In-plane Displacement (mm) [12]	1.049	0.944	24%	10%	1.11

(Number of test data point readings for each parameter shown in brackets [ ])

(c): Intermediate Load Combination 3: 2400 kN, 70 kPa

	Test Average	FEA Result	Test COV	COV Difference FEA vs Test	Test to Predicted Ratio
Von Mises Top/bottom Stress (MPa) [12]	200.6	201.4	21%	0%	1.00
Von Mises Edge Stress (MPa) [12]	129.0	160.8	7%	25%	0.80
Von Mises Midpanel Stress (MPa) [6]	155.5	158.8	3%	2%	0.98
Mid Panel Out-of-plane Deflection (mm) [6]	1.926	1.283	35%	33%	1.50
Quarter Point Out-of-plane Deflection (mm) [12]	1.497	0.952	41%	36%	1.57
In-plane Displacement (mm) [12]	1.607	1.410	15%	12%	1.14

(Number of test data point readings for each parameter shown in brackets [ ])

Table 5.5: Comparison of Finite Element Analyses with Test Results for the Three Ultimate Load Cases after the Application of Initial Transverse Pressure but Prior to Application of In-plane Load

(a): SPS-1: 207 kPa Test

	Test Average	FEA Result	Test-to-Predicted Ratio
Midpanel Out-of-plane Deflection (mm)	5.48	3.62	1.51
Quarterpoint Out-of-plane Deflection (mm)	4.14	2.70	1.53
Von Mises Strain at Panel Top and Bottom (microstrain)	361	756	0.48
Von Mises Strain at Panel Edges (microstrain)	252	990	0.25
Von Mises Strain at Midpanel (microstrain)	290	330	0.88

(b): SPS-2: 415 kPa Test

	Test Average	FEA Result	Test-to-Predicted Ratio
Midpanel Out-of-plane Deflection (mm)	12.1	7.374	1.64
Quarterpoint Out-of-plane Deflection (mm)	9.08	5.492	1.65
Von Mises Strain at Panel Top and Bottom (microstrain)	904	1249	0.72
Von Mises Strain at Panel Edges (microstrain)	444	1580	0.28
Von Mises Strain at Midpanel (microstrain)	681.2	673	1.01

(c): SPS-3: 690 kPa Test

	Test Average	FEA Result	Test-to-Predicted Ratio
Midpanel Out-of-plane Deflection (mm)	19.6	12.8	1.54
Quarterpoint Out-of-plane Deflection (mm)	15.0	9.51	1.57
Von Mises Strain at Panel Top and Bottom (microstrain)	744	2259	0.33
Von Mises Strain at Panel Edges (microstrain)	360	3543	0.10
Von Mises Strain at Midpanel (microstrain)	1028	1089	0.94

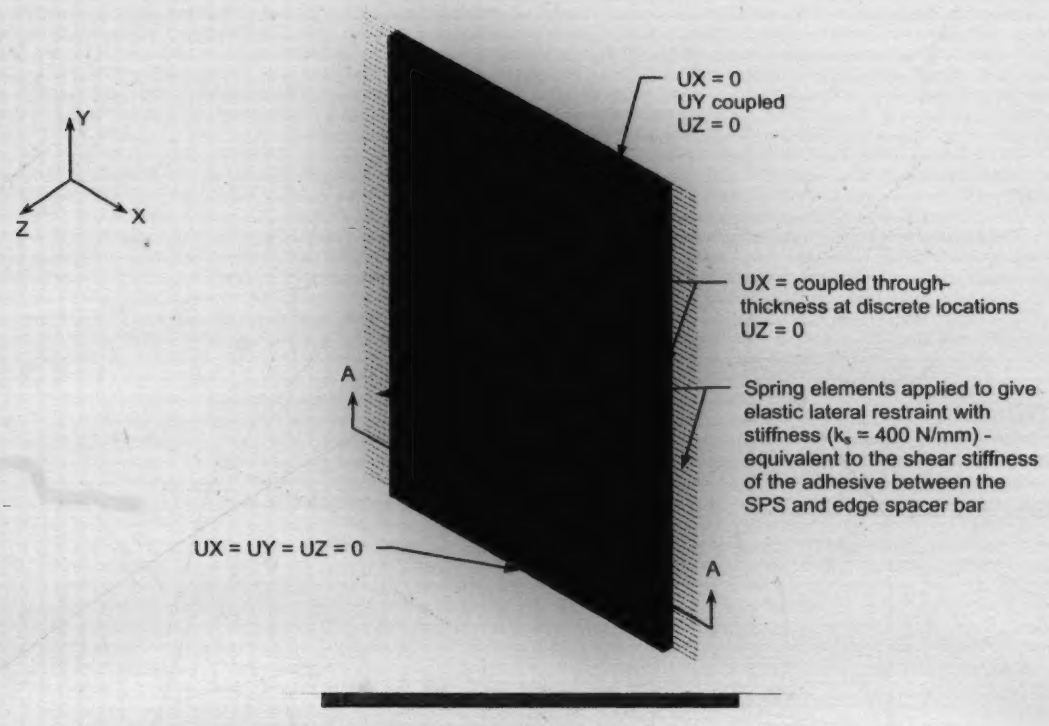
Y
Z
X
UX = 0
UY coupled
UZ = 0
UX = coupled through-thickness at discrete locations
UZ = 0
A
Spring elements applied to give elastic lateral restraint with stiffness (k_s = 400 N/mm) - equivalent to the shear stiffness of the adhesive between the SPS and edge spacer bar
UX = UY = UZ = 0
A

Section A-A

Loads:
First Load Step: Transverse loads applied to faceplate in first load step. Note that for zero transverse pressure a pressure of 2 kPa was applied to account for out-of-straightness.
Second Load Step: Axial compressive load applied as a displacement to the coupled set of nodes in UY direction.
Material & Model Properties
Steel (Solid Elements – SOLID45)
Multi-linear isotropic properties: see Figure 5.2
E = 199 290 MPa, ν = 0.3
Elastomer (Solid Elements – SOLID45)
Multi-linear isotropic properties - see Figure 5.2
E = 862 MPa, ν = 0.36
Springs (COMBIN14)
Number of Nodes = 26925
Number of Elements = 22350

Figure 5.1: Description of Finite Element Model

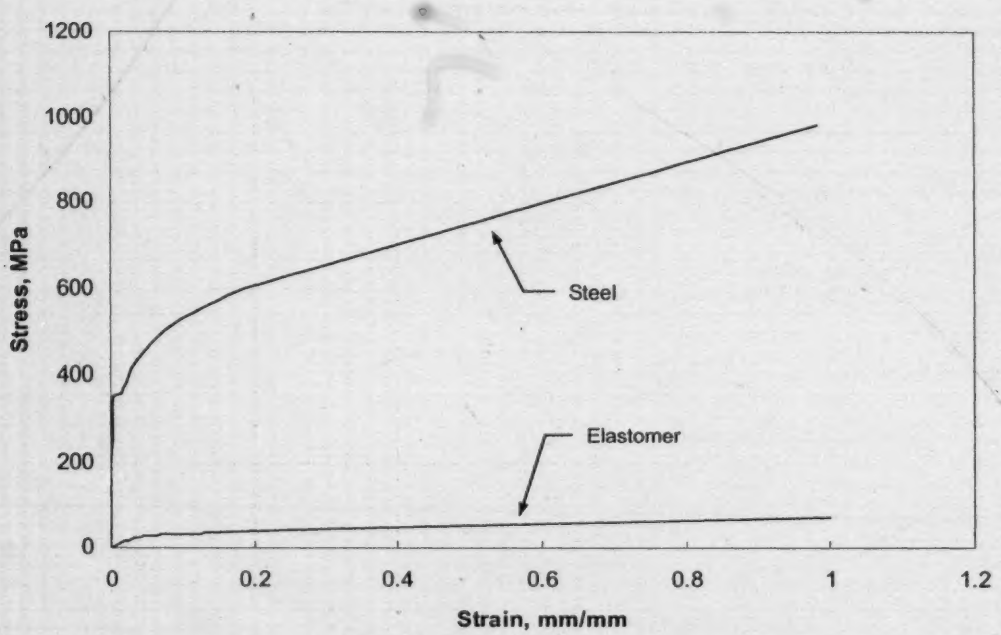

Figure 5.2: Steel and Elastomer Stress-Strain Curves Used in FE Models

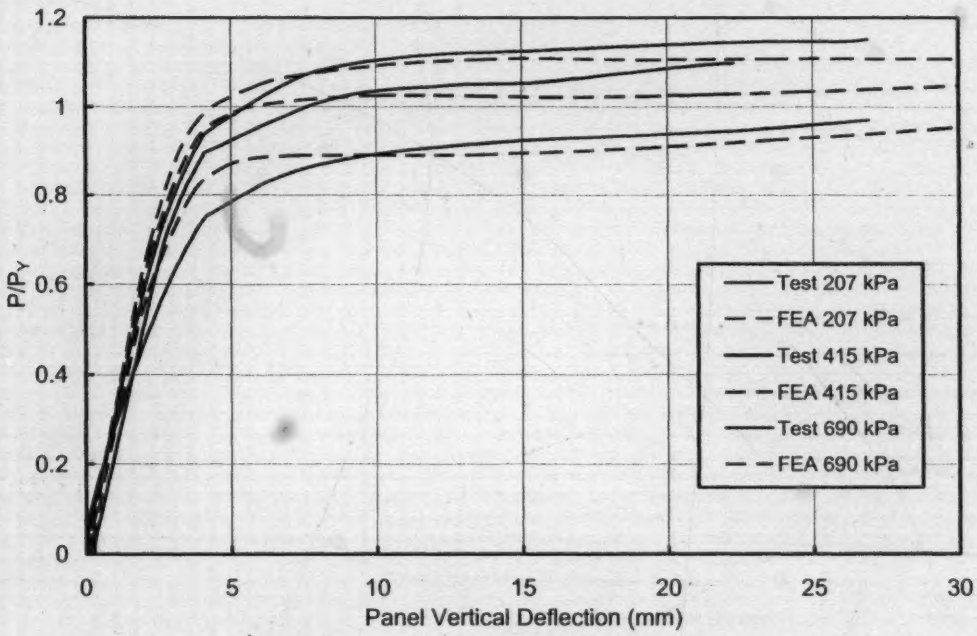

Figure 5.3: In-plane Load versus In-plane Deflection – FEA versus Test Results

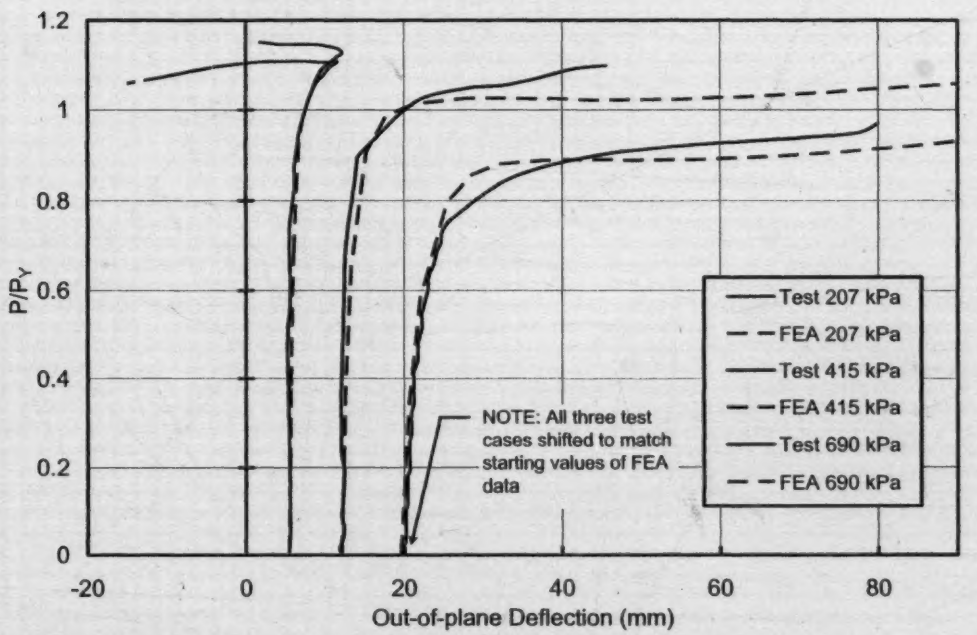

Figure 5.4: In-plane Load versus Out-of-plane Deflection of Panel Midpoint – FEA versus Test

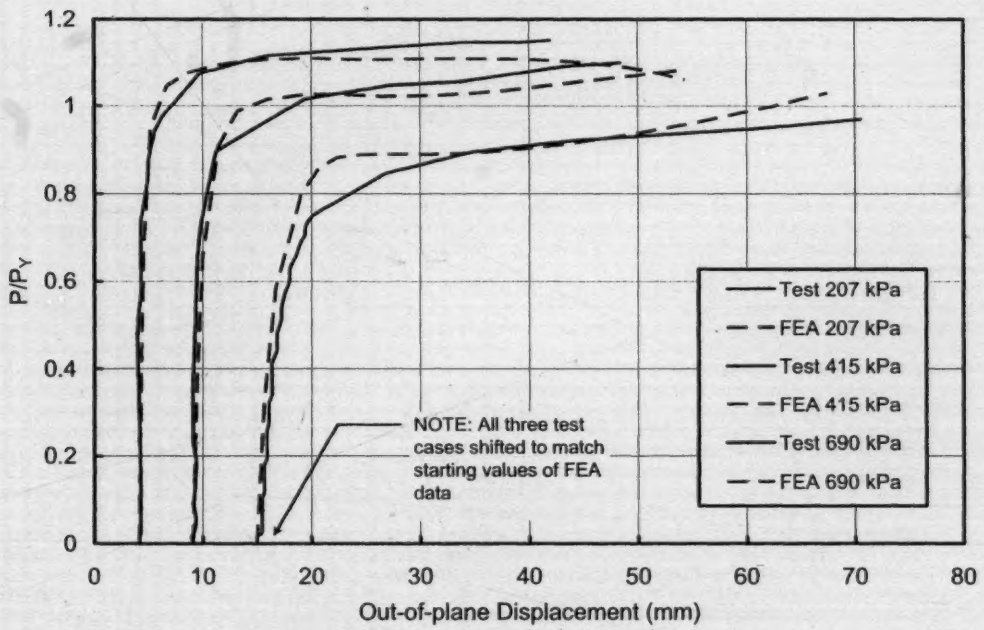

Figure 5.5: In-plane Load versus Out-of-plane Deflection at Panel Quarter Point – FEA versus Test

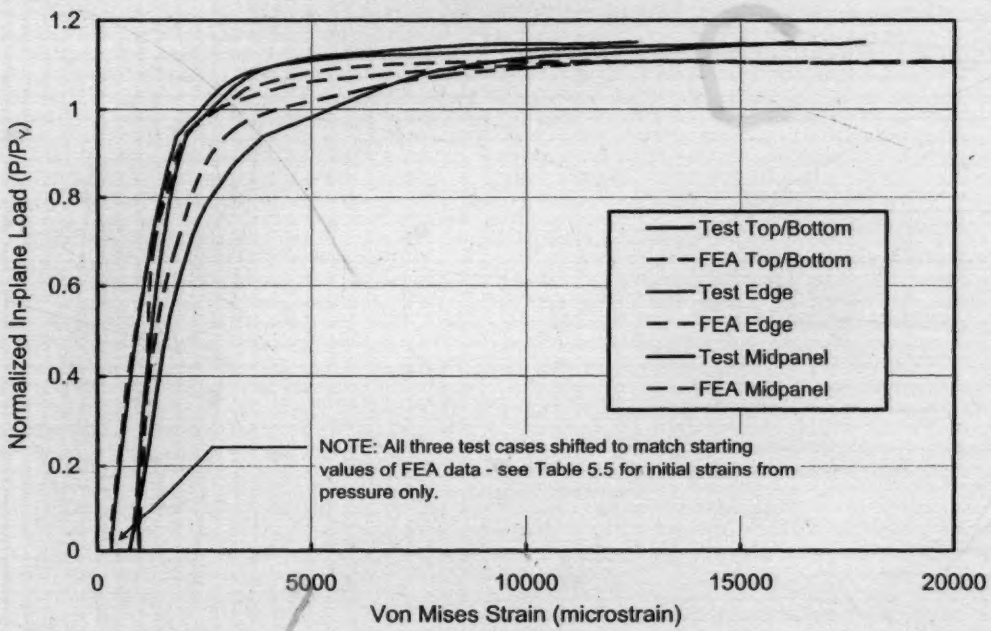

Figure 5.6: In-plane Load versus von Mises Strain for SPS-1 (207 kPa) – FEA versus Test

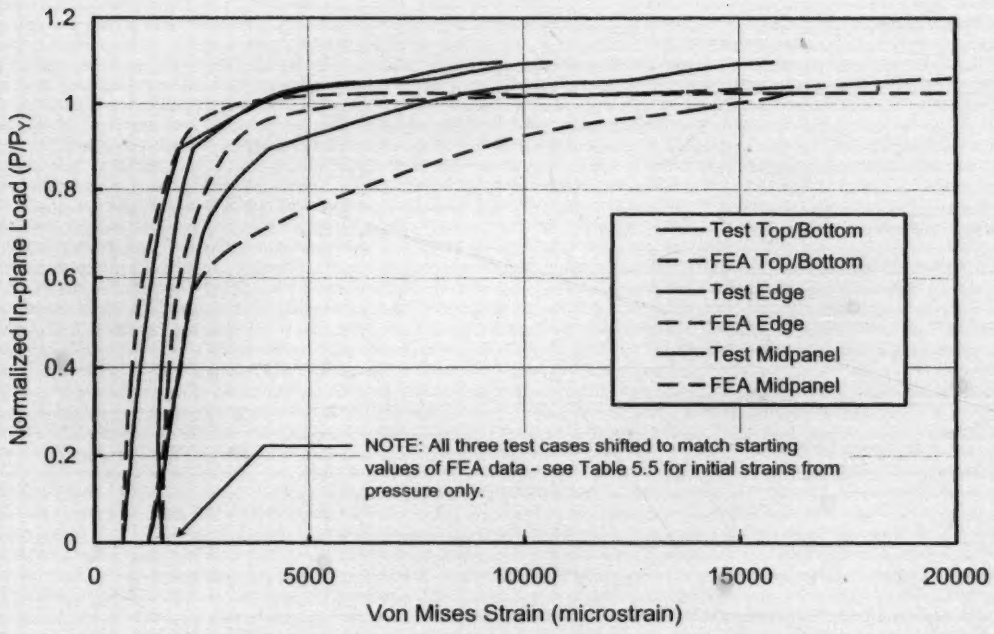

Figure 5.7: In-plane Load versus von Mises Strain for SPS-2 (415 kPa) – FEA versus Test

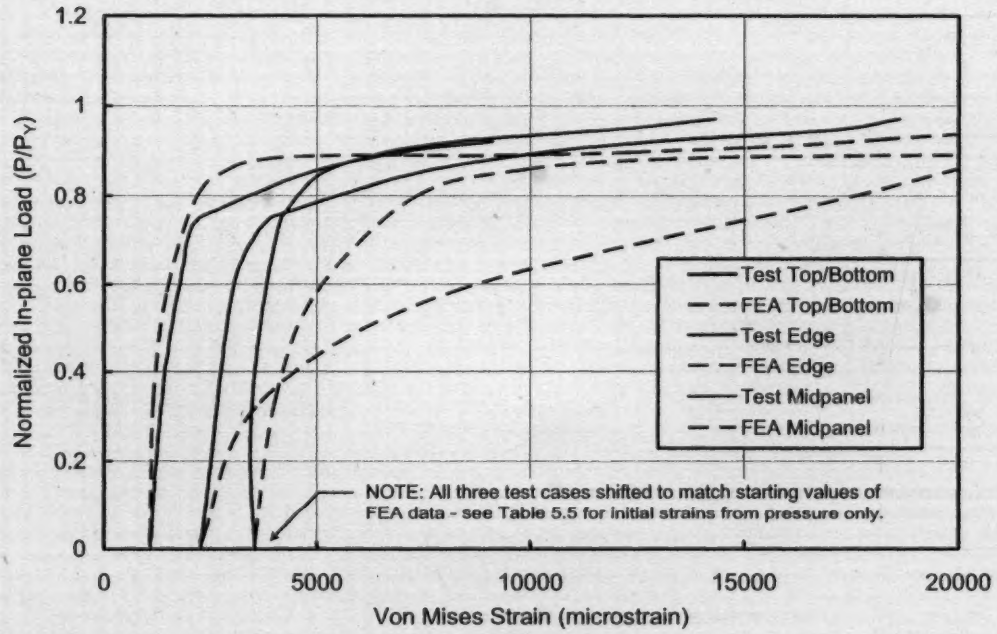

Figure 5.8: In-plane Load versus von Mises Strain for SPS-3 (690 kPa) – FEA versus Test

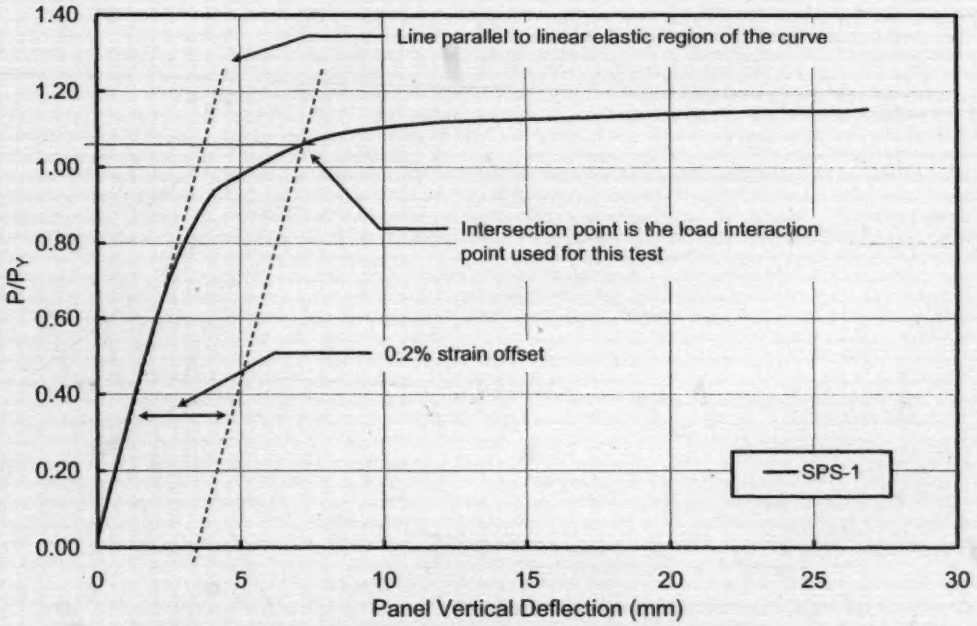

Figure 5.9: Determination of Interaction Point using 0.2% Strain Offset Method – SPS-1

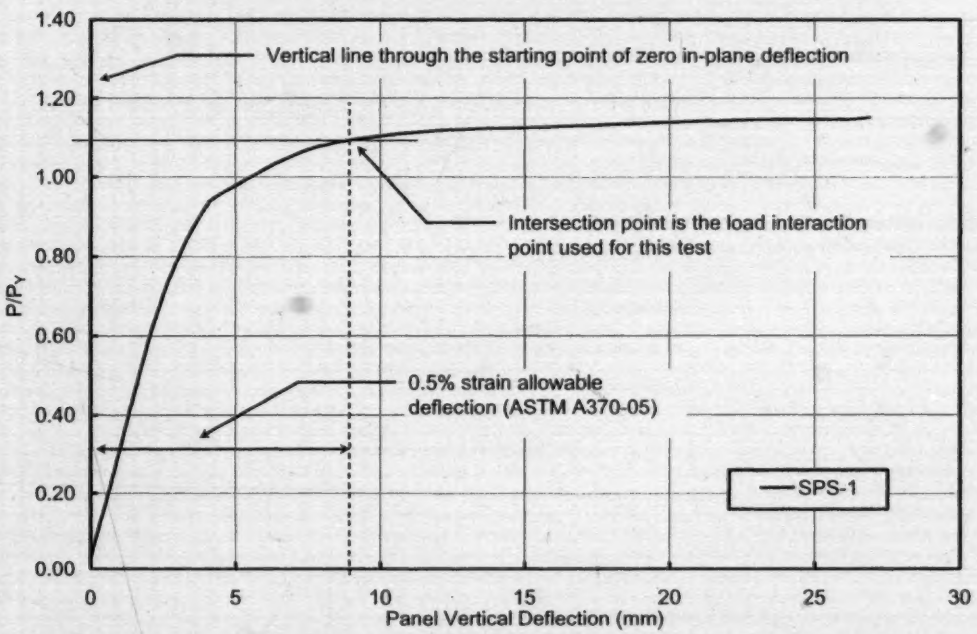

Figure 5.10: Determination of Interaction Point using 0.5% Allowable Deflection Method – SPS-1

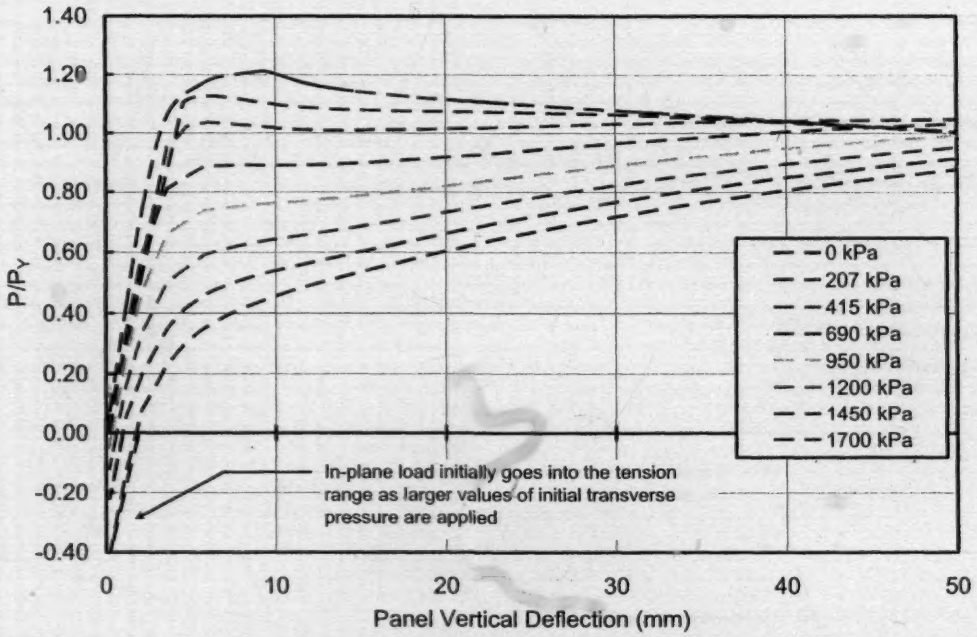

Figure 5.11: In-plane Load versus In-plane Deflection – Eight Load Cases for FEA Version 1 Model

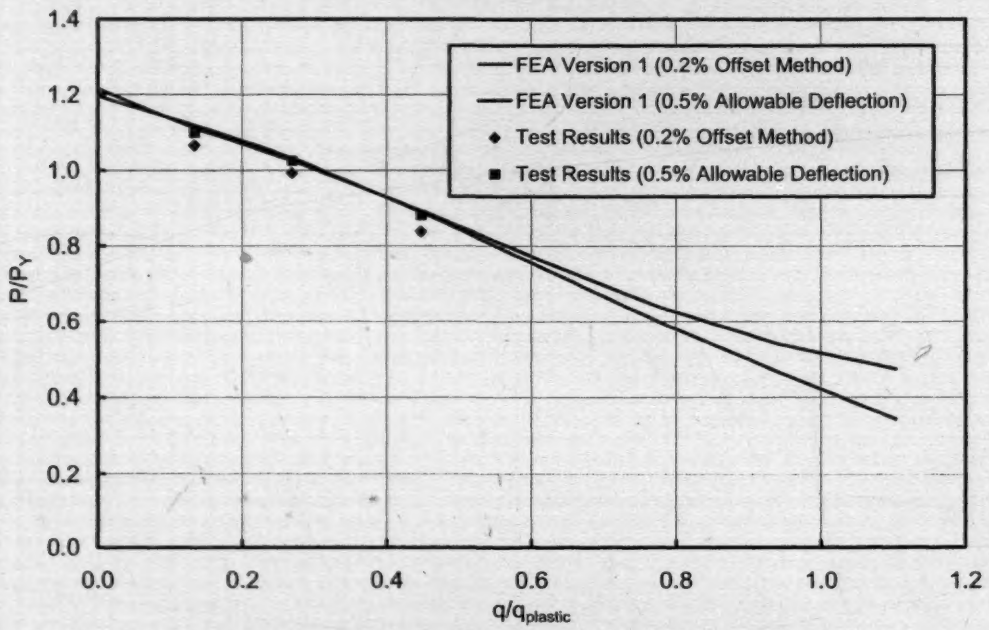

Figure 5.12: Interaction Diagram - FEA Version 1 and Test Results

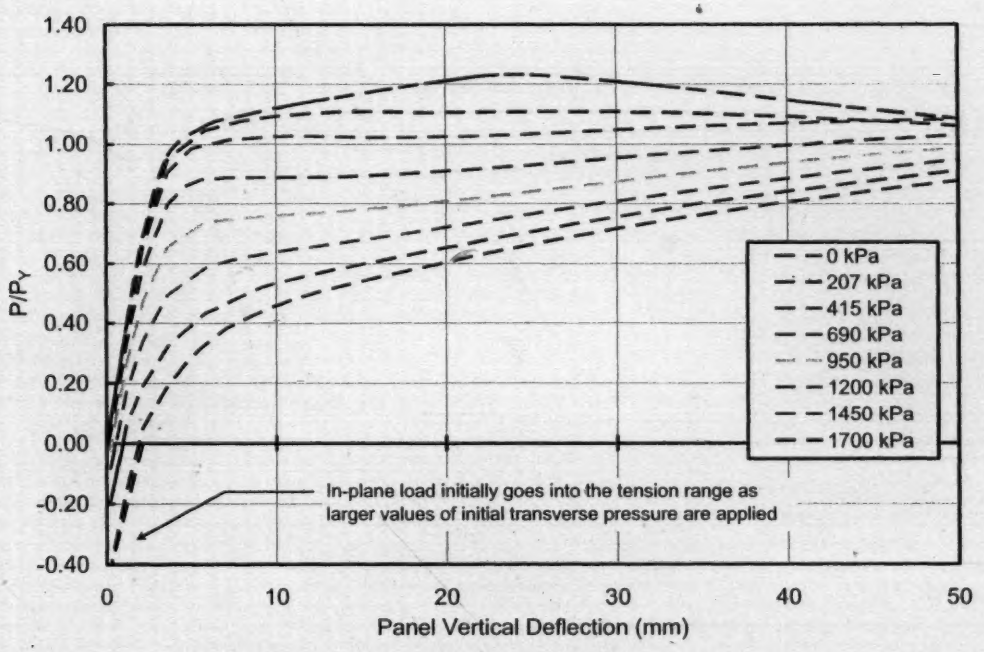

Figure 5.13: In-plane Load versus In-plane Deflection – Eight Load Cases for FEA Version 2 Model

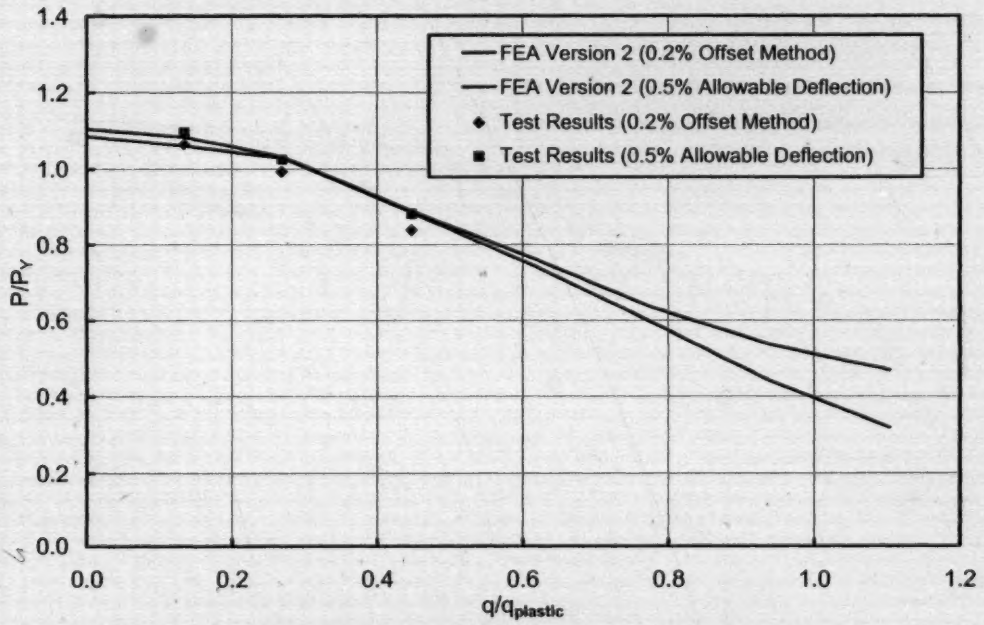

Figure 5.14: Interaction Diagram - FEA Version 2 and Test Results

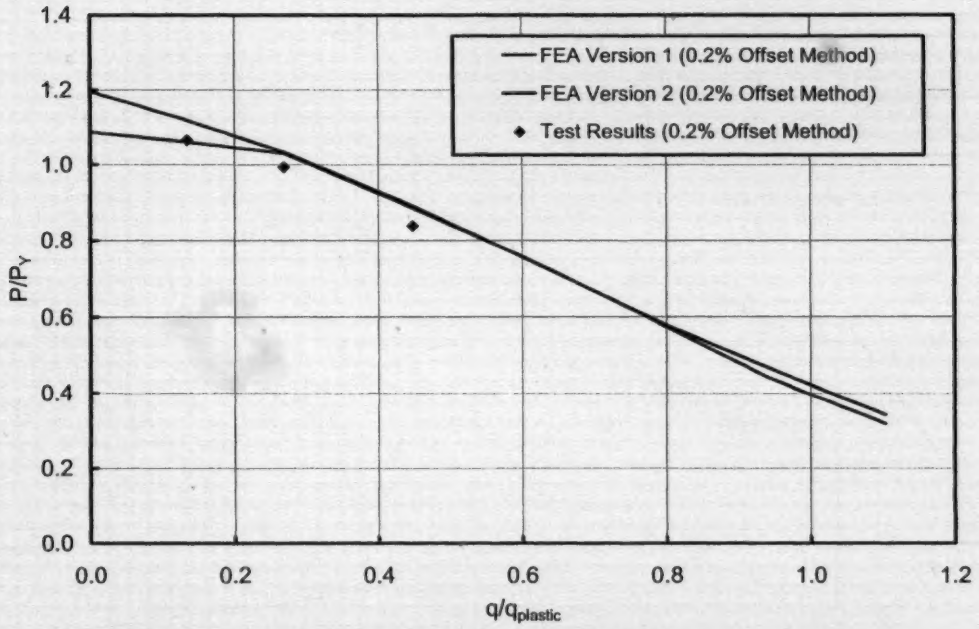

Figure 5.15: Interaction Diagram Obtained Using the 0.2% Offset Method – FEA Version 1 and 2

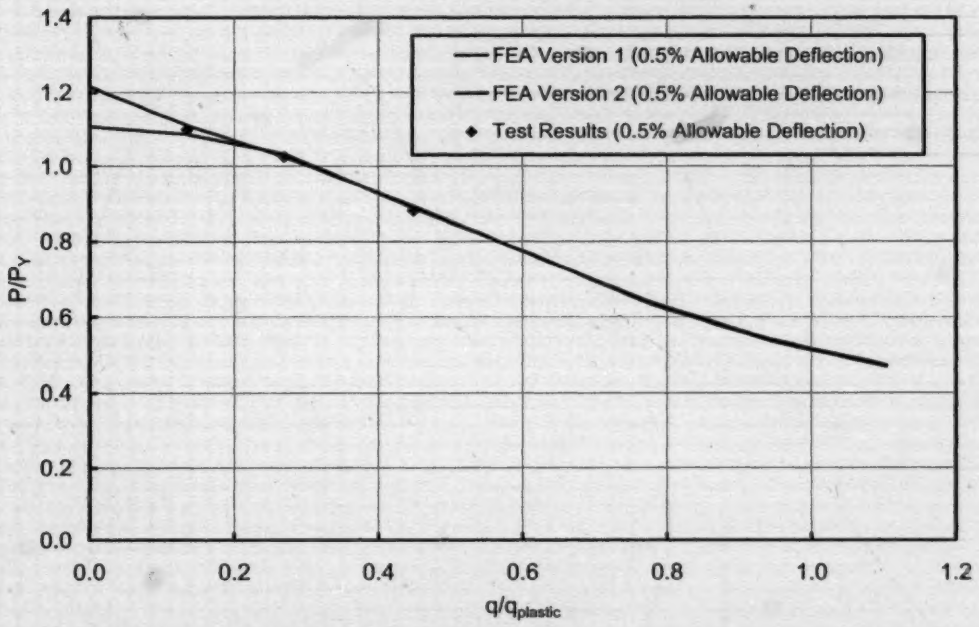

Figure 5.16: Interaction Diagram Obtained Using the 0.5% Allowable Deflection Method – FEA Version 1 and 2

6.0 Summary and Conclusions

6.1 Summary

The experimental program consisted of the testing of three Sandwich Plate System specimen sets under combined load cases of uniaxial in-plane compression and uniform transverse pressure. A test frame was designed to provide fixed boundaries on the panel perimeter and apply uniform in-plane and out-of-plane loads to the test specimen. The test frame was designed to test two SPS panels simultaneously. A test assembly consisted of two panels glued face to face with a shallow cavity formed between them where pressurized water provided the out-of-plane pressure. The in-plane load was transferred from a 15 MN testing machine through steel loading bars built into the top and bottom clamps of the test frame. Ancillary tension coupon tests were performed on the SPS plate steel to obtain material properties needed for a finite element analysis.

Each specimen set was loaded elastically at five different combinations of in-plane and transverse loads, with each specimen set undergoing the same five combinations as a means of comparing performance and variability between tests. Each specimen set was then taken to failure, with each of the three specimens subjected to a different magnitude of lateral pressure. Three failure points on the in-plane load versus lateral pressure interaction diagram for this SPS panel geometry were thus obtained.

A finite element model of a test specimen was developed to predict the strength and behaviour of SPS under combined loading. Two finite element models were created, with Version 1 being the theoretical case of perfectly fixed boundary conditions on the panel perimeter. The Version 2 model was identical to Version 1 with the exception of having softer lateral restraints along the unloaded edges. Results were compared in both elastic and ultimate load ranges, and in-plane load versus transverse load interaction diagrams were generated and compared for both models. A comparison of the numerical analysis results with the test results indicated that the finite element analysis is capable of predicting the test results accurately.

6.2 Conclusions

The significant observations and conclusions from the three SPS tests, the test frame design and the finite element analyses are as follows:

SPS Test Specimen Behaviour

1. In the elastic tests, panel out-of-plane deflections under lateral pressure only compared closely between all tests. In-plane deflections also compared well between tests under in-plane load only.
2. Notable variability was present in strains and von Mises stresses between tests at all load cases in the elastic load range, primarily at the gauges near the panel boundaries. Average coefficient of variation in the data was 19% for top and bottom von Mises stresses and 21% for the edge stresses.
3. Increasing lateral pressure on a panel results in a loss of axial stiffness at decreasing levels of in-plane load. The initial axial stiffness is not affected by the internal pressure.
4. Out-of-plane buckling under in-plane load progresses from a three half-sine-wave shape at low lateral pressures to a single half-wave as the lateral pressures become larger.
5. No local faceplate buckling or core-to-faceplate bond delamination was observed for any of the tests throughout all the loading ranges. Maximum in-plane deflection of the panels was 26 mm on average, translating into an average vertical strain of about 1.5%.

Test Frame Behaviour

1. The test frame successfully enforced equal in-plane load sharing between both SPS panels of a specimen set.
2. The adhesive seal between the SPS panels and the panel spacer bar did not perform as expected. Modifications to the seal should be made for future tests.

3. Because of the large strength and ductility of the SPS specimens, the test frame ran out of in-plane displacement allowance before the ultimate in-plane load capacity could be reached for any of the three specimen sets.
4. The roller bearing assemblies performed as expected, minimizing in-plane load transfer to the edge clamp bars.
5. The test frame clamps maintained a rotationally fixed boundary condition to the panel perimeter throughout all tests.

Finite Element Analyses versus Test Results

1. Overall panel behaviour for both in-plane and out-of-plane deflections compared very well with the Version 2 finite element model (with the flexible lateral edge restraints) throughout the in-plane loading range of all tests.
2. In response to lateral load only, the finite element models exhibited stiffer out-of-plane deflection behaviour than the tests; a result of seating issues in the test frame and lack of shear restraint on the test specimen edges.
3. Finite element results indicate that the panels are capable of carrying transverse pressures at higher levels than the so-called upper bound collapse pressure predicted using yield line theory.
4. Use of the 0.5% allowable deflection method (ASTM A370-05) provided the best comparison between the interaction points from test results and the interaction curves generated from the finite element models. All test-to-predicted ratios were between 0.99 and 1.01 for both finite element model versions.

6.3 Recommendations

To continue the program, future testing of Sandwich Plate System panels under this combined load case should focus on increasing the data required to generate reliable interaction diagrams. To begin, more tests should be done on SPS panels of the same geometry and 1.5 aspect ratio used in these tests, but at higher lateral pressures. Pressure

levels of 950 kPa, 1200 kPa and 1450 kPa would be the next logical set of three tests to fill in the interaction curve for this panel geometry.

The effect of plate aspect ratio should be investigated experimentally. A series of tests could be done on SPS panels of different aspect ratios; one set of six tests for panels of a 1.2 aspect ratio and another set of six tests for panels of a 1.7 aspect ratio. These are the lower and upper limits set by the Lloyd's Register Provisional Rules for the Application of Sandwich Panel Construction to Ship Structure (2005).

To improve on the test frame design, a greater clearance between the edge clamps and the top and bottom clamps would allow more in-plane deflection of the SPS panels, something that was required in this set of tests. The adhesive seal between the SPS and the panel spacer bars could be replaced by a rubber ring gasket fit into a small groove machined along both faces of each of the panel spacer bar components. In this case, butt joints in the spacer bar would be welded instead of glued.

The instrumentation used was adequate for this test, however the strain rosettes around the panel boundaries could be moved closer to the centre of the panel to reduce the boundary effects of the clamps and the high strain readings present right near the edges in the finite element models.

References

ASTM A370-05, (2005). *Standard Test Methods and Definitions for Mechanical Testing of Steel Products*. American Standard for Testing and Materials, 100 Barr Harbour Drive, West Conshohocken, Pa.

Bleich, F., (1952). *Buckling Strength of Metal Structures*. McGraw Hill, New York.

Brooking, M.A., and Kennedy, S.J., (2003). *The Performance, Safety and Production Benefits of SPS Structures for Double Hull Tankers*. Intelligent Engineering Ltd., Ottawa, Ontario.

Cao, J., Grenestedt, J.L., and Maroun, W.J., (2006). Testing and Analysis of a 6-m Steel Truss/Composite Skin Hybrid Ship Hull Model. *Marine Structures*, Vol. 19, pp 23-32.

Dally, J.W., and Riley, W.F., (1978). *Experimental Stress Analysis*. McGraw Hill, New York.

Foo, C.C., Chai, G.B., and Seah, L.K., (2006). Quasi-static and Low Velocity Impact Failure of Aluminium Honeycomb Sandwich Panels. *Proceedings of the Institution of Mechanical Engineers, Part L: Journal of Materials: Design and Applications*, Vol. 220, pp 53-66.

Ghoneim, M.G., and MacGregor J.G., (1992). *Strength and Stability of Reinforced Concrete Plates Under Combined In-plane and Lateral Loads*. Structural Engineering Report No. SER 176, Department of Civil and Environmental Engineering, University of Alberta, Edmonton, Alberta.

Hughes, O.F., (1983). *Ship Structural Design: A Rationally-Based, Computer Aided, Optimization Approach*. John Wiley and Sons, Hoboken, N.J.

Lloyd's Register, (2005). *Provisional Rules for the Application of Sandwich Panel Construction to Ship Structure*. Lloyd's Register, London, U.K.

Lui, G.K., and Alexander, S.D.B., (2003). *Fatigue of Steel Plate – Elastomer Composite Beams*. MSc. Thesis, Department of Civil and Environmental Engineering, University of Alberta, Edmonton, Alberta.

Roberts, J.C., Boyle, M.P., Wienhold, P.D., Ward, E.E., and White, G.J., (2002). Strains and Deflections of GFRP Sandwich Panels Due to Uniform Out-of-plane Pressure. *Marine Technology*, Vol. 39, pp 223-231.

Salvadori, M., and Levy, M., (1981). *Structural Design in Architecture.* Prentice-Hall, Englewood Cliffs.

Appendix A

Shop Drawings of Test Frame Components

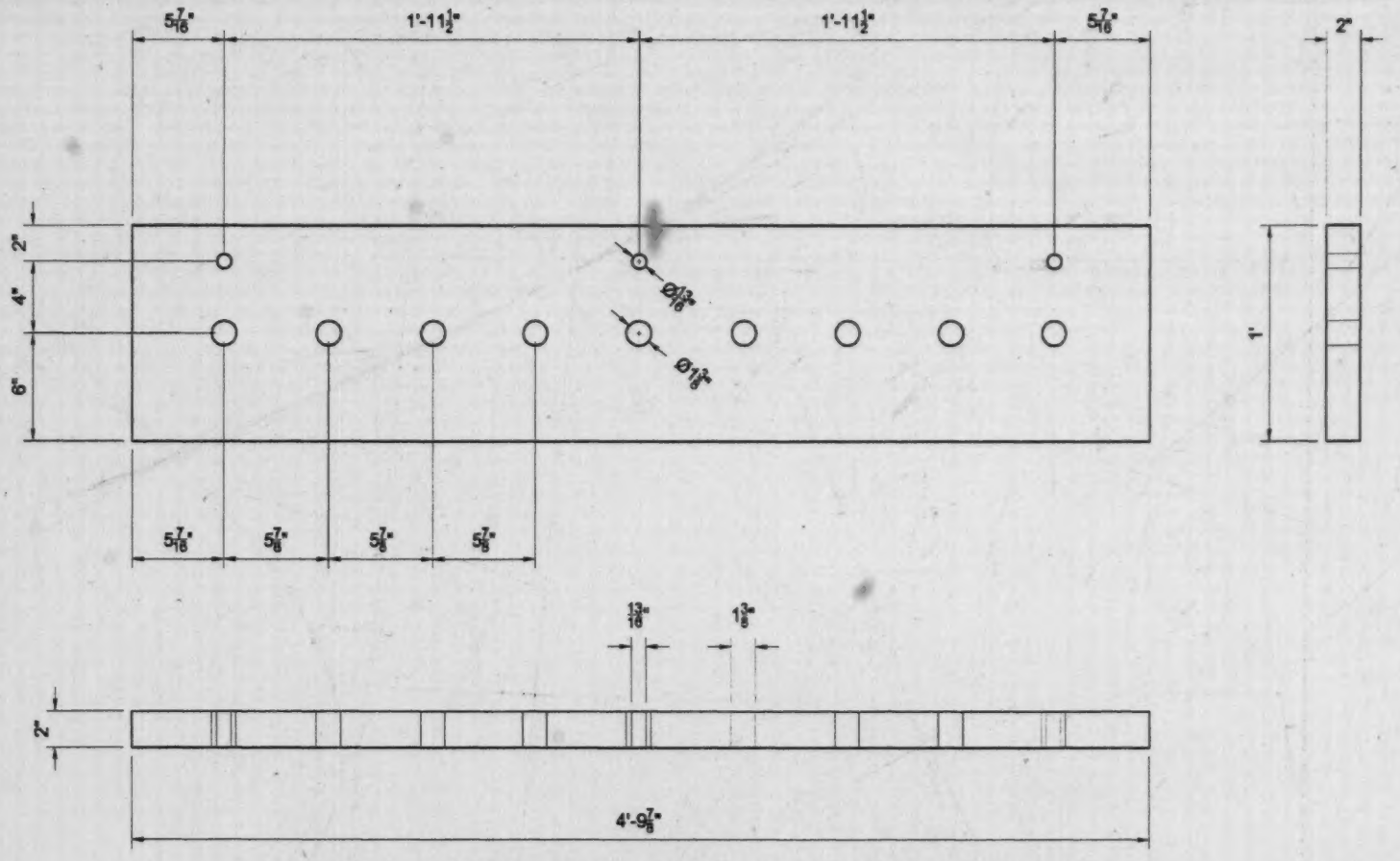

Figure A1: Top Outer Clamp Bar (4 Pieces Required) – Fabrication Drawing with Imperial Units

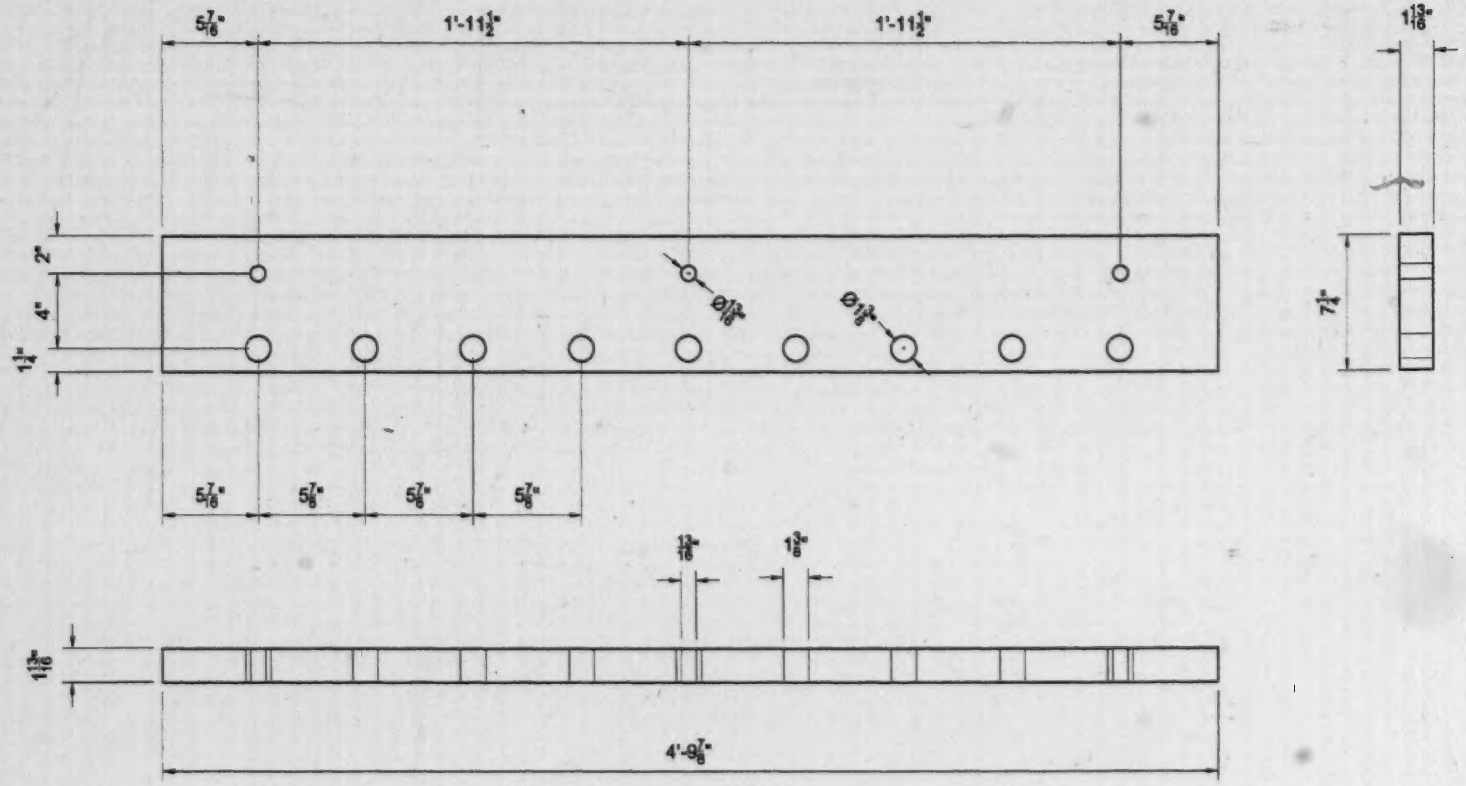

Figure A2: Top In-plane Loading Bar (4 Pieces Required) – Fabrication Drawing with Imperial Units

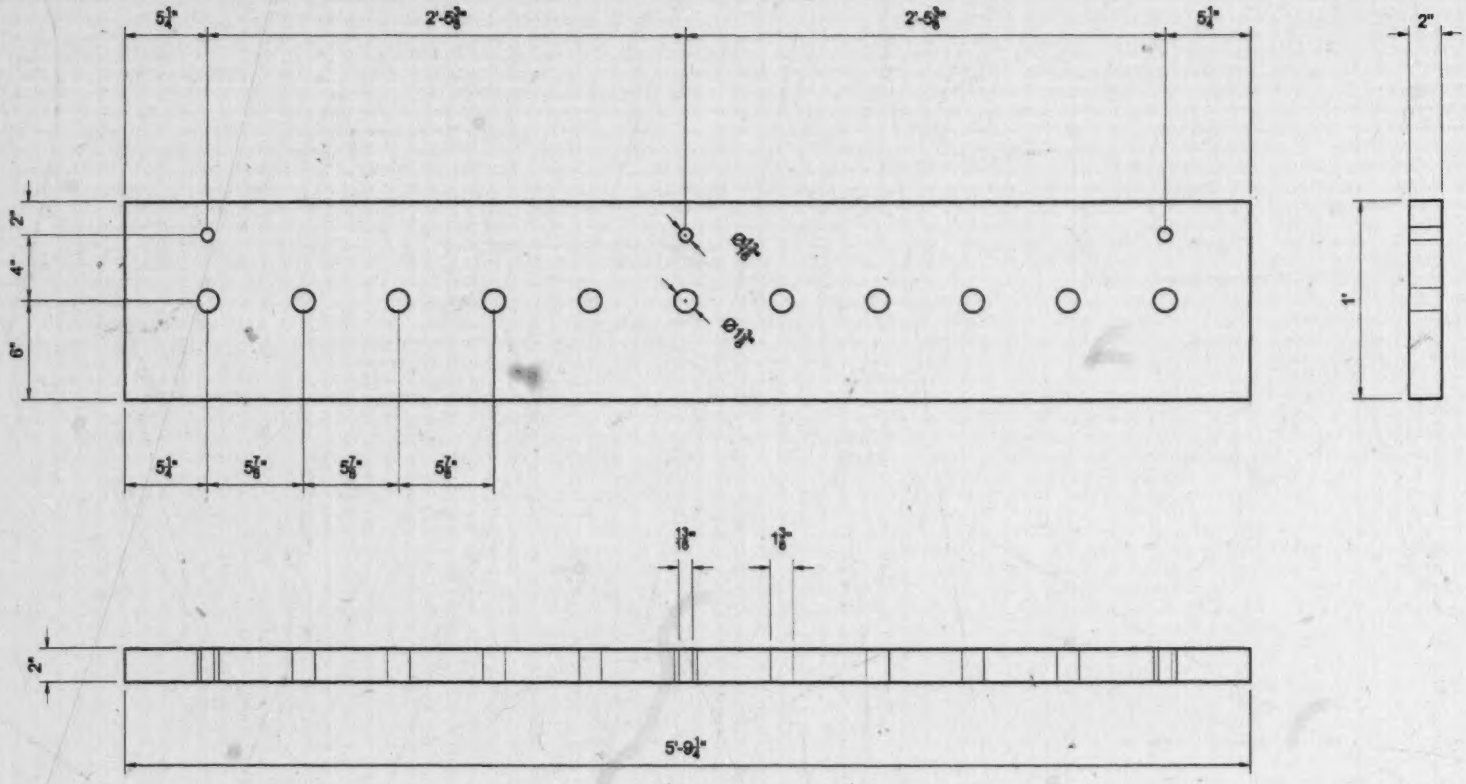

Figure A3: Edge Clamp Outer Bar (4 Pieces Required) – Fabrication Drawing with Imperial Units

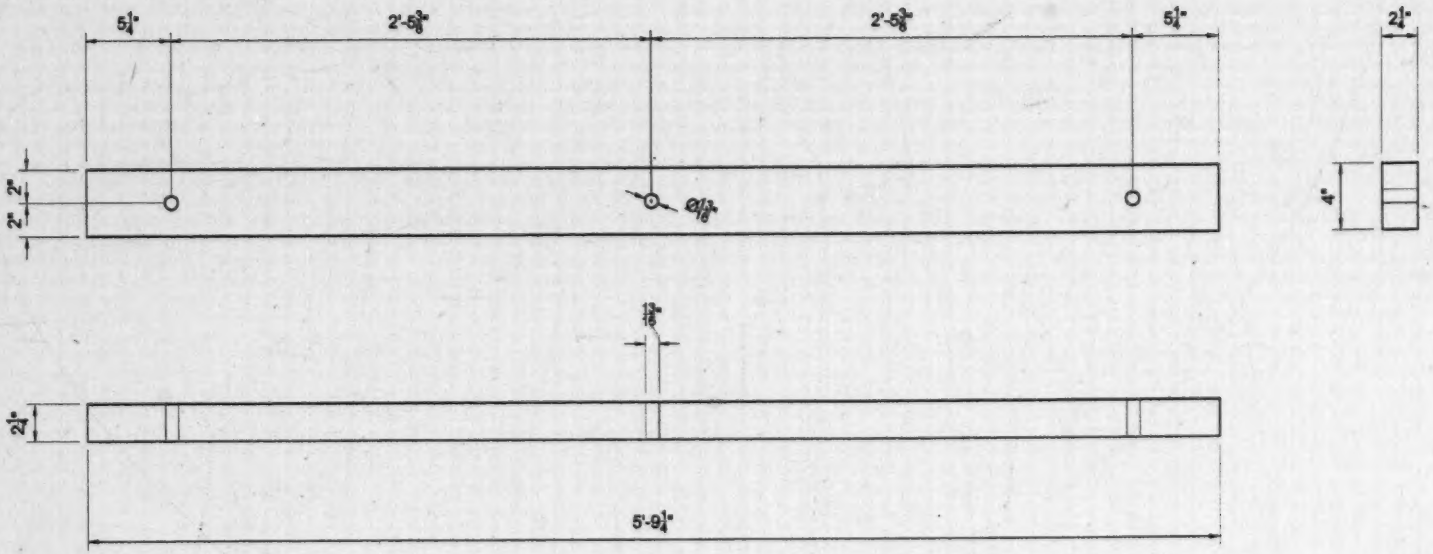

Figure A4: Edge Clamp Spacer Bar (2 Pieces Required) – Fabrication Drawing with Imperial Units

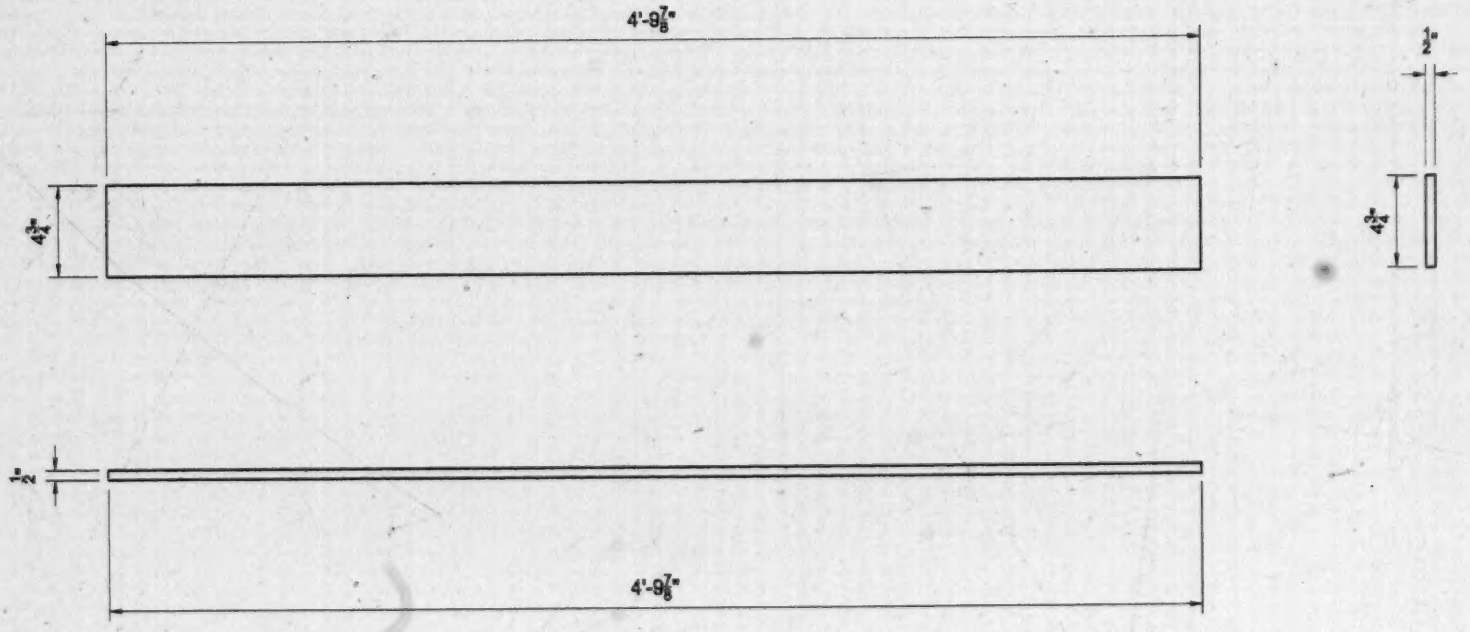

Figure A5: Top Panel Spacer Bar (2 Pieces Required per Specimen Set) – Fabrication Drawing with Imperial Units

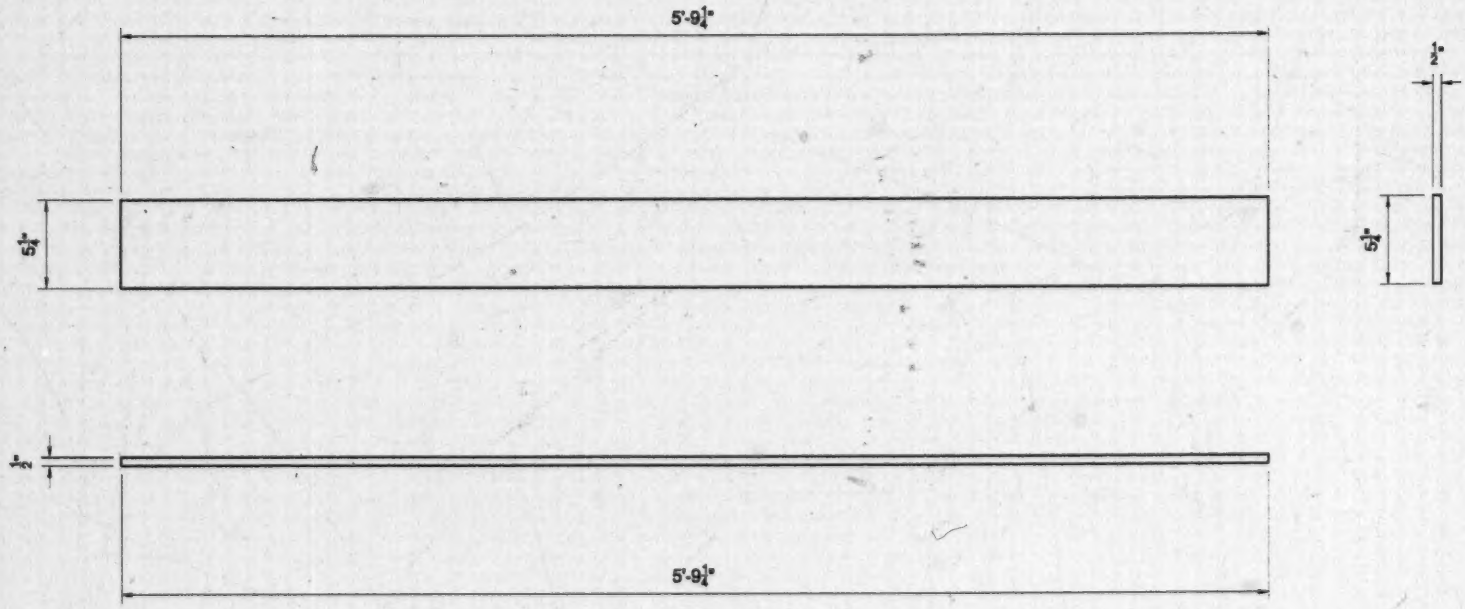

Figure A6: Edge Panel Spacer Bar (2 Pieces Required per Specimen Set) – Fabrication Drawing with Imperial Units

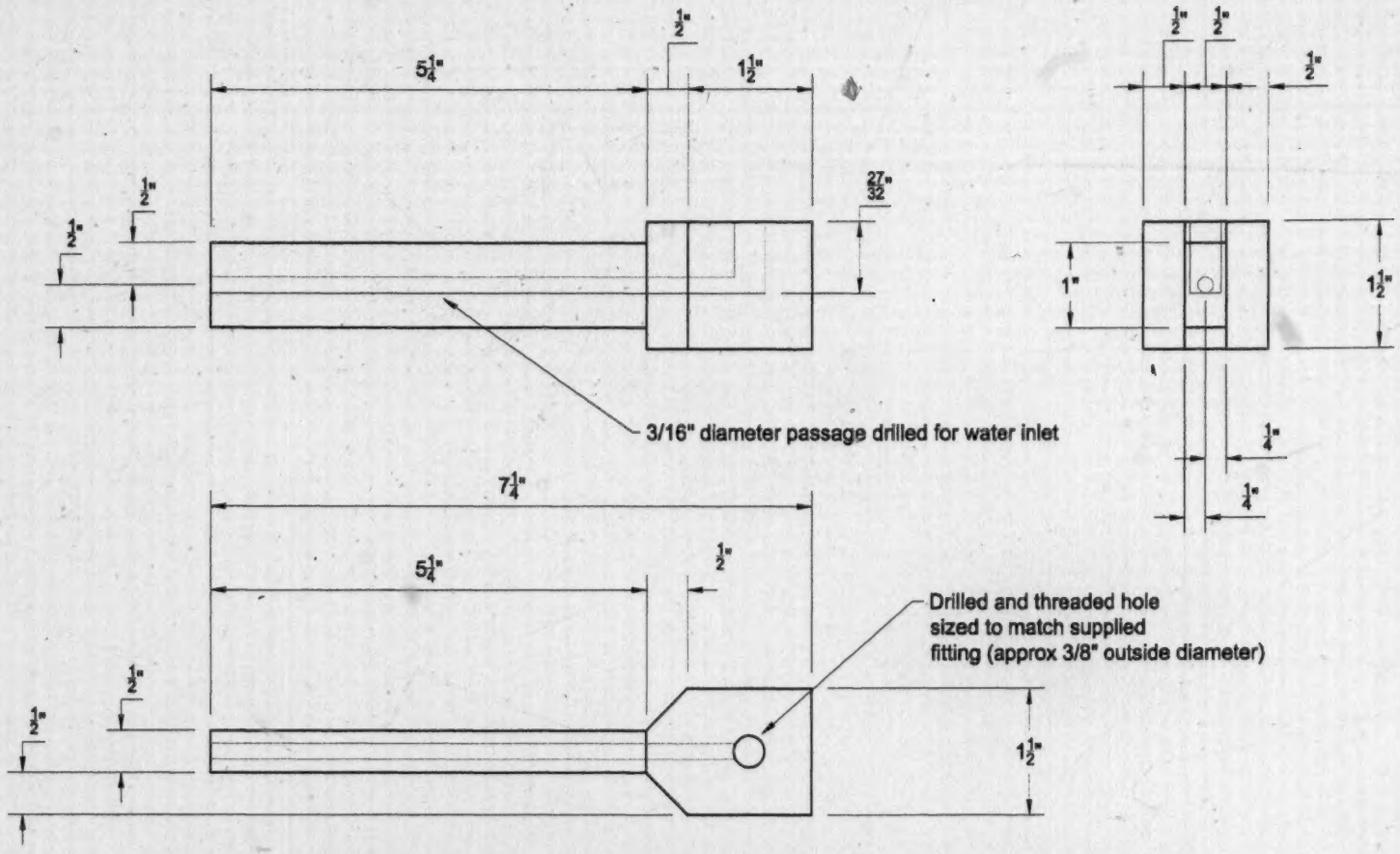

Figure A7: Water Inlet Spacer Insert (2 Pieces Required per Specimen Set) – Fabrication Drawing with Imperial Units

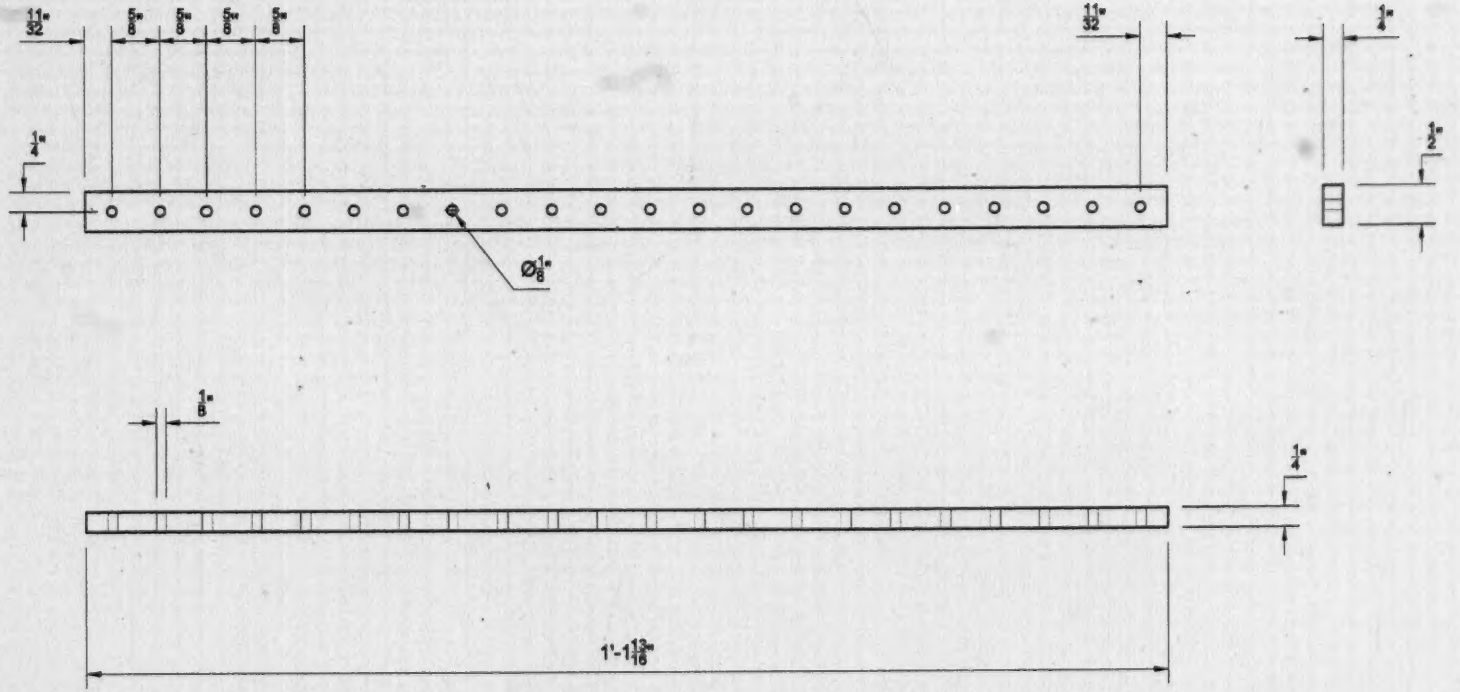

Figure A8: Nylon Retaining Strip for Roller Bearing Assemblies (40 Pieces Required) – Fabrication Drawing with Imperial Units

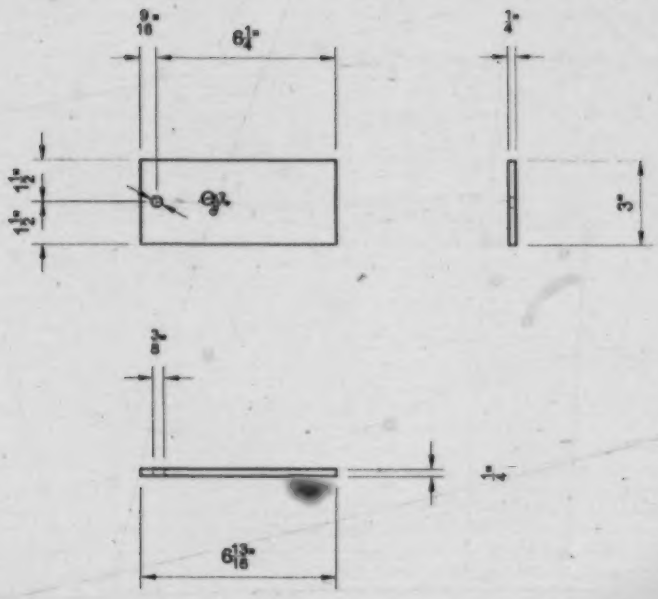

Figure A9: Inner Bearing Plate for Roller Bearing Assemblies (40 Pieces Required) – Fabrication Drawing with Imperial Units

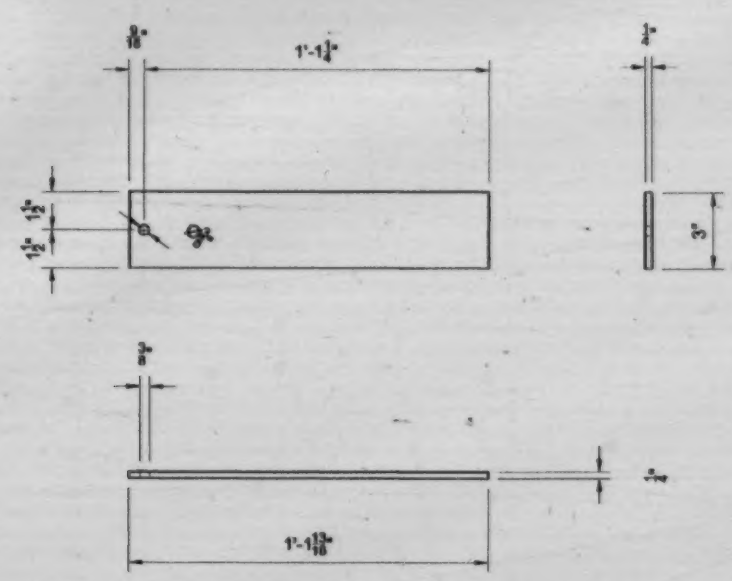

Figure A10: Outer Bearing Plate for Roller Bearing Assemblies (20 Pieces Required) – Fabrication Drawing with Imperial Units